INSTITUTO TECNOLÓGICO Y DE ESTUDIOS SUPERIORES DE MONTERREY

CAMPUS MONTERREY

DIVISIÓN DE INGENIERÍA

PROGRAMA DE GRADUADOS EN INGENIERÍA

EXPERIMENTAL INVESTIGATION OF TEXTILE COMPOSITES STRENGTH SUBJECT TO BIAXIAL TENSILE LOADS

TESIS

PRESENTADA COMO REQUISITO PARCIAL PARA OBTENER EL GRADO ACADÉMICO DE:

DOCTOR EN CIENCIAS DE INGENIERÍA

CON ESPECIALIDAD EN MECATRÓNICA

POR

DAVID ALEJANDRO ARELLANO ESCÁRPITA

MONTERREY, N.L. MAYO DE 2011

INSTITUTO TECNOLÓGICO Y DE ESTUDIOS SUPERIORES DE MONTERREY

CAMPUS MONTERREY

DIVISIÓN DE INGENIERÍA

PROGRAMA DE GRADUADOS EN INGENIERÍA

EXPERIMENTAL INVESTIGATION OF TEXTILE COMPOSITES STRENGTH SUBJECT TO BIAXIAL TENSILE LOADS

TESIS

PRESENTADA COMO REQUISITO PARCIAL PARA OBTENER EL GRADO ACADÉMICO DE:

DOCTOR EN CIENCIAS DE INGENIERÍA

CON ESPECIALIDAD EN MECATRÓNICA

POR

DAVID ALEJANDRO ARELLANO ESCÁRPITA

MONTERREY, N.L. MAYO DE 2011

INSTITUTO TECNOLÓGICO Y DE ESTUDIOS SUPERIORES DE MONTERREY

CAMPUS MONTERREY

DIVISIÓN DE INGENIERÍA
PROGRAMA DE GRADUADOS EN INGENIERÍA

Los miembros del Comité de Tesis recomendamos que este documento de disertación presentado por David Alejandro Arellano Escárpita sea aceptado como requisito parcial para obtener el grado académico de:

Doctor en Ciencias de Ingeniería con

Especialidad en Mecatrónica

Comité de Tesis:

Dr. Hugo Ramón Elizalde Siller
Asesor

Dr. Oliver Matthias Probst Oleszewski
Sinodal

Dr. Jaime Bonilla Ríos
Sinodal

Dr. Carlos Rubio González
Sinodal

Dr. Elías Rigoberto Ledesma Orozco
Sinodal

Dr. Alex Elías Zúñiga
Director del Programa Doctoral en Ciencias de Ingeniería

Mayo de 2011

ABSTRACT

Engineering textile composites are built of a polymeric resin matrix reinforced by a woven fabric, commonly glass, kevlar or carbon fibres. The woven architecture confers multidirectional reinforcement while the undulating nature of fibres also provides a certain degree of out-plane reinforcement and good impact absorption; furthermore, fibre entanglement provides cohesion to the fabric and makes mould placement an easy task, which is advantageous for reducing production times. However, the complexity of textile composites microstructure, as compared to that of unidirectional composites makes its mechanical characterization and design process a challenging task, which often rely on well-known failure criteria such as maximum stress, maximum strain and Tsai-Wu quadratic interaction to predict final failure. Despite their ample use, none of the aforementioned criteria has been developed specifically for textile composites, which has led to the use of high safety factors in critical structural applications to overcome associated uncertainties. In view of the lack of consensus for accurate strength prediction, more experimental data, better testing methods and properly designed specimens are needed to generate reliable biaxial strength models.

The aforementioned arguments provide motivation for this thesis, which presents the development of an improved cruciform specimen suitable for the biaxial tensile strength characterization. A glass-epoxy plain weave bidirectional textile composite is here selected as study case, as a representative material used on many industrial applications. The developed cruciform specimen is capable of generating a very homogeneous biaxial strain field in a wide gauge zone, while minimizing stress concentrations elsewhere, thus preventing premature failure outside the biaxially loaded area. Seeking to avoid in-situ effects and other multilayer-related uncertainties, the specimen is designed to have a single-layer gauge zone. This is achieved by a novel manufacturing process also developed in this research, which avoids most drawbacks found in typical procedures, such as milling. Once the suitability of the specimen was demonstrated, an original biaxial testing machine was designed, built, instrumented and calibrated to apply biaxial loads; the apparatus included a high definition video recorder to get images for digital image correlation strain measurement. An experimental tests program was then conducted to generate a biaxial tensile failure envelope in the strain space. Based on the experimental results, a phenomenological failure criterion based on experimental results and physical textile parameters such as the number of layers and unit cell dimensions was developed. The predicted failure envelope predicted by this criterion achieves very good agreement with the experimental data.

DEDICATORIA

Dedico este trabajo a mis Padres, quienes siempre me han apoyado y a mi hija Valeria, quien ha sido mi motivación durante estos años.

AGRADECIMIENTOS

Deseo agradecer a las siguientes personas sus valiosas contribuciones a la realización de este trabajo de investigación.

- A Ricardo Karthe Escobedo y al Ingeniero Tomás Rosales Ontiveros, quienes me introdujeron al mundo de los materiales compuestos y con quienes aprendí muchas de las técnicas empleadas en la preparación de los especímenes cruciformes empleados para el desarrollo experimental.

- Al Doctor Alex Elías Zúñiga, a quien debo la invitación de enrolarme al programa doctoral del ITESM y quien siempre tuvo la disposición para apoyarme en los aspectos académicos y administrativos.

- Al Doctor Ricardo A. Ramírez Mendoza, quien me acogió en el Centro de Innovación en Diseño y Tecnología y en la Cátedra de Autotrónica, dándome la libertad de desarrollar mi investigación en un tema de mi interés.

- A mi asesor, el Doctor. Hugo R. Elizalde Siller, por su paciencia y su disposición para apoyarme en el transcurso de mi investigación.

- Al Doctor Oliver Matthias Probst Oleszewski por sus valiosos consejos y el apoyo de la cátedra de Energía Eólica para la instrumentación de la máquina biaxial.

- Al Ingeniero Pablo Vargas Cortés por su apoyo en el diseño y construcción de la máquina biaxial, indispensable para el desarrollo de este trabajo y también por brindarme su amistad y apoyo en todos los aspectos de mi vida como estudiante de posgrado.

- A mis compañeros y amigos, especialmente a Luis Alfredo Payán Rodríguez y Diego Ernesto Cárdenas Fuentes por haber estado siempre presentes.

- A Jaime G. Sada Salinas por facilitar el equipo de captura de video para las pruebas experimentales y mas importante aún por su amistad.

- Al Consejo Nacional de Ciencia y Tecnología CONACYT por financiar la construcción de la máquina biaxial a través del fondo de la convocatoria SEP-CONACYT I0003 (CB-2007-01 Ciencia Básica 2007)

Table of contents

List of Figures

List of Tables

Chapter 1.
Introduction

1.1. Composite materials overview

Despite its recent introduction in advanced engineering applications, structural composite materials have been present in nature millions of years ago, in the form of animal's bones, constituted of a calcium ceramic phase which provides hardness, agglutinated by collagen fibres, which provides cohesion and flexibility [62]; or in the form of wood, conformed by cellulose fibres agglutinated by lignin [26]. This type of mixed materials architecture provides to wood and bones high resistance and comparative low weight, essential conditions for high performance structural applications, result of millions of years of evolution. Both cases exemplify the convenience of synergic application of two or more materials for structural purposes. More recently, mankind used composites materials since early civilization; a good example of primitive artificial composite material is that used on building blocks called adobes, made of clay reinforced with straw; this formula allows wet clay to dry without cracking due the hygro-thermal stresses associated with the drying process [63], allowing our ancestress to take advantage of widely available resources to provide edifications. In this case, both the matrix and reinforcement phases were natural.

Today is possible to artificially synthesize specific constituents to create composites designed for specific purposes; as result, new high performance composites have appear, such that fibre-reinforced polymers composite materials (FRPC) which are increasingly found in structural applications, where their excellent mechanical properties generate significant performance improvements for those systems that requires light, stiff and strong materials such those demanded by the aeronautics, wind energy or sport-cars industries. Figure 1.1 compares the specific strength and stiffness (strength/stiffness per

unit of density) for different advanced engineering materials, which specific strength and modulus normalized to that of typical aluminium alloy used in previously mentioned industries, thus allowing direct comparison against this well known material. Three of the most representative FRPC families (glass, aramid and carbon reinforced polymer composites) are represented on that figure.

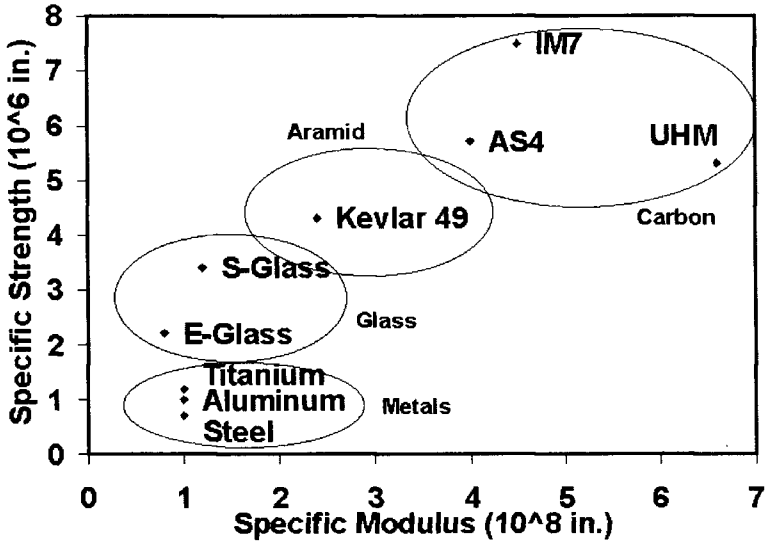

Figure 1.1: Specific strenght vs specific modulus of different high performace structural materials, both normalized to typical aluminium alloys values. [49]

Figure 1.1 presents the specific strength and stiffness of various structural materials as compared with aluminum alloys; this plot evidences the advantages of FRPC over metallic alloys for structural purposes, as they can be as much as seven times stronger and six times as rigid (per weight unit) than aluminum alloys; also, they are less susceptible to degradation by fatigue or corrosion and allows building larger structural single-parts, eliminating mechanical joins and weight [58]; unfortunately, as the well known adage cited by Raymer [61] states: "There's no such thing as a free lunch"; for the case of composite materials this implies that for successfully exploiting the full potential of composites for structural applications, design engineers require of considerably more complex and sophisticated design tools as well as characterization methods than those traditionally employed for conventional metallic alloys, to predict the complex mechanical behavior inherent to heterogeneity and anisotropy [57],[58],[32]. Also new manufacture

methods and techniques to monitor the quality and structural integrity must be developed to bring these materials to commercial applications. Although high performance composites have been commercially available since 1960´s decade, promoting a boom in experimental aircraft (i.e. Burt Rutan all-composite-mold less designs) [47], FRPC have seen only limited applications on large commercial transport airplanes, mainly for non-critical, secondary structural applications. This started to change in the mid of 1980´s decade, when Airbus introduced some structural parts in the A310´s and more extensively in 320 model, as shown in the Figure 1.2, which illustrates the growth of composites on commercial transport aircraft (expressed as a percentage of structural weight) during the last decades.

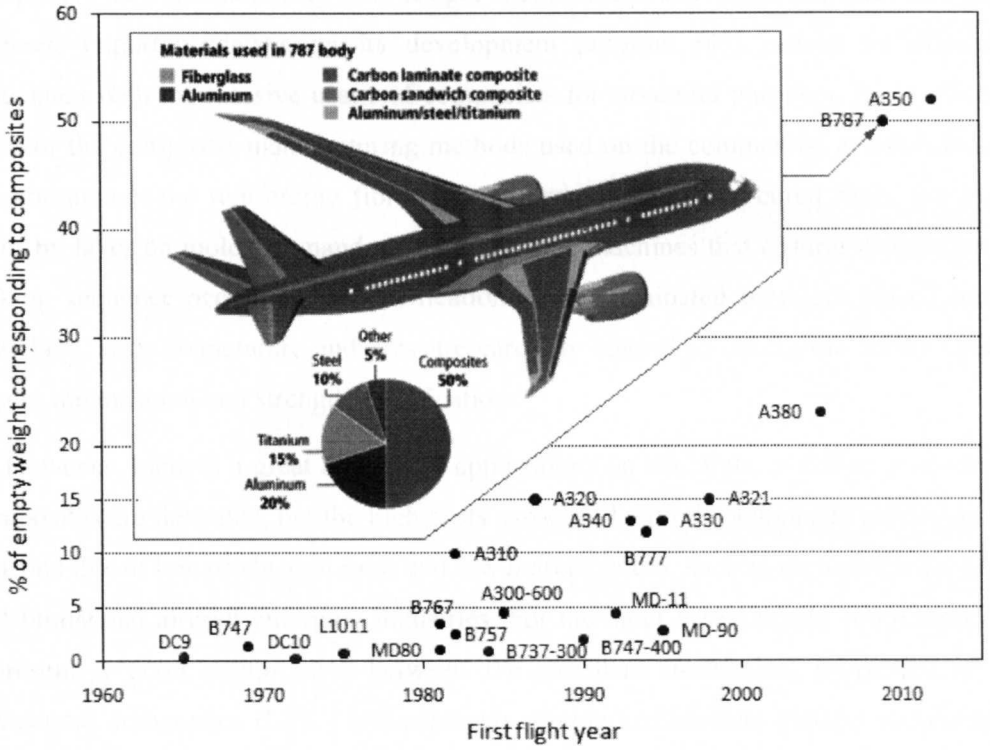

Figure 1.2: Composite usage trends in commercial transports aircraft [16]. Inserted: extensive use of composites on the Boeing 787 (Reproduced from Boeing Co.)

After experience gained on this assays, on mid of 2000´s decade, Airbus, along with the University of Delft, developed the GLARE, a hybrid aluminum sheets-fiberglass

laminated composite [39] which was extensively used on large fuselage sections of the A380, the biggest commercial aircraft ever built.

However, the most significant breakthrough on the structural use of composites for airframe construction was made by the Boeing Company with the introduction of the revolutionary Boeing 787, which realized it maiden flight in December 2009. This aircraft is built on 50%-weight of FRCM; if compared by volume, this number increases to 80% (considering the relative low density of composites), which means that in fact almost all the primary structural components are built on composites, as shown in the inserted sketch of Figure 1.2. For comparison, the previous model of Boeing, the B777, used 12% of total weight of composites [16],[46]. To achieve this quantum leap, Boeing had to develop a completely new methodology for design, manufacture and certificate the 787, which suffered important delays on its development program [45] caused by difficulties associated with the massive usage of composites for structural purposes. As in this case, most of the composite manufacturing methods used on the commercial aviation industry are automated: the reinforcing fibres, once impregnated on pre-cured resin, are placed layer by layer on molds or mandrels by automated machines that ensures orientation and staking sequence according to specifications; then, laminated parts are placed into an autoclave, with temperature and pressure carefully controlled during the curing cycle to ensure dimensional and strength specifications.

However, there is a great amount of applications on which the excellent properties of composites are desirable, but the high costs associated with the automated process are not justified due to low production rates and low market values, such as the small wind energy and unmanned aircraft emerging industries. For the latter cases, textile composites (TC) represent a good compromise between the excellent mechanical properties of uni-directional composites (UDC) and relatively simple manufacture process requirements. This can be achieved due to fibres entanglement in TC, providing cohesion in the same fashion as in a fabric, which can then be easily manipulated, placed and impregnated with non-cured, low viscosity matrix using manual hand lay-up processes.

Again, and according to the "There's no such thing as a free lunch" principle, such manufacturability advantages come at a price: the intricate 3D fibre-entangled architecture of TC adds even more complexity to the yet complex mechanical behaviour; derived

uncertainties oblige designers to use high safety factors, reducing the weight-saving advantages that could be achieved if better failure models were available. Moreover, most efforts directed to develop strength prediction models have focused on UDC due to a specific interest of the aeronautical industry, thus delaying the development of TC failure models.

Based on the aforementioned exposition, it is one objective of this thesis to contribute on the experimental characterization of glass/epoxy TC.

1.2. Organization of Contents

Chapter 2 presents a literature survey about micro-structural architecture and mechanics of composite materials (CM); elastic and strength models are introduced, and special attention is paid to describing failure modes related to CM heterogeneity and failure prediction strategies for UDC and TC are presented.

In Chapter 3 results of survey on biaxial testing methods is presented, focusing on biaxial specimens and data acquisition and reduction methods. A generic cruciform specimen geometry was here selected due to its relative straightforward capability to generate biaxial loads. Also, the Digital Image Correlation (DIC) technique for full strain field measurement is presented and identified as the most adequate for primary data acquisition system.

As result of this literature review, the objectives and scope of this research are defined in Chapter 4, which states as main objectives: i) design of a suitable methodology for biaxial tension-tension strength characterization of single-layer TC, including the development of a properly designed specimen, biaxial testing machine and data acquisition system, ii) to obtain an experimental failure envelope for single-layer TC, and iii) to formulate a dedicated TC phenomenological failure criterion.

On Chapter 5, a finite element (FE) evaluation of a widely used cruciform specimen evidences the need of better specimens. This fact motivated this author to propose a novel rhomboid-windowed cruciform specimen which, after optimization via FE analyses and Design of Experiments methodology, demonstrates a great improvement over similar

specimens. Once an adequate geometry was achieved, an apparatus capable to apply pure biaxial loads was required to conduct the experimental test program.

On Chapter 6, biaxial testing machines survey is presented, resulting on the identification of desirable requirements and features for biaxial testing. As a result, an original biaxial testing machine was designed, built, instrumented and calibrated.

Chapter 7 describes the experimental setup, including a novel manufacture process which avoids micro-damage by machining into the cruciform's rhomboidal window. The cruciform's experimental validation and failure envelope are also presented in this chapter.

On chapter 8, a phenomenological failure criterion for biaxial tension-tension loads is presented, based on experimental results and physical parameters.

Finally, conclusions and recommendations for future work are presented in Chapter 9.

Chapter 2.
Mechanics of composite materials

2.1. Composites materials: definition and classification

Composite materials are characterized by:

- Engineering materials made from 2 or more components, physically distinct and mechanically separable.
- Having several chemically distinct phases, completely insoluble with each other and separated by an interface.
- Properties superior to the sum of the properties of individual components (synergy)

Under these assumptions, engineering composite is defined as a material which is constituted by at least two elements: the matrix and the reinforcement: matrix is responsible of agglutinating and transmitting loads to reinforcement, while the latter provides elasticity and strength.

Due to practically infinite number of possible combinations, systematic classification of composites is necessary for analysis. A well accepted classification is by the type of matrix, as shown in Figure 2.1. Due to its importance in wind energy and aerospace industry, areas of special interest for the research group in which this author collaborates, polymeric thermo-stable matrix was selected to conduct this research, specifically epoxy resins which exhibit excellent mechanical properties, environment stability and competitive costs as compared with other thermo stable resins. Once the matrix is defined, reinforcement spectrum is reduced to carbon, glass, aramid and boron fibres, which are the most commonly reinforcement employed in epoxy resins. From these, glass fibres were selected as they are representative of many industrial applications and because their comparative low cost, which allow more tests for certain budget.

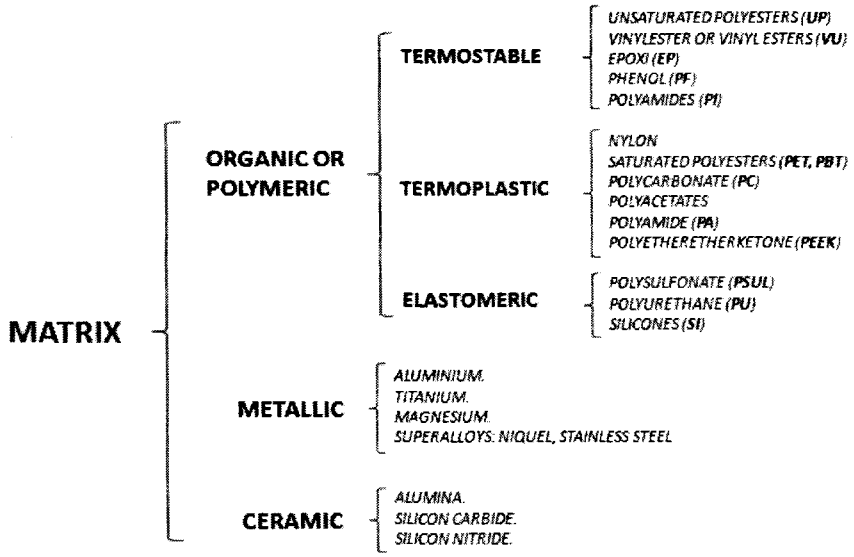

Figure 2.1: Composites classified by matrix.

Other classifications can be done as function of the fibres arrangement: referring to the fibres, if there is no mechanical linkage between individual fibres, then the composite is considered unidirectional (UD); if groups of fibres (yarns) are entangled as in fabric fashion, as sketched on Figure 2.2, the composite is catalogued as a textile composite (TC) [32].

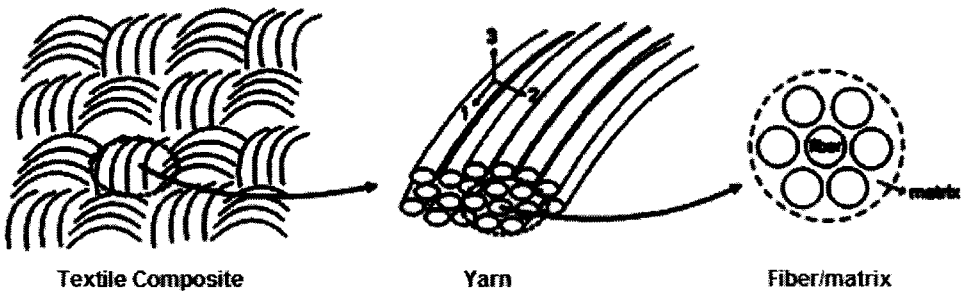

Figure 2.2: Squematic hierarchical structure of textile composites. Reproduced from [41]

The woven architecture confers multidirectional reinforcement while the undulating nature of fibres also provides a certain degree of out-plane reinforcement and good impact absorption [38]; furthermore, fibre entanglement provides cohesion to the fabric and

makes mould placement an easy task, which is advantageous for reducing production times [14]. These features make TC an attractive alternative for the manufacture of high-performance, lightweight structural components [73]. Another interesting feature of TC is that they can be entangled on a variety of patterns, depending of the specific applications intended; on Figure 2.3 unit cells corresponding to well known composite fabric styles are sketched; the unit cell is the minimum size of the textile required to specify it. The simplest, the plain weave (Figure 2.3a), is selected for this research as, in this author's opinion, obtained data could be easily extrapolated to other types.

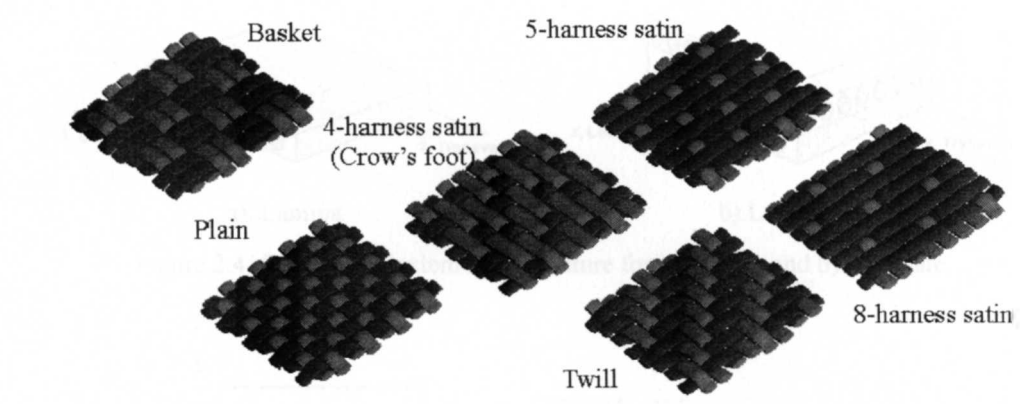

Figure 2.3: Illustration showing various fiber weave architectures. Reproduced from [51].

Despite fundamental differences, essentially the same elastic and damage models are used for both TC and UDC; although standard elastic orthotropic models can yield a reasonably good approximation to TC's structural response, there is not enough experimental data to validate whether UDC failure models can predict accurately or not strength for combined load states, as revealed in the following sections.

2.2. Anisotropic elastic models

To describe the elastic models employed in this work, a reference frame is established next: consider a single unidirectional lamina (Figure 2.4), on which an orthogonal coordinate system is defined with axis 1 parallel to fibres direction, axis 2 lies in the lamina plan and transversal to the fibres while axis 3 is perpendicular to the lamina plane.

When various laminas are stacked at different orientation forming a laminate, a local coordinate reference system is defined, with x as the longitudinal direction, y as the transversal and z as the through-thickness direction. Notice that, during a global laminate analysis, each individual ply (or lamina) conserve its own reference system, which direction is defined by the angle formed between the lamina longitudinal axis 1 and laminate longitudinal axis x .

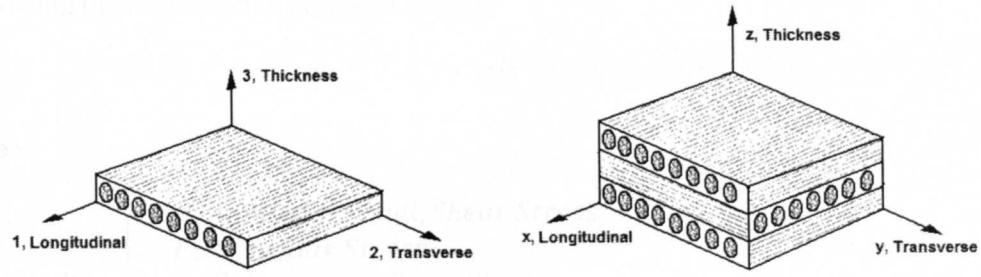

a). Lamina b).Laminate [0/90/0]

Figure 2.4: Coordinate system nomenclature for a). lamina and b). laminate.

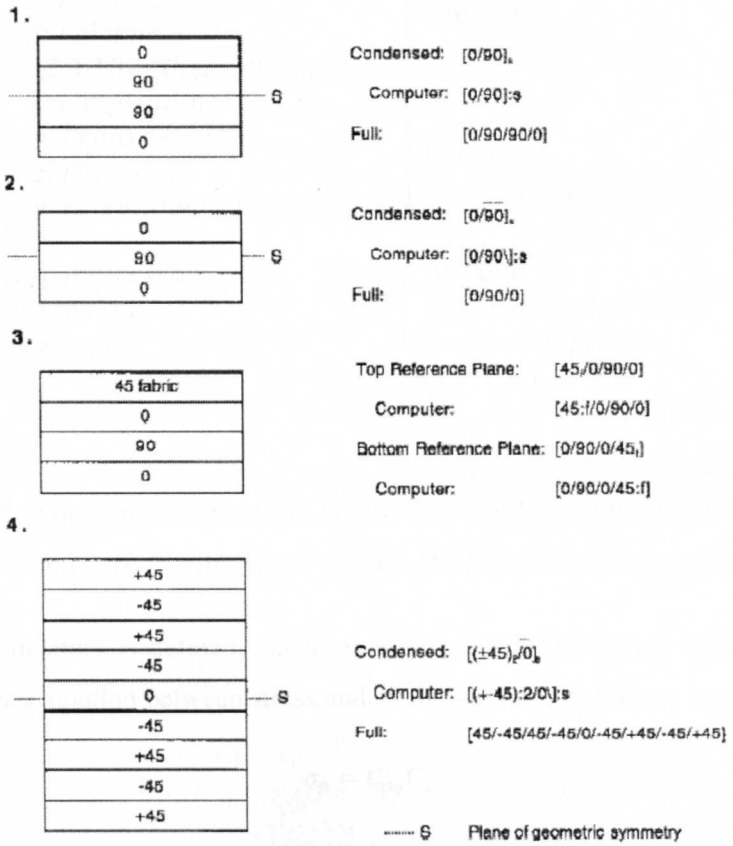

Figure 2.5: Laminate orientation codes. Reproduced from [5]

To define laminates, the code established in ASTM D6507 Standard Practice for Fibre Reinforcement Orientation Codes for Composite Materials [5] is used for all laminates descriptions in this work. In Figure 2.5 some examples of laminate codes are presented, extracted from the ASTM D6507 standard. For this work, the elastic and strength properties are defined with respect to the coordinate systems presented in Figure 2.4, following the next notation proposed in [51]:

$$H_i^{jk}$$

where:

$$H = \begin{cases} \sigma, \tau; Applied\ Normal, Shear\ Stress \\ F; Allowable\ Stress \\ \varepsilon, \gamma;\ Extensional, Shear\ Strain \\ E, G; Young's, Shear\ Modulus \\ v; Poisson's\ Ratio \end{cases}$$

$$i = \begin{cases} 1; Longitudinal \\ 2; Transverse \\ 3; Thickness \\ 12, 13, 32; Shear, Poisson's \end{cases} Lamina$$

$$\begin{cases} x; Longitudinal \\ y; Transverse \\ z; Thickness \\ xy, xz, zy; Shear, Poisson's \end{cases} Laminate$$

$$j = \begin{cases} c; compressoin \\ t; tension \\ s; shear \end{cases} \qquad k = \begin{cases} y; yield \\ u; ultimate, Not\ Used\ for\ Striffness \end{cases}$$

Examples:

$$F_2^{tu} = Lamina\ Ultimate\ Transverse\ Tensile\ Allowable\ Stress$$

$$E_z^c = Laminate\ Compressive\ Young\ Modulus, thickness\ direction$$

Once nomenclature is defined, elastic models used in FE models for composites are described. Linear relation between stress and strain is given by Hooke's law, expressed as:

$$\sigma_p = C_{pq}\varepsilon_q \qquad Eq.\ 2.1$$

Where stress σ, material elastic properties $\boldsymbol{C}$ and strains ε are defined for three dimension anisotropic case as:

$$\{\boldsymbol{\sigma}\} = \begin{Bmatrix} \sigma_1 \\ \sigma_2 \\ \sigma_3 \\ \tau_{23} \\ \tau_{31} \\ \tau_{12} \end{Bmatrix} \quad \{\mathrm{E}\} = \begin{Bmatrix} \mathrm{E}_1 \\ \mathrm{E}_2 \\ \mathrm{E}_3 \\ \gamma_{23} \\ \gamma_{31} \\ \gamma_{12} \end{Bmatrix} \quad [\boldsymbol{C}] = \begin{bmatrix} C_{11} & C_{12} & C_{13} & C_{14} & C_{15} & C_{16} \\ C_{21} & C_{22} & C_{23} & C_{24} & C_{25} & C_{26} \\ C_{31} & C_{32} & C_{33} & C_{34} & C_{35} & C_{36} \\ C_{41} & C_{42} & C_{43} & C_{44} & C_{45} & C_{46} \\ C_{51} & C_{52} & C_{53} & C_{54} & C_{55} & C_{56} \\ C_{61} & C_{62} & C_{63} & C_{64} & C_{65} & C_{66} \end{bmatrix} \quad \textit{Eq. 2.2}$$

For a thin, single lamina with thickness much smaller than the other two dimensions, plane stress assumption becomes a good approximation ($\sigma_3 = \tau_{23} = \tau_{31} = 0$); if additionally, material is considered linearly orthotropic, Hooke's Law for in-plane elastic behaviour can be reduced to:

$$\begin{bmatrix} \sigma_1 \\ \sigma_2 \\ \tau_{12} \end{bmatrix} = \begin{bmatrix} C_{11} & C_{12} & 0 \\ C_{12} & C_{22} & 0 \\ 0 & 0 & C_{66} \end{bmatrix} \begin{bmatrix} \mathrm{E}_1 \\ \mathrm{E}_2 \\ \gamma_{12} \end{bmatrix} \quad \textit{Eq. 2.3}$$

where:

$$C_{11} = \frac{E_1}{1 - v_{12}v_{21}} \qquad C_{12} = \frac{v_{12}E_2}{1 - v_{12}v_{21}} = \frac{v_{21}E_1}{1 - v_{12}v_{21}} \qquad C_{22} = \frac{E_2}{1 - v_{12}v_{21}}$$

$$C_{66} = G_{12} \quad \textit{Eq. 2.4}$$

Then, four independent engineering constants are required to define the in-plane elastic response of an orthotropic material: E_1, E_2, v_{12}, G_{12}; note that v_{21} is not independent as it must satisfy C_{12}. For more practical cases, TC and UDC are treated as orthotropic due to their symmetry planes. Detailed derivation and of this model and its application to laminates is described in [32].

2.3. Strength of composite materials

Elastic properties are needed to determine structural response, while strength properties allow establishing limit loads. Unfortunate, the same features that confer CM their excellent specific stiffness also make strength characterization a challenge. Experimental investigations on strength of CM's [69],[27],[21],[67],[36],[84] demonstrate that their

heterogeneous structure influence the manner in which material fails (i.e. distinct failure modes or mechanisms), according to the following general principles:

- ❖ Failure modes are highly dependent on the properties of individual constituents.
- ❖ Also depend on the type of applied load.
- ❖ In general, they can be independent.

Most frequent failure modes observed in CM´s are:

Delamination: separation of adjacent plies due to fracture at their interface. This defect is not visible on the surface, making it difficult to detect in early stages. Predicting initiation and propagation of this failure mode can be performed via numerical analysis using de-cohesion elements, implemented in some commercial finite element software. This formulation is based on the estimation of the energy required to produce fracture in the interface region. Delamination modes can be classified according to the type of load: Mode I (Figure 2.6 a) is related to out-of-plane loads, while Modes II and III (Figure 2.6 b and 1c, respectively) are due to in-plane shear stresses at the interface [11].

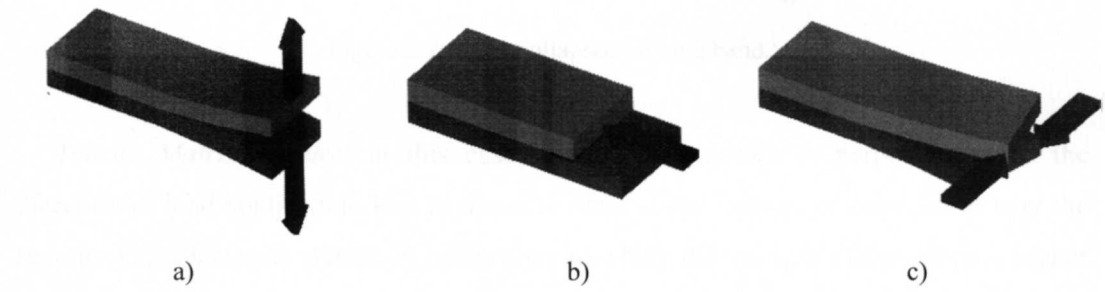

Figure 2.6: Delamination modes: a).Mode I, b). Mode II, c). Mode III

Matrix compression failure: although known as compressive, this failure mode is related to shear stress; in fact, the fracture surface occurs at a certain angle with the direction of the compressive load, which reveals the shear nature of this failure mode. Specifically, the fracture angle for laminates of fibre glass and epoxy resin is approximately 53° to the direction of loading [57]; researchers who observed this phenomenon suggested that the friction between fibres and matrix is a factor that play a

dominant role in the compression fracture; this would explain the departure from the 45° angle typically observed in compressive failure of homogeneous brittle materials.

Fibre compression failure: formation of collapsed regions due to fibre buckling. This failure mode is highly dependent on shear behaviour of the matrix, as well as defects in the laminate (misalignment in the fibres or voids in the matrix). It is typically accompanied by small-scale emergence of collapsed fibre bands or "kinking bands" [67] resulting from buckling instability in the fibres by shear failure in the matrix or fracture in the fibres (Figure 2.7).

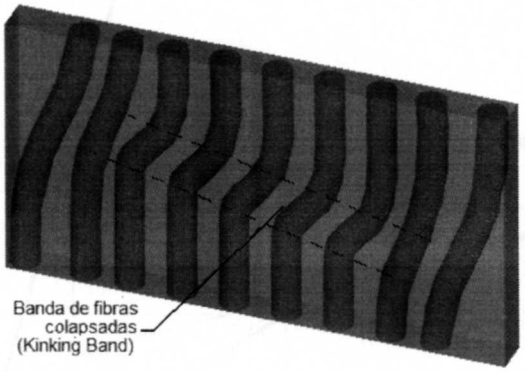

Figure 2.7: Fiber collapsed kinking band.

Tensile Matrix Failure: in this case, the fracture surface is perpendicular to the direction of load application. It is common to observe the fracture of some fibres near the region of the damaged matrix. In composites in which the strength of the fibres is higher than the matrix, this type of damage is not catastrophic because the stress loads are redistributed between fibres and intact matrix regions. Experimentally, and particullary for TC, this manifests as a change in the slope of the stress-strain curve (Figure 2.8). Once it reaches a certain level of damage in the matrix, behaviour of material is dominated by the fibres and remains nearly bi-linear until final failure, corresponding to a stress significantly higher than for the matrix damage onset. However, the micro damage in the laminate can cause leakage of a pressurized fluid, issue that must be considered in pressure vessels.

Tensile fibre failure: this type of failure is considered catastrophic because of the large amount of energy released by the rupture of the fibres. Of course, the state of stress

required to break the fibres causes a wide damage upon failure, so that the load cannot be redistributed. This condition is regarded as the last effort of the material under tension. Some studies [37] demonstrate that failure by tension in fibres depends only on the longitudinal stress component, so this failure mode is completely independent of fibre-matrix interactions.

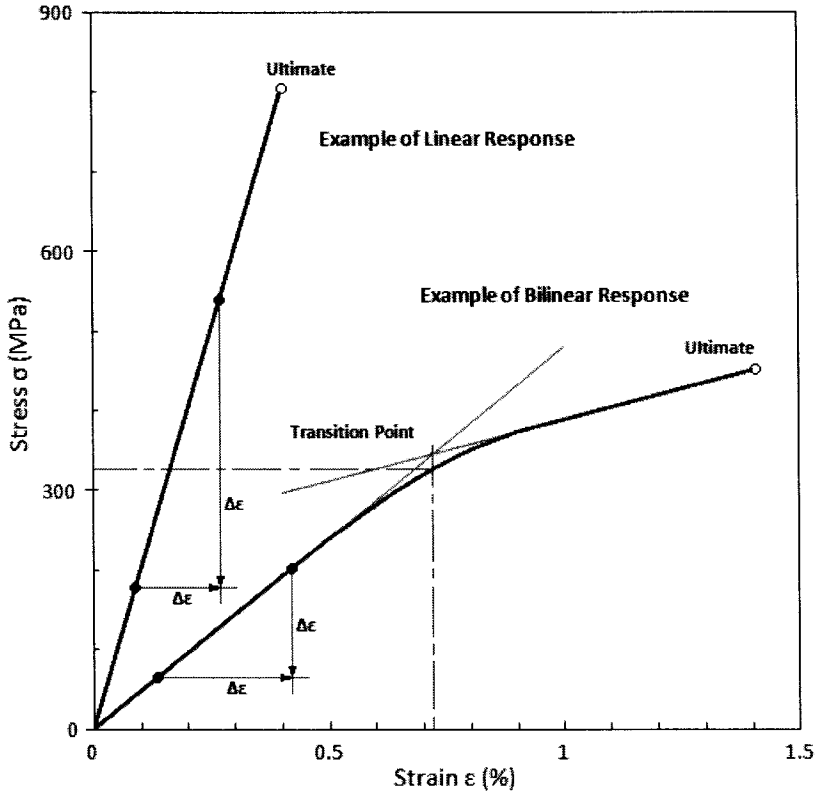

Figure 2.8: Typical tensile stress-strain curves observed in uniaxial testing of composites. Linear response is typical of longitudinally loaded UD lámina, while bilinear response is typically observed in textile composites (Reproduced from ASTMD3039 [Adapted from [4]).

Despite the excellent in-plane mechanical properties exhibited by composites, their bending stiffness is comparatively low due to the inherent instability of thin films under bending or compressive loads. This problem can be solved through the use of sandwich structures [58], which consist of a thick sheet of lightweight material of comparatively low rigidity and resistance (core) which outer surfaces are laminated composited plies (skins). The skins carry most of the loads in the plane, while the core increases the effective moment of inertia, thereby increasing stability and out plane flexural rigidity.

Usually, the material used for cores is polymeric foam, lightweight wood or honeycomb. However, the fact of adding another constituent adds new failure mechanisms. The most commonly observed are the following [15], [66]:

Failure by indentation: occur when a concentrated load is applied on the surface of the sandwich. The failure is characterized by the collapse of the core directly under the load, forming a cavity on the surface of the laminate. As a result, a complex elasto-plastic stress state arises around the indented area, weakening the skins and destabilizing the sandwich structure, making it prone to collapse under compressive loads (Figure 2.9 a).

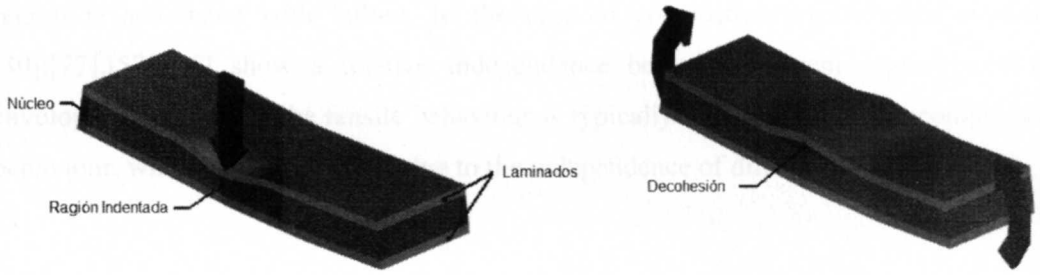

a. Indentation b. Core/skin decohesion.

Figure 2.9: Typical failure modes exhibited by sandwich structures..

Core failure: this failure occurs when the core stress reaches a critical value. For thick laminates (relative to the direction of loading) this is dominated by shear, while for thin laminates the compressive and bending stresses can become comparable in magnitude [66].

Core/laminate de-cohesion: this failure mode is similar to delamination, but in this case defining a separation between the skin and core (Figure 2.9 b). The triggering of this failure mode may be due to manufacturing defects or external factors such as impact. Decohesion between core and laminate reduces the bending rigidity and makes the laminated susceptible to buckling instability [66].

2.4. Failure criteria review

It is now an accepted fact that there is no single failure criterion which can predict the complex failure behaviour observed in composite materials [60],[34],[76]. Unlike isotropic and homogeneous metallic materials, which ductile yielding can be accurately predicted using simple and elegant models such as Von Mises, failure criteria for composites must consider inherent anisotropy to achieve an accurate failure prediction, as evidenced by the different failure modes presented on the last section. Most failure criteria represent a geometric envelope within a tensor space (stress, strain, energy) associated with a load state; the region within the envelope represents the safe zone, while the outer region is associated with failure. In the case of composites, experimental evidence [30],[77],[57],[15] show a relative independence between different segments of the envelope, for example, the tensile behaviour is typically independent of the compression behaviour, which is not surprising due to the independence of different failure modes.

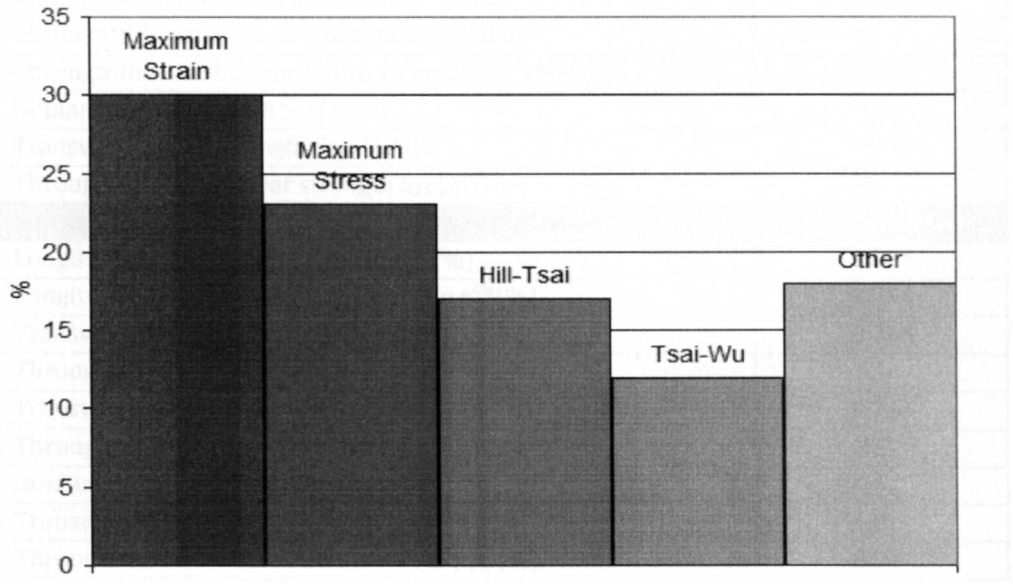

Figure 2.10: Usage of different failure criteria by composite structural designers. (Reproduced from [55])

Table 2.1. Unidirectional E Glass/MY755 epoxy mechanical properties [37].

Fibre type	E-Glass
Matrix	MY750
Elastic properties	
Fibre volume fraction V_f (%)	60.0
Longitudinal modulus E_1 (GPa)	45.6
Transverse modulus E_2 (GPa)	16.2
Through-thickness modulus E_3 (GPa)	16.2
In-plane shear modulus G_{12} (GPa)	5.83*
Transverse shear modulus G_{13} (GPa)	5.83*
Through-thickness shear modulus G_{23} (GPa)	5.7
Major Poisson's ratio υ_{12}	0.278
Major transverse Poisson's ratio υ_{13}	0.278
Through-thickness Poisson's ratio υ_{23}	0.4
Strength properties: maximum allowable stresses	
Longitudinal tensile strength F_1^{tu} (MPa)	1280
Longitudinal compressive strength F_1^{cu} (MPa)	800
Transverse tensile strength F_2^{tu} (MPa)	40
Transverse compressive strength F_2^{cu} (MPa)	145**
Through-thickness tensile strength F_3^{tu} (MPa)	40
Through-thickness compressive strength F_3^{cu} (MPa)	145**
In-plane shear strength S_{12} (MPa)	73**
Transverse shear strength S_{13} (MPa)	73**
Through-thickness shear strength S_{23} (MPa)	50
Strength properties: maximum allowable strains	
Longitudinal tensile failure strain ε_1^{tu} (%)	2.807
Longitudinal compressive failure strain ε_1^{cu}(%)	1.754
Transverse tensile failure strain ε_2^{tu}(%)	0.246
Through-thickness compressive failure strain ε_2^{cu} (%)	1.2
Transverse tensile failure strain ε_3^{tu}(%)	0.246
Through-thickness compressive failure strain ε_1^{cu} (%)	1.2
In-plane shear failure strain γ_{12}^{u} (%)	4.0
Transverse shear failure strain γ_{13}^{u} (%)	4.0
Through-thickness shear failure strain γ_{23}^{u} (%)	0.88

* Initial modulus

** Nonlinear behaviour and stress strain curves and data points are provided

\+ Please note that values are considered to be low, compared with typical data for the same material published somewhere else or quoted by the manufacturers.

Broadly speaking, the failure criteria used in composite materials can be classified as: parametric, phenomenological, micromechanics and probabilistic [55],[21]. Despite simple phenomenological and parametric criteria are the most commonly used by designers (see Figure 2.10), there exist a large number of more complex, more or less successfully criteria developed for composites. A brief description and examples of the most commonly used is presented next. E-glass/Epoxy unidirectional composite was selected to compare the failure envelope predicted by each criterion, using material properties of Table 2.1.

2.4.1. Parametric failure criteria

These criteria are based on empirical observations, seeking to fit mathematical expressions to experimental data to generate a failure envelope. Parametric criteria are widely used, due to their success in predicting certain failure conditions and relative simplicity of implementation. Another important factor is their frequent use in many texts. Among main mishaps is that they do not distinguish between different failure modes, so results can hardly be extrapolated; accordingly, they might not offer a physical explanation about the origin and spread of damage. Most of these criteria are given in quadratic form, the best known being the Tsai-Hill, Tsai-Wu, to which other variants are often compared. Tsai-Wu criterion [55],[21] expresses the failure envelope as:

$$f = K_i\sigma_i + K_{ij}\sigma_i\sigma_j \qquad i,j = 1 \dots 6 \text{ (Repeated indices indicate summation)} \qquad \textit{Eq. 2.5}$$

where $f \geq 1$ denotes failure. Input values σ_i correspond to the stress state, while parameters K_i *and* K_{ij} must be experimentally obtained to fit the experimental failure envelope. To ensure that failure envelope is closed and convex, the interaction terms K_{ij} must satisfy [75]:

$$K_{ii}K_{jj} - {K_{ij}}^2 \geq 0 \qquad \textit{Eq. 2.6}$$

Such condition implies that $K_{ii} \geq 0$. These parameters include the ultimate stresses experimentally observed on uniaxial tension and compression tests in longitudinal and transverse directions and also ultimate shear stress; the simplification for plane-stress orthotropic materials is:

$$K_1\sigma_1 + K_2\sigma_2 + K_{11}{\sigma_1}^2 + K_{22}{\sigma_2}^2 + K_{66}{\tau_{12}}^2 + 2\,K_2\sigma_1\sigma_2 = 1 \qquad \textit{Eq. 2.7}$$

where the parámeters are defined as:

$$K_1 = \frac{1}{F_1^{tu}} - \frac{1}{F_1^{cu}}; \quad K_2 = \frac{1}{F_2^{tu}} - \frac{1}{F_2^{cu}}; \quad K_{11} = \frac{1}{F_1^{tu}F_1^{cu}}; \quad K_{22} = \frac{1}{F_2^{tu}F_2^{cu}}$$

$$K_{66} = \frac{1}{F_{12}^{su^2}}; \; K_{12} = \frac{F_{12}^*}{\sqrt{F_1^{tu}\,F_1^{cu}\,F_2^{tu}\,F_2^{cu}}} \qquad \textit{Eq. 2.8}$$

The bilinear interaction parameter F_{12}* ranges between 1 and -1, the specific value being determined by the properties of each laminate; however, it is difficult to find in the literature recommended values for each type of composite. A value of -1/2 is generally used if not information is available, as it corresponds to the general form of the Von-Mises criterion. The effect of this parameter is shown in Figure 6.

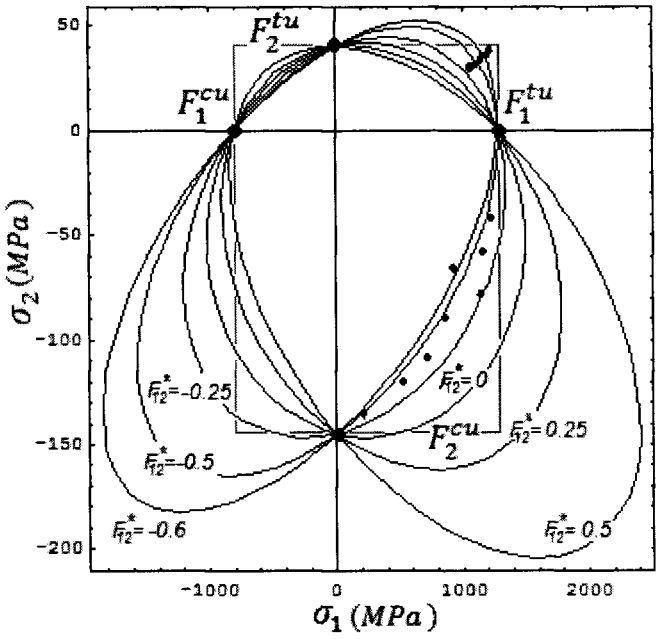

Figure 2.11: efect of bilinear interaction parameter F12* on Tsai-Wu predicted failure envelope.

One advantage of this approach is that the safety factor for lamina under a given stress state is the inverse of the value of the criterion, which facilitates interpretation for design purposes. A modification of the Tsai-Wu criterion is the Tsai-Hill criterion [21],[55], which proposes a piece-wise failure envelope, distinguishing between the different quadrants of the stress space.

$$K_1 = 0; \quad K_2 = 0; \quad K_{11} = \frac{1}{F_1^{ju}}; \quad K_{22} = \frac{1}{F_2^{ju}}$$

$$K_{66} = \frac{1}{F_{12}^{su2}}; \quad K_{12} = -\frac{1}{2F_1^{ju2}} \quad \text{where } j = \begin{cases} c; compression \\ t; tension \end{cases} \qquad \textit{Eq. 2.9}$$

This piecewise definition of the Tsai-Hill failure envelope is defined by specific sets of parameters for each quadrant, depending if the loads are tensile or compressive. Failure envelopes generated for this criterion are shown in Figure 2.12: Tsai-Hill criterion appears to be conservative for the quadrant 1, while fits very well experimental data on quadrant IV. Some recent works [72] have developed quadratic criterion considering out-plane shear terms, extending the usability of the criterion for thick beams under flexure load condition.

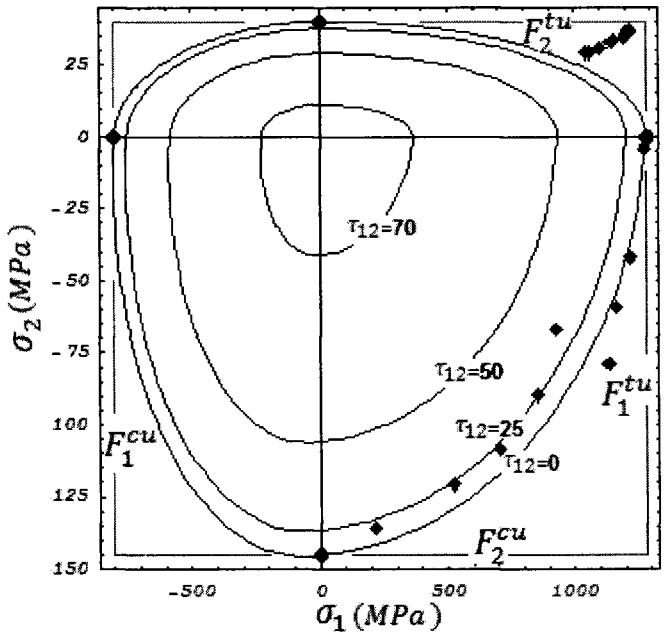

Figure 2.12: Tsai-Hill failure criterion envelope.

2.4.2. Phenomenological failure criteria

Also known as failure criteria based on failure modes, these are based on understanding the failure modes of the material at the macroscopic level to build models addressing each mode separately. As in the case of metals, it is assumed material homogeneity. Some criteria are:

a. Maximum Stress and Maximum Strain Criteria. [30]. They are among the most frequently used criteria due to its simplicity, predicting failure when some of the stress or strain components in a given direction reaches a critical value determined by uniaxial experimental tests. A disadvantage is that it does not consider interactions under multiaxial load states. Failure envelopes for these criteria are given by the expressions:

$$f_{max.\ stress} = max\left\{\left|\frac{\sigma_1}{F_1^{tu}}\right|, \left|\frac{\sigma_1}{F_1^{cu}}\right|, \left|\frac{\sigma_2}{F_2^{tu}}\right|, \left|\frac{\sigma_2}{F_2^{cu}}\right|, \left|\frac{\tau_2}{F_2^{su}}\right|\right\} \geq 1$$

Eq. 2.10

$$f_{max.\ strain} = max\left\{\left|\frac{\varepsilon_1}{\varepsilon_1^{tu}}\right|, \left|\frac{\varepsilon_1}{\varepsilon_1^{cu}}\right|, \left|\frac{\varepsilon_2}{\varepsilon_2^{tu}}\right|, \left|\frac{\varepsilon_2}{\varepsilon_2^{cu}}\right|, \left|\frac{\gamma_{12}}{\gamma_{12}^{u}}\right|\right\} \geq 1$$

Eq. 2.11

Both equations predict failure when $f \geq 1$.

b. Hashin criterion and its multiple variants (eg Hashin-Rotem [30], Modified Hashin, etc.) was one of the first to differentiate between failure modes associated with the matrix and fibres. The envelope generated by this criterion is obtained from the following equations:

$$f = \begin{cases} \dfrac{\sigma_1}{F_1^{ju}} \geq 1 \\ \left(\dfrac{\sigma_{22}}{F_2^{ju}}\right)^2 + \left(\dfrac{\tau_{12}}{F_{12}^{su}}\right)^2 \geq 1 \end{cases} \quad \text{where } j = \begin{cases} c; compression \\ t; tension \end{cases}$$

Eq. 2.12

Hashin also developed 3-dimensional criteria, which have been implemented in the commercial software MSC Dytran [53].

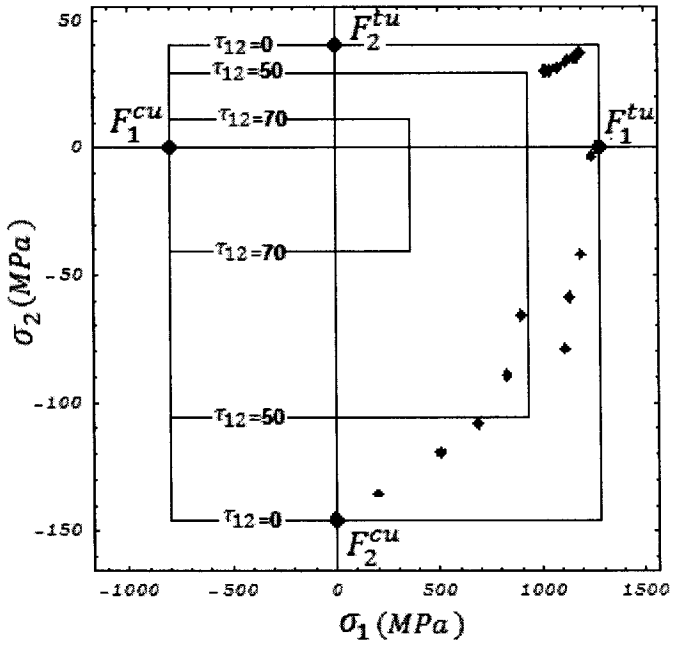

Figure 2.13: Hashin failure envelope

c. LaRC04. This criterion models the interaction between individual constituents, proposing different mathematical models related for each failure mode. This approach makes one of the best criteria, capable of predicting relatively accurate failure envelopes for a wide array of load conditions, specifically compression and shear. The complete criteria consist on a set of six independent equations, each corresponding to a specific failure mode. The shear failure model in the matrix is based on the Mohr-Coulomb theory and predicts not only the maximum load, but also the plane angle in which fracture appears. The model for compression fibre failure is determined by an initial misalignment, and the plane which produces the collapsed fibre band is predicted by the model. The full set of equations [57] that conforms the LArC04 criterion are:

$LaRC04\ \#1: Tensile\ matrix\ failure\ (\sigma_2 \geq 0)$

$$FI_M = (1-g)\frac{\sigma_2}{F_{2\,is}^{tu}} + g\left(\frac{\sigma_2}{F_{2\,is}^{tu}}\right)^2 + \frac{\Lambda_{23}^0 {\tau_{23}}^2 + x(\gamma_{12})}{x(\gamma_{12|is})}$$

Eq. 2.13

$LaRC04$ #3: $Tensile\ fibre\ failure\ (\sigma_1 \geq 0)$

$$FI_F = \frac{\sigma_1}{F_1^{tu}}$$

Eq. 2.14

$LaRC04$ #2: $Matrix\ compressive\ failute\ (\sigma_1 \geq -F_2^{cu})$

$$FI_M = \left(\frac{\tau^T}{S^T - \eta^T \sigma_n}\right)^2 + \left(\frac{\tau^L}{S^L{}_{is} - \eta^T \sigma_n}\right)^2$$

Eq. 2.15

$LaRC04$ #5: $Matrix\ compressive\ failute\ (\sigma_1 < -F_2^{cu})$

$$FI_M = \left(\frac{\tau^{Tm}}{S^T - \eta^T \sigma_n^m}\right)^2 + \left(\frac{\tau^{Lm}}{S^L{}_{is} - \eta^L \sigma_n^m}\right)^2$$

Eq. 2.16

$LaRC04$ #4: $Fiber\ compressive\ failute\ (\sigma_{2m2m} < 0)$

$$FI_F = \left(\frac{\tau_{1m2m}}{S^L{}_{is} - \eta^L \sigma_{2m2m}}\right)^2$$

Eq. 2.17

$LaRC04$ #6: $Fiber\ compressive\ failute\ (\sigma_{2m2m} \geq 0)$

$$FI_{M/F} = (1-g)\frac{\sigma_{2m2m}}{F_{2\,is}^{tu}} + g\left(\frac{\sigma_{2m2m}}{F_{2\,is}^{tu}}\right)^2 + \frac{\Lambda_{23}^0 \tau_{2m3\psi}{}^2 + x(\gamma_{1m2m})}{x(\gamma_{12|is})}$$

Eq. 2.18

The meanings and relationships to determine the involved parameters can be found in reference [57]. There is a good correlation with experimental data for compression and shear combined loads, as shown on Figure 2.14. For longitudinal tensile quadrants it is identical to maximum stress criterion. Figure 2.15 shown a full failure envelope generated with LaRC04 criterion, indicating the specific equation applied for each load condition. It is remarkable the poor fit in the IV quadrant, considering the relative accuracy achieved by other load combinations.

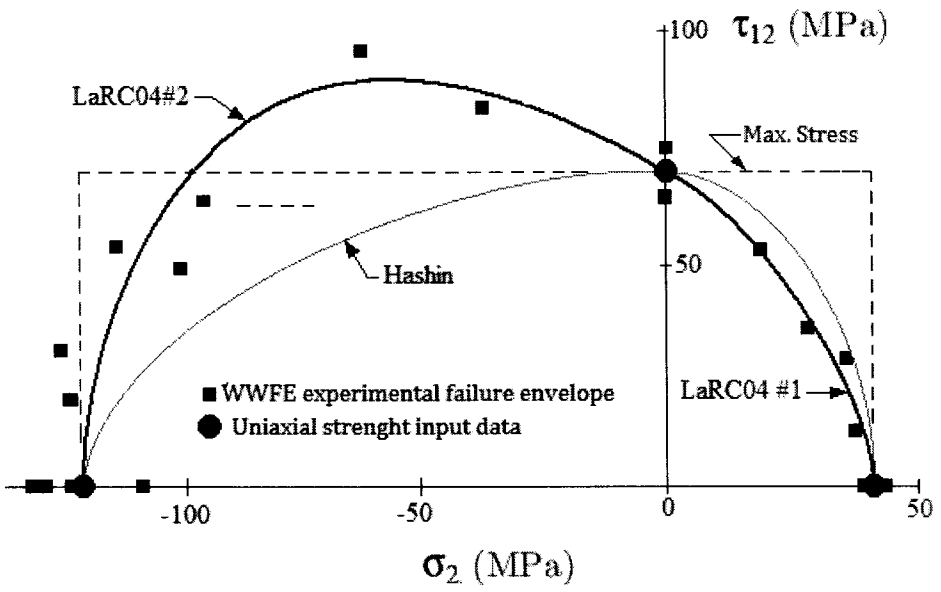

Figure 2.14: LaRC04, Hashin and Maximum Stress criteria predicted failure envelopes.

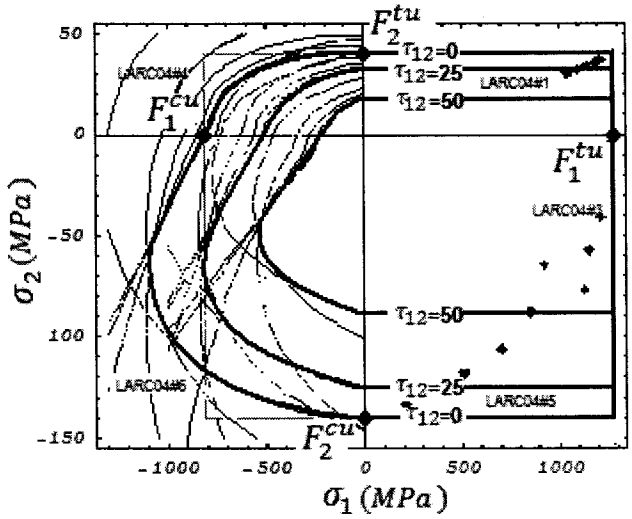

Figure 2.15: LaRC04 failure envelope

2.4.3. Micromechanics strength prediction

Micromechanical approaches are based on modelling separately the fibres and matrix of a composite to predict overall mechanical properties such as elastic modulus and strength; the simplest micromechanical models consider homogeneous, linear elastic,

perfectly aligned and isotropic fibres and matrix, with perfect (no voids or discontinuities) interfaces in-between; other complex models represent more realistic effects including voids, fibre-misalignments, fibre length variations, voids and interface strength. This can be approached in the following ways:

a). The mechanics of materials approach, which attempts to predict the behaviour of simplified models of the composite material. Best known approach is the rule of mixtures, which despite being a very simple model based on volumetric fibre to matrix ratio is capable to predict with reasonable accuracy the longitudinal elastic modulus of UDC, but fails on transverse modulus prediction because stress concentrations around the fibres generate a non homogeneous strain field which significantly affects the material behaviour in that direction; the model must be corrected using theory of elasticity, described next.

b). The theory of elasticity approach, which is often aimed at producing upper and lower bound exact analytical or numerical solutions. Best known example is the Eschelby equivalent homogeneous inclusion approach [32], which is based on analytical solutions of the stress/strain fields of coupled ellipsoid inclusion surrounded by a matrix deformation, which accurately predicts transverse properties of UDC; however, textile composites usually have much more complex microstructures which require a three-dimensional representation, thus analytical methods become inadequate; for this reason, the next micromechanical approach has been selected for this study.

c). The finite element (FE) approach: based on 2D or 3D FE modelling of composite micro-structure, depending of its complexity and required detail. FE models are especially suitable to study the strength of TC because of their complex entangled geometry [38],[40],[50], as illustrated on Figure 2.16. One of the most successful methods based on micromechanics approaches for TC is the so-called Multi-Continuum Theory (MCT), which in principle is capable of describing the multiple phases which co-exist within a single material point. As damage in composites typically begins at individual constituent level, MCT authors proposed that failure onset must be in fact limited to only one constituent, developing a combination of micromechanics and the classic strain decomposition approach of Hill [33], extracting constituent stresses from those acting on the composite.

Figure 2.16: FE strain distribution into a plain weave textile unit cell

The constituent stresses are then used as input of quadratic stress-interactive constituent-based failre criteria [50]. The result is a progressive, nonlinear analysis technique for the simulation of failure in composite structures [83].

Despite good results, the MTC and other micromechanics-based methodologies do not generate a typical failure criterion in the form of mathematical expressions which can be easily implemented as design tools. Also, analysis is time-costly.

2.4.4. Probabilistic criteria

Some authors have proposed probabilistic approaches to generate failure envelopes by using statistical methods for random functions based on experimental measurements. Although these criteria do not consider interactions of individual constituents, can they can generate complex envelope fails to fit well with experimental data. However, as in the case of parametric criteria, the expressions obtained cannot be extrapolated to different load conditions. An example of these criteria is the criterion of Kriging [55] which is based on a statistical technique for evaluating proposed natural resources.

2.5. Concluding Remarks

- Composite materials exhibit anisotropic behaviour due to complex architecture, and strength is highly dependent on the type of loads applied and corresponding failure modes. Despite the wide interest of TC for industry applications, most of the research efforts have been focussed on UDC, resulting in a large amount of failure theories developed for UDC (around 20, as inferred from the WWFE conclusions [70]), where best known theories are used indistinctly for UDC and TC. On Figure 2.10 most commonly used failure criteria are presented; it is remarkable that, in spite of significantly different predictions (see Figure 2.17), 80% of designers use Maximum Strain, Maximum Stress, Tsai-Hill and Tsai-Wu [37], used indistinctly for UDC or TC.

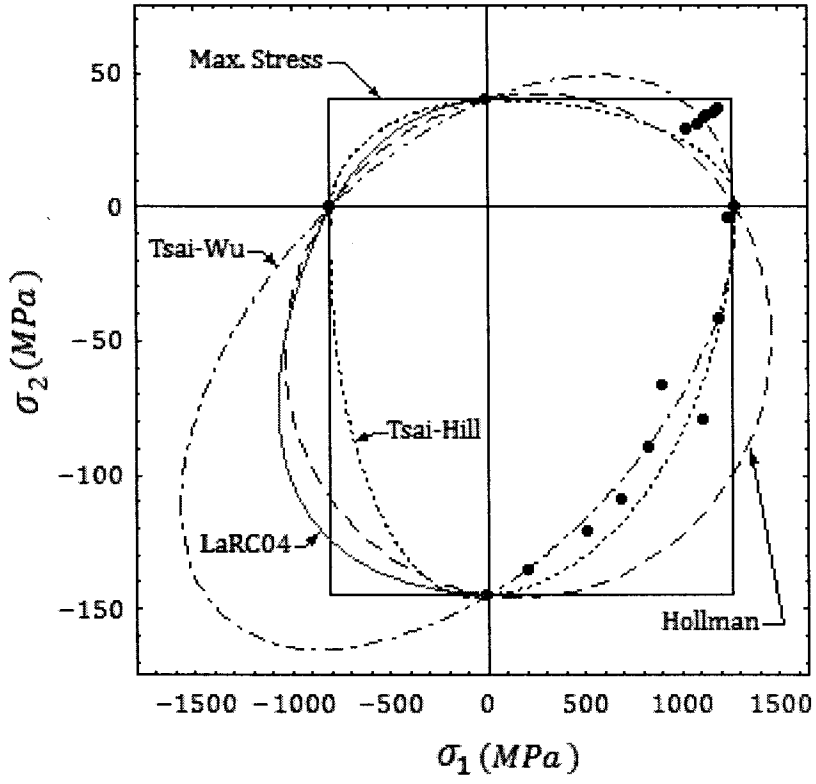

Figure 2.17: Failure criteria comparisson

- Despite their ample use, none of the aforementioned failure criteria has been developed specifically for TC, which has led to the use of high safety factors in critical structural applications to overcome associated uncertainties [44].
- The most successful approaches to predict TC strength are based on phenomenological modelling of interactions between constituents at different scales (matrix-yarn-fibre), providing new insight on TC failure mechanisms. However, implementation as design tool is considerably more complex than standard failure criteria, while still exhibiting significant deviation from experimental data [83].
- The most widely used failure criteria are presented in Figure 2.10; although not the most precise, simplicity is arguably the reason why they are preferred over more sophisticated models. This argument will be here considered for developing a dedicated TC failure criterion based on phenomenological considerations.
- After extensive review, a main obstacle for improving TC models identified was the scarcity of experimental data required to validate or reject new theories. Recent investigations reported biaxial tensile strength tests in 2D-triaxial TC employing tubular specimens, which suggested that the failure envelope predicted by the maximum strain criterion fits well the experimental data in the tension-tension (T-T) quadrant [74]. Other tests performed on cruciform specimens indicated that the maximum stress criterion is more adequate [83]; however, the authors of those researches expressed some concerns about the generality of the experimental methodology for non quasi-isotropic lay-up configurations, such as the one studied in this work.
- In view of the lack of consensus for accurate TC strength prediction [80],[82], and as stated by researchers who participated in the World Wide Failure Exercises (WWFE) [70] more experimental data, better testing methods and properly designed specimens are needed to generate reliable biaxial strength models.
- The aforementioned arguments provide motivation for this work, which aims to contribute on the TC tensile biaxial strength characterization and prediction state of the art.

Chapter 3.
Biaxial testing review

Combined multi-axial elastic and strength characterization of mechanical properties has become a necessity since composite materials emerged as cost-efficient alternative for structural applications; nonetheless, these are far from straightforward, requiring three basic elements: i). an apparatus capable of applying multi-axial loads, ii) a specimen capable of generating a homogeneous stress and strain field in a predefined gage zone, producing failure inside this zone for correct strength characterization, and iii) a measurement system capable of acquiring the applied loads and resulting specimen strains. Although these requirements are basically similar to those of uni-axial testing, they represent significant complications when applied for biaxial tests; the required equipment is scarce and costly, available only for some of the most advanced research centres. This limit advance of experimental characterization required to explode the full potential of composite materials.

Regarding specimens, the ability of generating a homogeneous multi-axial strain field inside a pre-specified gage zone is not straightforward mainly due to geometric stress concentrations. Moreover, the data acquisition system requires a free surface to take direct measurements. These factors limit in practice the number of combined loads that can be applied on a single specimen to only two, although some researchers have proposed apparatus designed to apply tri-axial loads although at the expense of limiting the access for full field strain measurements. Efforts on multi-axial testing had been disperse and rather unsuccessful in defining adequate methodologies, as evidenced by the lack of standardization by international organisms which have otherwise generated well known standards for uni-axial characterization of composites.

In the following there are listed some of the most commonly used standards relative to uni-axial characterization of uni-axial tensile properties of composites: ASTM D3039 (standard testing procedures for obtaining tensile properties of polymer matrix composites), British Standard: BS 2782: Part 3: Method 320A-F: Method for obtaining mechanical properties of plastics, BS EN ISO 527 Part 5: Plastics. Determination of tensile properties and test conditions for unidirectional fibre-reinforced plastic composites, CRAG (Composite Research Advisory Group) Test Methods for the Measurement of the Engineering Properties of Fibre Reinforced Plastics, Standard ASTM D6856: Testing procedures for textile composite materials, Japanese Industrial Standard JIS K7054: Tensile Test Method for Plastics Reinforced by Glass Fibre, Russian Standards GOST 25.601-80: Design Calculation and Strength Testing Methods of mechanical testing of polymeric composite materials. In brief, seven standards for tensile uni-axial characterization vs. none for bi-axial is a strong evidence about the need of enhancing current biaxial testing methodologies.

The objective of this chapter is to review the state of art related to the main elements required to perform multiaxial tests, whit emphasis on biaxial tensile specimens, testing machines and data measurement systems. The reasons for attend this particular case are:

- Complexity of testing systems arises considerably whit the number of independent loads which must apply. Due all the testing equipment and techniques must be developed during this research, biaxial tensile strength case was defined as feasible research topic.
- Most of the structural application of composites uses thin skins, resulting in shell structures, in which the laminates thickness are significantly lower than the other dimensions, which means that for compressive loads the buckling failure modes are the limiting factors [54]; then, the structural strength not depends on the material's strength but mainly on the geometry and stiffness; on the other hand, when tensile loads are applied to shell, the structures tends to be stable, and the final failure depends on the material's strength.
- To study interactions between failure modes is desirable to test pair of loads in order to facilitate the identification of their interactions.

3.1. Multiaxial specimens

To generate useful strength data, a biaxial specimen must be capable to meet the next requirements [19],[20],[22],[29]:

- A sufficiently wide homogeneous biaxially-stressed zone must be generated for strain measurements.
- Failure must occur within this zone.
- No spurious loads (other than tension/compression) should be acting on the gage specimen.
- The specimen should accept arbitrary biaxial load ratios.

The very design of specimens that recreate biaxially loaded components has become a constantly-evolving field, aiming to provide optimal geometry, manufacture and general arrangement for a valid and reliable test [65]. Specimens designed for biaxial testing can be identified in three main groups: i) tubes, ii) thin plates and iii) cruciforms. A review of these and their main features is next given:

3.1.1. Tubular specimens

Multiaxial stress states were formerly created with thin-walled tubes subjected to internal pressure, torsion and axial loads [19],[20],[68]. These specimens allow simultaneous application of tension/compression longitudinal and tangential and shear loads, becoming a versatile alternative to conduct multi-axial characterization (Figure 3.1).

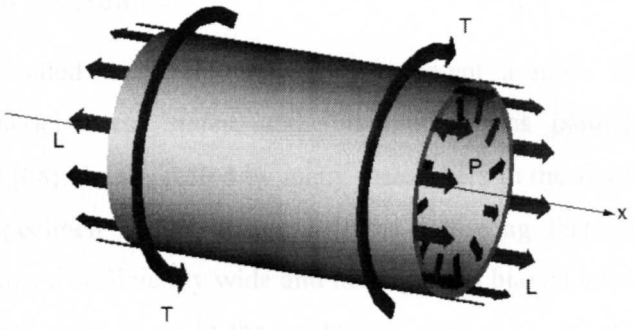

Figure 3.1: Thin-walled tube specimen.

However, the existence of stress gradients across the tubular wall makes this method less accurate than setups based on flat plates, which are also more representative of common industrial applications than the tubular geometry [1]. Some studies also reveal high stress concentrations on the gripping ends. A further disadvantage is a pressure leakage after the onset of matrix failure, although some correction can be provided by internal linings [68].

3.1.2. Thin plates

Round or elliptical flat sheets subject to pressure in the hydraulic bulge test [9], as shown in Figure 3.2, can develop a biaxial stress state, although the technique suffers several disadvantages, for example, non-homogeneous stress distributions induced by gripping of the edges [17]. Also, just like the rhomboidal plate case, the loading ratio is shape-dependant [10], thus it cannot be varied during the test to obtain a full characterization.

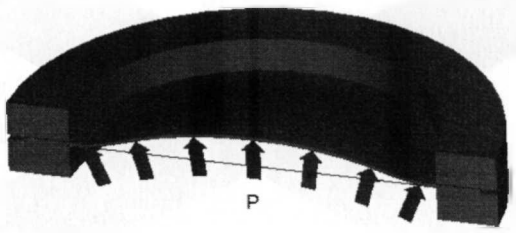

Figure 3.2: Elliptical flat sheet used in the bulge test.

3.1.3. Cruciform specimens

Testing biaxially-loaded cruciform specimens represent a more direct approach for obtaining true biaxial stress states, and this method has gained wide acceptance [80],[82],[19],[20],[68]. As suggested by many researchers in the field [80],[19],[29], an ideal cruciform specimen should accomplish the following features: *i*) It should be capable of generating a sufficiently wide and homogenous biaxial stress/strain field in the gage area, *ii*) failure must occur in the predefined gage zone, *iii*) the cruciform should accept arbitrary biaxial load ratios for generating a complete failure envelope (within a desired range), *iv*) both the tested and the reinforcement layers should be of the same

material, *v*) the transition between the gage zone and the reinforced regions should be gradual enough as to avoid undesirable high stress concentrations, *vi*) the cruciform fillet radius should be as small as possible for reducing stress coupling effects, and *vii*) stress measurements in the test area should be comparable to nominal values obtained by dividing each applied load by its corresponding cross-sectional area. Although various cruciform geometries containing a central-square thinned gage zone have been proposed in the literature, none can claim full satisfaction of the above requirements due to difficulties inherent to biaxial tests [19]. A cruciform with a thinned central region and a series of limbs separated by slots is presented in Figure 3.3 [52]; the slotted configuration allows greater deformations to occur in the thinned section, thus enforcing failure there. Nevertheless, thickness-change can induce undesirable stress concentrations that usually lead to premature failure outside the gage zone. Also, the extensive machining required for thinning is an undesirable feature.

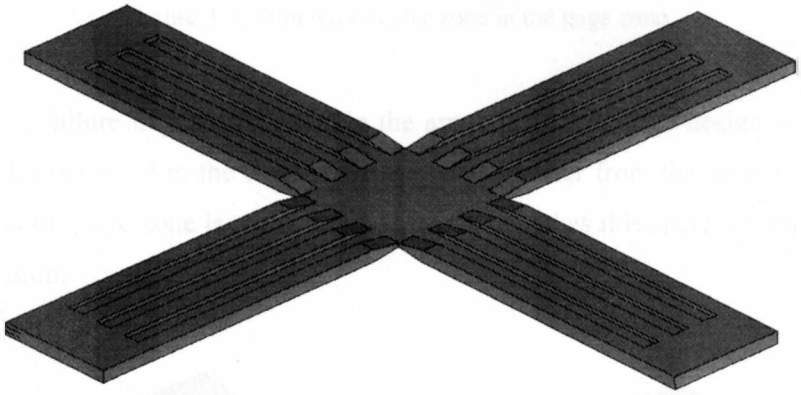

Figure 3.3: Slotted configuration [Ref].

Another cruciform with a thinned circular zone in the gage area [29] exhibit failure outside it, mainly because manufacture defects caused unexpected higher strength in one axis. The implementation of a rhomboidal shaped test zone is suggested in (Sacharuk), although, to this author knowledge, results were not reported. Some experiments concluded that loading must be orthogonal to the fibre orientation to produce failure in the test zone [22].

The main difficulty in obtaining an optimal configuration is eliminating stress concentrations in the arms joints. To solve this, an iterative optimization process (numerical/experimental) yielded optimum geometric parameters of the specimen [85]. Results from this study led to a configuration characterized by a thinned square test zone and filleted corners between arms.

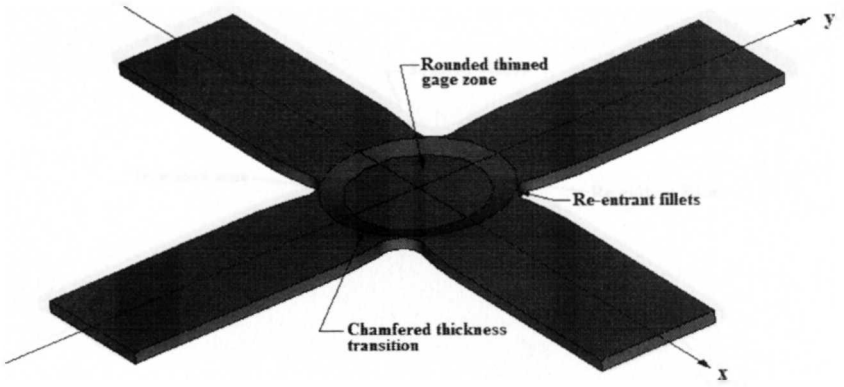

Figure 3.4: Thinned circular zone in the gage zone.

Given that failure is prone to occur in the arms, [3] presented a design where a small cruciform slot is placed in the centre to cause load transfer from the arms to this region. Nevertheless the gage zone is much reduced, and this makes this specimen useless for TC characterization.

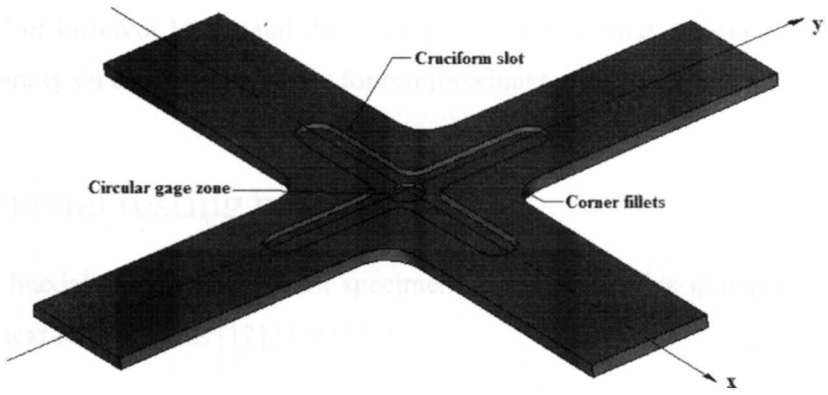

Figure 3.5: Inner cruciform slot.

In the cruciform proposed by Ebrahim et al [19] failure in the gage zone is achieved. The design is characterized by a thinned rounded square gage zone and considers a gradual thickness reduction in the biaxially loaded zone, and also filleted corners as shown in Figure 3.6. Results were satisfactory, but it was found that the top and bottom edges of the depression presented high strain gradients [3].

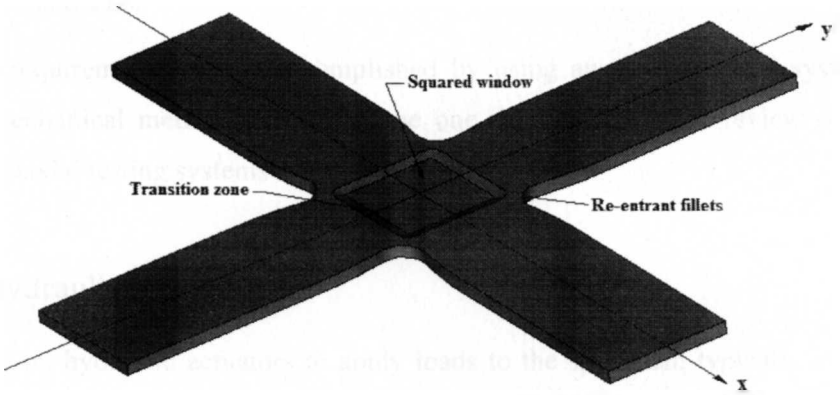

Figure 3.6: Cruciform with thinned rounded square gage zone and filleted corners.

Based on the aforementioned references, a parallel research carried out a comprehensive study aimed at obtaining an improved cruciform design. The rhomboid shaped gauge zone is improved yielding better results because of the alleviation of stress concentrations due to the short distance between the gauge zone and the corners of the arms which are filleted to avoid another zone of stress concentration. This specimen is comprised of different layers and the inner layer is under study, whereas the outer ones (equal quantity on each side) are only for reinforcement.

3.2. Biaxial testing machines

To apply biaxial loads on cruciform specimens a specific device is required, which can meet the next requirements [12],[13],[22],[23]:

- The loads applied to a cruciform specimen must be strictly in tension or compression, avoiding spurious shear or bending loads.

- The restriction previously stated implies that orthogonality among load axes must be guaranteed at all times during the test.
- The restriction previously stated implies, in turn, that the centre of the specimen must remain still or that the load axes must displace with it.
- An efficient method to ensure the previous condition is to apply equal displacements in the loaded axis.

These requirements can be accomplished by using an active control system, or by passive mechanical methods, such that the one described later. A review of the most common biaxial testing systems is presented next.

3.2.1. Hydraulic systems

Are based on hydraulic actuators to apply loads to the specimen; typically uses double-acting pistons with a closed-loop servo control system which sensing both, displacements and/or loads as feedback, as implemented in the design of Pascoe and de Villiers [56].

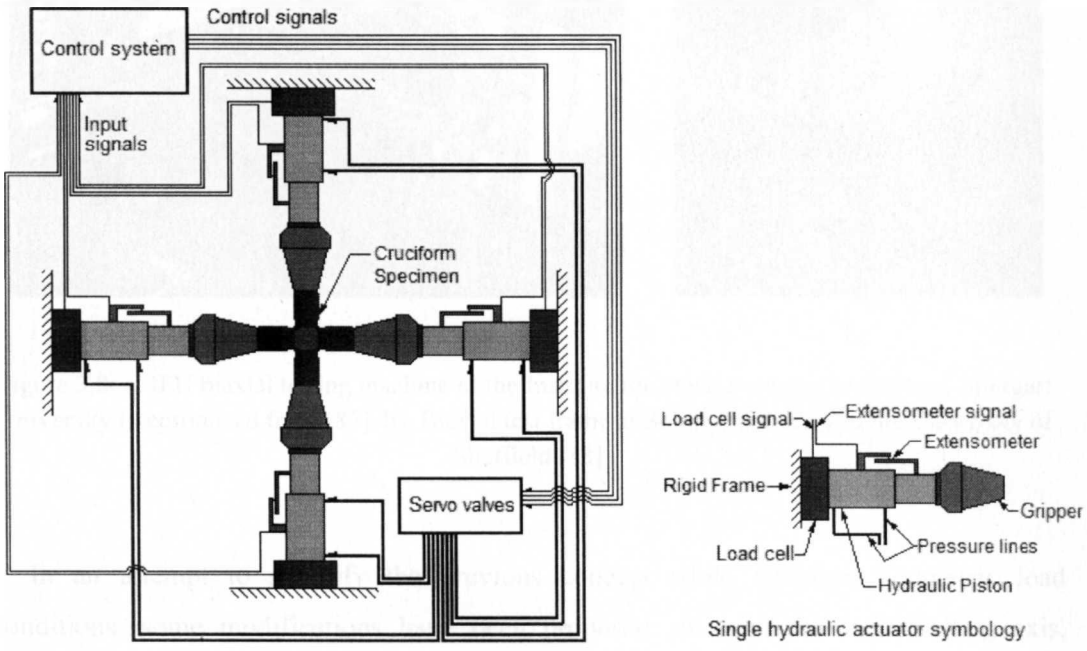

Figure 3.7: Use of independent actuator per load applied.

This configuration, which comprises the use of independent actuator per each applied load, which allows the centre of the specimen to move during the test, which is an undesirable condition; this adverse feature can be avoided by implementing a control system that ensures synchronization of opposite actuators [81[10] so there is no motion of the centre of the specimen. This configuration also permits load ratios can be varied to obtain a full failure envelope. None of these systems could ensure equal displacement in both extremes of each axis, even the one using synchronization control, therefore the centre of the specimen could move and, even though systems are implemented to counteract this problem, this increases the design costs. Fessler [25] proposed a machine in which motion is allowed only in one direction at one arm for each cruciform axis. This is the most common basic configuration found in the literature related to biaxial characterization of composites [48],[81].

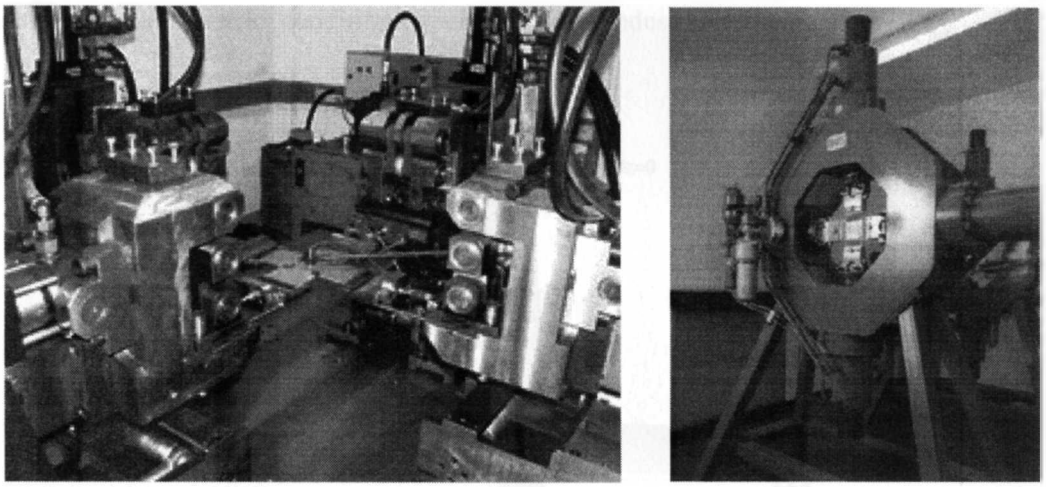

a. b.

Figure 3.8: a. IFU biaxial testing machine of the Institute for Metal Forming Technology Stuttgart University (Reproduced from [87]. b). Biaxial test frame at Solids Laboratory of the University of Sheffield [88]

In an attempt to simplify the previous concept while maintain symmetric load conditions, some modifications have been proposed; as example, each loading axis, consist of a pair of opposite hydraulic actuators, can be connected to a common hydraulic line so the force exerted by each side is the same and thus eliminates movements of the

centre of the specimen. Although the common hydraulic line ensures equal force in both extremes of one axis this system does not ensures equal displacements.

Another variation to hydraulic systems is described in the US Patent No. 5279166, which describes a biaxial testing machine consisting of two independently orthogonal loading axes capable of applying tension and/or compression loads; two ends of the specimen are gripped to fixed ends while the complementary ends are fixed to grips attached to actuators that apply the load, made in an attempt to reduce the complexity and hence the costs of biaxial testing machines. This configuration results in significant displacements of the centre of the specimen, although it is stated that the machine has a mechanism that helps maintain the centre of the specimen and the loads are always orthogonal despite this, under large displacements the mechanism used will not be capable of maintain the orthogonally of the loads as shown a quick finite element evaluation, whose results are shown in Figure 3.9; moreover, the resulting displacement field is completely asymmetric, condition which generates undesirable shear stress.

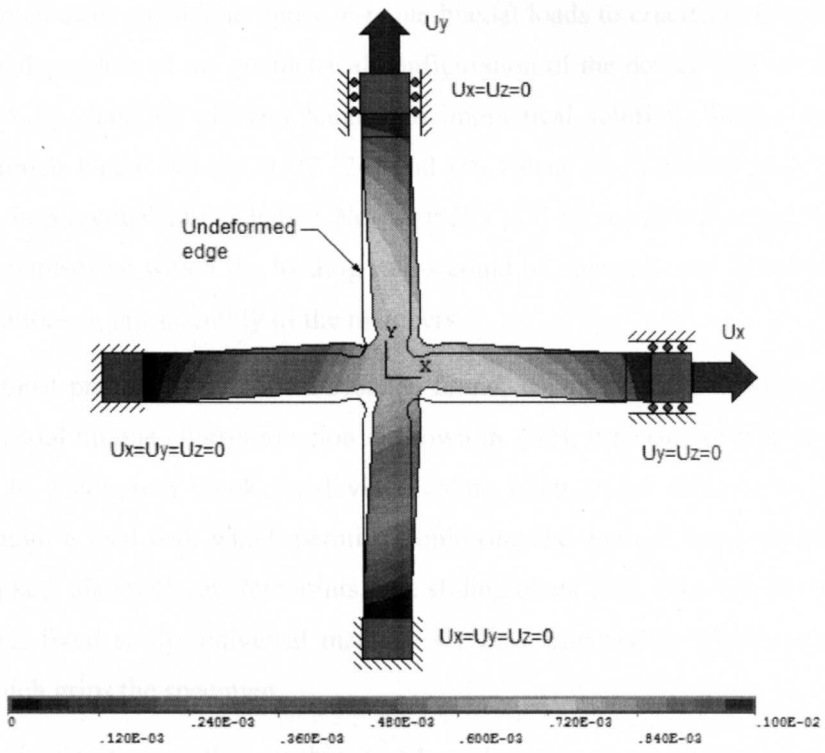

Figure 3.9: Qualitative contou plots of displacement vector magnitude result of one end of each axis fixed and other displaced.

Despite most of the biaxial testing hydraulic machines are original developments, a commercial biaxial testing machine has been developed by the enterprise MTS in conjunction with the NASA. It uses four independent hydraulic actuators, each with a load cell and hydraulic grippers, and an active alignment system for the specimen (MTS). Being this system created on a commercial scope, its cost is too high for entry-level composites development laboratories.

3.2.2. Mechanical systems

So called because they are based on the kinematics of it mechanisms to maintain the load symmetry, despite the actuators can be hydraulic or mechanic or even the application of deadweight to the specimen through systems of ropes, pulleys, levers and bearings, as presented by Hayhurst et al [31] . In the practice, the mechanical systems proposed for composite materials characterization are mainly test rigs designed to be adapted on conventional uniaxial testing machines; basically they are mechanisms consisting of coupled jointed-arms capable to apply in-plane biaxial loads to cruciform specimens. The load ratio is dependent of the geometrical configuration of the device [23] which permits to be varied by changing element length, an impractical solution. Similar devices are found in French Patent No. 2579327 [24] and US Patent No. 7204160 [64]. A simpler mechanism is presented in US Patent No. 5905205 [13] by using a four-bar rhomboidal shaped mechanism on which the loading ratios could be changed only before the test by certain variations in the assembly of the members.

One of most practical mechanical systems found, which has been used on polymeric materials biaxial fatigue characterization is shown in [42]; it consist of four arms, joined at on side to a common block fixed via revolute joints to an universal test machine actuator trough a load cell, which permits monitoring the applied force, while the other sides are linked, also with revolute joints, to a sliding block each; those blocks slides over an flat plate, fixed to the universal machine's frame. The sliding blocks assemble the grippers which grips the specimen.

After reviewing the existing machines and mechanisms on which biaxial tests can be carried out, some characteristics can be drawn; for some of them, the lack of a mechanism

that automatically counteracts any load difference that could lead to the displacement of the centre of the specimen makes them unsuitable to perform reliable tests with; or, in case there is such mechanism, it is controlled by means of an active system that increases design complexity and costs. Therefore, the design proposed later on this thesis contemplates these drawbacks, as well as testing requirements previously stated; in addition, construction costs are considerably low compared to other systems.

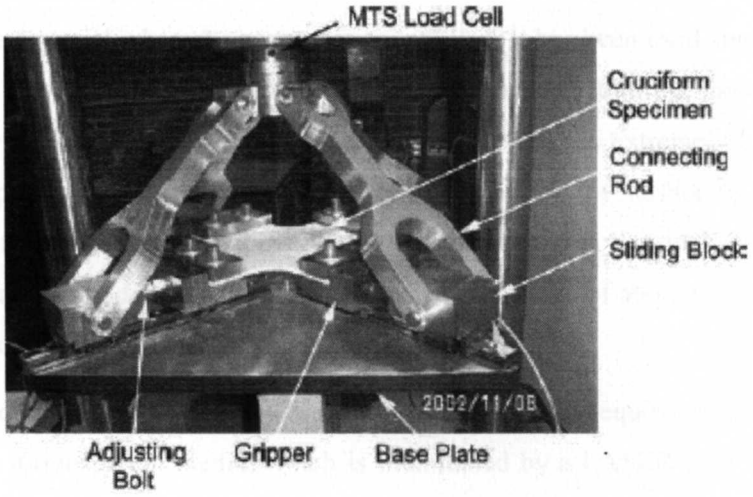

Figure 3.10: Test rig designed to be mounted on a universal testing machine, capable to apply equibiaxial loads to a cruciform specimen. Reproduced from [42].

3.3. Data acquisition techniques

Unlike uni-axial tensile tests in which ultimate failure stress and strains data can be straightforward reduced from the collected data, biaxial strength characterization using cruciform specimens data cannot be inferred from the typical load and extension applied to the specimen because corresponding fields are not homogeneous along the specimen due the complex geometry. For this reason biaxial testing requires a method capable to measure the full stain field into the biaxially loaded zone into the specimen. Due strain cannot be directly measured is necessary to measure the displacement field, from which the strain field can be easily calculated, and from this and through a constitutive model the stress can also be calculated. However, full field techniques are not standard data

acquisition methods and to identify the most suitable technique for this research a survey was realized.

3.3.1. Full field strain measurement methods

The first method considered was the reflective photo-elasticity: it is based on the birefringence, a physical property which consists on the change of the refraction coefficient of some material when shear stresses are applied. It has been used since 1950s decade [18], so is a well characterized technique. However, some limiting factors have been identified for this project: 1). the preparation of the samples is extremely laborious and requires the application of a layer of birefringent material on the surface to observe, with a thickness of about millimetres [18], which if compared with the thickness of the composite layer that is intended to characterize, having thicknesses of about 0.2-0.3mm is clearly that the measurement method affect significantly test results.

Another technique was considered Moiré interferometer. This requires to printing a pattern of lines on a transparent media, which is illuminated by a LASER source, which generates a interference pattern which depends of specimen deformation [59]. However, this method has the disadvantage that the data reduction process is tedious and complicated [28], and the results depend heavily on the analyst's experience.

After considering these options, a technique called digital image correlation (CDI) was identified from biaxial testing literature [19], [20], [43]. The basic concept is to obtain digital images of studied geometry on it initial, non-deformed state and after suffering a deformation. The surface of the part under study is pre-printed with a random speckle pattern, so that relative displacements between each points on photographs corresponding to non-deformed and deformed states can be identified by a computer algorithm. This method has some advantage over the aforementioned such as stated in [8]:

1). Simple experimental setup and specimen preparation: only one fixed CCD camera is needed to record the digital images of the test specimen surface before and after deformation.

2). Low requirements in measurement environment: 2D DIC does not require a laser source. A white light source or natural light can be used for illumination during loading. Thus, it is suitable for both laboratory and field applications.

3). Wide range of measurement sensitivity and resolution: Since the 2D DIC method deals with digital images, thus the digital images recorded by various highspatial-resolution digital image acquisition devices can be directly processed by the 2D DIC method.

So, it can be said that the 2D DIC method is one of the current most active optical measurement technologies, and demonstrates increasingly broad application prospects.

Nevertheless, the 2D DIC method also suffers some disadvantages:

1). The test planar object surface must have a random gray intensity distribution.

2). The measurements depend heavily on the quality of the imaging system.

3). At present, the strain measurement accuracy of the 2D DIC method is lower than that of interferometric techniques, and is not recommended as an effective tool for non-homogeneous small deformation measurement.

The low cost associated with equipment and specimen preparation makes the DIC technique despite its disadvantages, which can be avoided by 1). Develop a technique capable to be used as reference by the DIC program available, 2). to use the better high definition commercial camcorder available and 3). The designed specimen generates relative homogeneous strain field, and expected values cannot be considered as small, so the potential disadvantages of the method are not concern, and DIC was selected to be used as primary full field strain measurement technique.

3.4. Concluding Remarks

Literature review related to former multiaxial testing methodologies conducted to the following decisions respect to the specimen, test equipment and data acquiring technique to be developed and be used on this research:

- Cruciform specimens represent a straightforward and suitable approach to recreate biaxial tensile load state, reason because is going to be preferred over the other identified specimens on this review. Nevertheless, some mishaps have been identified on cruciforms, such as premature failures and fail to recreate true biaxial strain states; to overcome this problems, program oriented to enhance the cruciforms will be conducted prior any other activity, to ensure the feasibility of the proposed research.
- Commercial biaxial testing machines are based on hydraulic actuated and electronically controlled systems, which arises costs which exceeds the budget assigned to this research. On the other hand, other systems described on literature consists on mechanical rigs designed to be installed on universal testing machines, but these systems exhibit significant mishaps to be used on the experimental program; as part of this research, a mechanism driven biaxial test machine will be developed.
- The use of cruciforms specimens requires for full field strain method to identify the strain failure at the fail zone. Digital image correlation was identified as powerful, easy to implement full field strain measurement technique as compared with other comparable techniques, and it relative disadvantages are non-relevant for the experimental conditions expected on this research.

Chapter 4.
Objectives and scope of research

To exploit the full potential advantages of textile composite materials is fundamental to characterize it strength behavior. After the literature survey performed, important mishap on biaxial tensile experimental data, as well as a lack of experimental evidence required validating or proposing new failure models for textile composites have identified fields that requires research efforts. This work pretends to contribute on both areas by characterizing biaxial tensile strength of tensile composites. To make relevant contributions on this topic, the following objectives are pursued: 1). studying the former experimental methodologies to characterize the biaxial tensile strength on composites, adapting or enhancing it if necessary; 2). to generate experimental failure envelope data corresponding to such load condition and 3). Proposing a useful failure criteria based on the on the experimental data collected on the testing program. The following specific stages are performed:

1). Biaxial Testing Facilities Development

Due the lack of biaxial testing equipment, specimens and methodologies standardization, a program focused on developing the facilities and abilities required to conduct biaxial testing program is performed. The scope of work includes:

a. To research and select the specific type of biaxial test to implement. This includes the study of suitability of specimens employed for textile characterization. In case of be necessary, an adaptation of the specimens going to be realized.
b. Development of a biaxial test apparatus, based on an intensive investigation of other biaxial testing apparatus and on the specifications and features established as necessary or desirable for this and subsequent researches.

c. To conduct the design, testing and validation of an appropriate testing methodology. It includes all the significant aspects involved on the experimental procedure, such as the specimens manufacture, preparation and gripping, data acquisition systems settings, and data reduction methods.

2). Biaxial Characterization Program

The objective of this stage is to obtain an experimental failure envelope for the tension-tension quadrant, which provide evidence enough to understand the failure mechanisms involved on the final tensile biaxial strength of textile composites.

3). Phenomenological failure criterion

Based on results obtained in the characterization program, a failure criterion for the studied load condition will be proposed, preferentially based on phenomenological considerations and which takes the geometrical dimensions of the unit cell as input parameters.

Chapter 5.
Enhanced cruciform specimen

Biaxial stress states were formerly created with thin-walled tubes subjected to internal pressure and axial loads [19],[20],[68]. However, the existence of stress gradients across the tubular wall makes this method less accurate that setups based on flat plates, which are also more representative of common industrial applications than the tubular geometry [1]. A further disadvantage is a pressure leakage after the onset of matrix failure, although some correction of this effect can be provided by internal linings [68].

Testing biaxially-loaded cruciform specimens represents a more direct approach for obtaining true biaxial stress states, and this method has gained wide acceptance [80],[82],[19],[20],[68]; Figure 5.1 illustrates a typical cruciform specimen, illustrating the main geometric and material features.

As suggested by many researchers in the field [80],[19],[20],[29], an ideal cruciform specimen should accomplish the following features: *i*) It should be capable of generating a sufficiently wide and homogenous biaxial stress/strain field in the gauge area, *ii*) failure must occur in the predefined gauge zone, *iii*) the cruciform should accept arbitrary biaxial load ratios for generating a complete failure envelope (within a desired range), *iv*) both the tested and the reinforcement layers should be of the same material, *v*) the transition between the gauge zone and the reinforced regions should be gradual enough as to avoid undesirable high stress concentrations, *vi*) the cruciform fillet radius should be as small as possible for reducing stress coupling effects, and *vii*) stress measurements in the test area should be comparable to nominal values obtained via dividing each applied load by its corresponding cross-sectional area. Although various cruciform geometries containing a central-square thinned gauge zone have been proposed in the literature, none can claim full satisfaction of the above requirements due to difficulties inherent to biaxial tests [19].

The present research paid much attention to features *i)* to *v)*, while *vi)* and *vii)* were considered of lesser relevance as they are based on the assumption that the data reduction method consists on a stress calculation based on applied loads, later corrected with a by-pass factor [83]; instead, a digital image correlation (DIC) technique was used in this work, allowing a direct full strain field measurement just before final failure occurs.

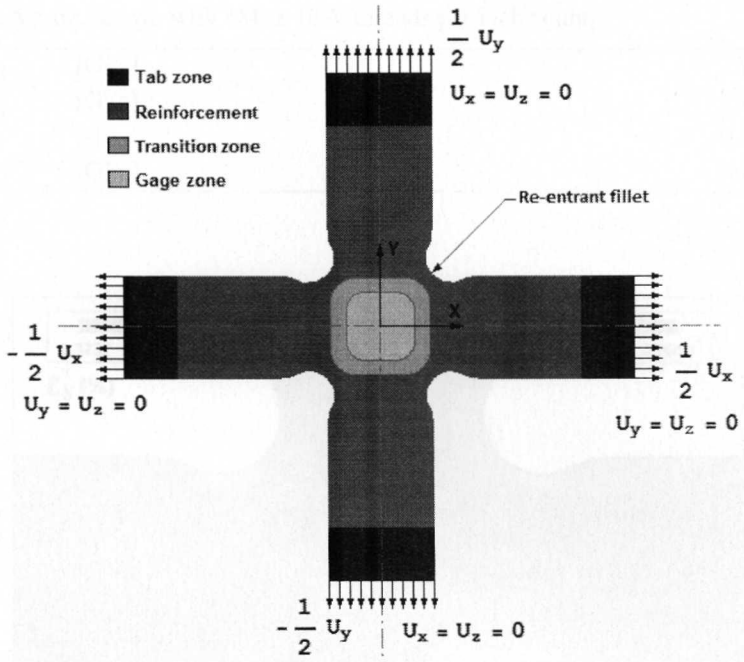

Figure 5.1: Typical cruciform specimen. Also shown are the boundary conditions imposed on all FE cruciform's models analyzed in this paper.

5.1. Reference cruciform

For comparison purposes, a well-known cruciform specimen having a square-windowed thinned gauge zone [19], here called Model 1, was taken as a reference design and analyzed via a linear Finite Element (FE) model. The boundary conditions were parametrically defined as shown in Figure 5.1 with U_x and U_y chosen to produce a maximum strain (ε_x or ε_y) of 2% inside the gauge zone, corresponding to typical failure strain values reported for glass-epoxy TC [83]; identical BC were applied for all subsequent analyses. The material properties correspond to a generic plain weave bidirectional textile, as presented in Table 5.1. Results of the analysis are shown in Figure 5.2 which splits the geometry into top and bottom sections for simultaneously illustrating

the ε_x and γ_x strain fields, respectively, in a single graph; due to full symmetry, the ε_y strain field is identical to the ε_x field when rotated by 90°.

Table 5.1. In-plane mechanical properties for a TC conformed of: Epoxy West System 105/206 reinforced with fibreglass cloth style #7520, bidirectional plain weave 8.5 oz./sq. yd, with 18L x 18W threads per inch count.

E_{11}	[GPa]	25.0
E_{22}	[GPa]	25.0
v_{12}	[-]	0.2
G_{12}	[GPa]	4.0

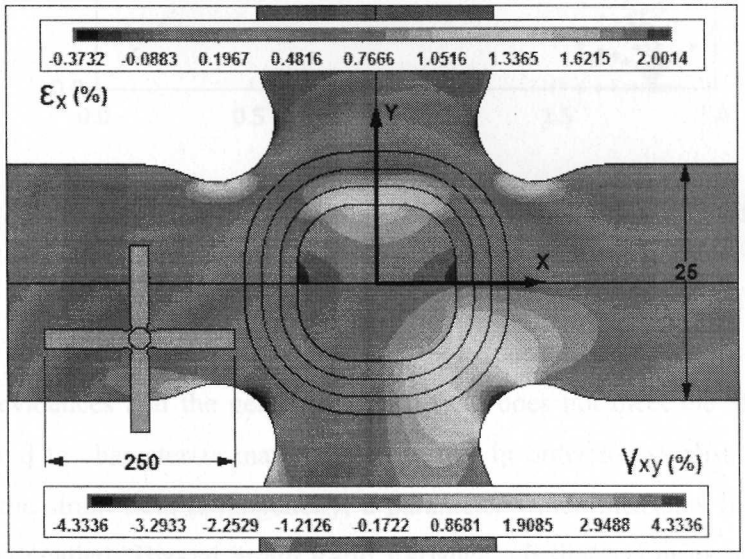

Figure 5.2. Strain fields of the reference cruciform (Model 1) obtained via linear FE analysis. Top and bottom sections represent, respectively, εx and γxy strain fields. Length dimension is given in mm, other dimensions and layup are described in [19].

An ideal biaxial specimen subject to 1:1 imposed displacements would exhibit $\varepsilon_x=\varepsilon_y$ as well as $\gamma_{xy}=0$ in most of the gauge zone, thus deviations from this condition can be taken as a measure of the specimen's ability to generate a true biaxial load state. To objectively evaluate the reference specimen, ε_y vs. ε_x and γ_{xy} vs. ε_x nodal values inside the gauge zone were plotted in Figure 5.3.

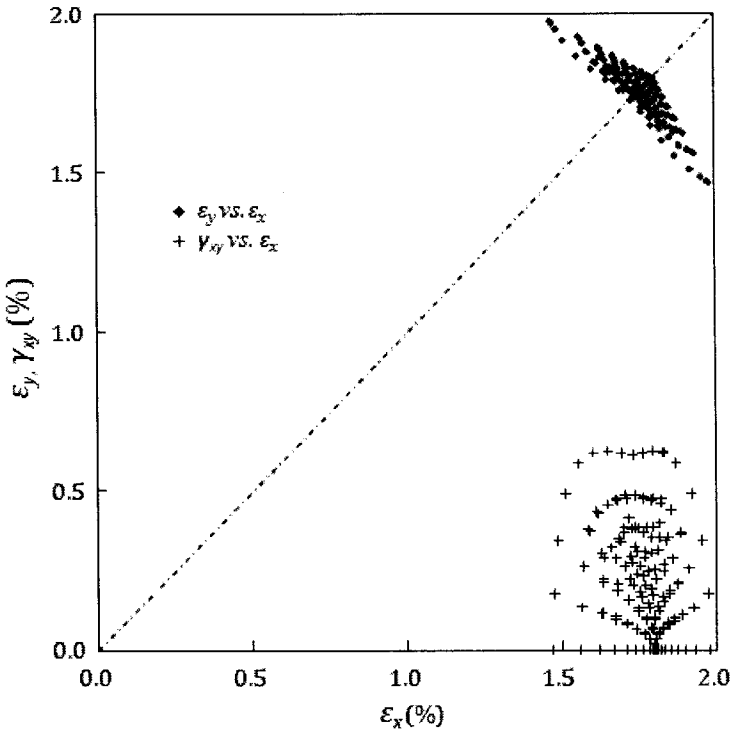

Figure 5.3. Gauge zone nodal strains εy vs. εx (*) and γxy vs. εx (+) corresponding to the reference cruciform (Model 1) for equi-biaxial imposed displacements Ux=Uy=0.9mm.

Both data clouds deviate significantly from the expected homogeneous biaxial strain state, which evidences that the generated strain field does not meet the aforementioned criteria required to characterize material's strength. In order to establish a quantitative criterion for the strain field homogeneity, a parameter which measures the biaxial ratio dispersion, here called "Biaxial Strain Ratio Variance" (BSRV), is proposed and defined as follows:

$$BSRV = \frac{1}{n}\sum_{1=1}^{n}(BR_i - \overline{BR})^2 \qquad \textit{Eq. 5.1}$$

where n is the number of nodal measurements i=1..n, and $\overline{BR}$ is the mean value of all measurements BR_i, each defined by:

$$BR_i = \frac{\varepsilon_{x_i}}{\varepsilon_{y_i}} \qquad \textit{Eq. 5.2}$$

To monitoring the shear strain dispersion inside the gauge zone in a similar manner as with the BSRV, a parameter called "Shear strain to Y strain Ratio Variance" (SYRV) is defined as follows:

$$SYRV = \frac{1}{n}\sum_{1=1}^{n}(SR_i - \overline{SR})^2 \qquad \textit{Eq. 5.3}$$

Where shear to y strain ratio SR is defined as:

$$SR_i = \frac{\gamma_{xy_i}}{\varepsilon_{y_i}} \qquad \textit{Eq. 5.4}$$

Both BSRV and SYRV values calculated for Model 1 are presented in Table 5.2

Table 5.2. BSRV, SXRV and maximum γ_{xy} (%) for Models 1 and 2.

	BSRV [-]	SXRV[-]	γ_{xy} max [%]
Model 1 (Figs. 2 & 3)	0.01476	0.04898	4.333
Model 2 (Figs. 4 & 5)	0.01359	0.01446	4.354

5.2. Proposed cruciform specimen

Based on previous results, and in an attempt to improve the strain distribution generated by this cruciform specimen, some modifications are proposed in this work:

a) Given that fillets are prime examples of stress concentrators, both the cruciform's and gauge zone's fillets should be as far apart as possible from each other, thus favouring a rhomboid-windowed gauge zone. This modification also intends to minimize regions of stress interactions, which cause lack of homogeneity in the strain field and even premature failure, as reported for some square-windowed specimens [2]. Traditional (instead of re-entrant) fillets were preferred to maintain this stress concentrator as separated as possible from the gauge zone.

b) Because the focus of this research are TC, the proposed specimen, labelled Model 2 from here onwards, also features wider arms and a larger gauge zone, seeking to reduce the textile unit cell vs. gauge zone length ratio. This modification is in tune with ASTM standards on testing procedures for textile composites [6].

c) To avoid polluting the obtained strength data with in-situ effects, adhesion between adjacent layers and other multilayer-related uncertainties, characterization is sought for a single-layer central gauge zone, while a number of reinforcement layers are added outside the gauge zone to enforce failure inside it. The resulting rhomboid windowed cruciform shape was similar to other specimens employed for fatigue characterization of ABS plastic, which report a smooth biaxial strain field at the gauge zone [42]. Basic dimensions were selected from a specimen reported in literature [27]: arm width = 50mm (twice than that of Model 1), and cruciform fillets R=25mm. The rhomboid window length l was set identical to the arm width, while the window's fillet radius r was set as 10% of l; the geometry is sketched in Figure 5.4. The lay-up consists of a single flat central layer (containing the gauge zone) with two reinforcement rhomboid-windowed layers at each side; the latter configuration was chosen after extensive simulation, yielding a relatively homogeneous strain field while maintaining the shear strain at cruciform fillets below the failure values. Due to the difficulty in generating a geometrically smooth transition between the gauge and reinforced zones in the real specimen without incurring in test layer damage, this feature was omitted.

To test these design concepts, a FE analysis was conducted on Model 2; strain results are shown in Figure 5.4 in the same partitioned fashion as in Figure 5.2 and with BC imposed as in Figure 5.1; the gauge zone's nodal strain values ε_y vs. ε_x and γ_{xy} vs. ε_x are shown in Figure 5.5. Compared to the reference specimen (Model 1), Model 2 generates a more uniform strain distribution, as suggested by the lower BRSV value obtained (see Table 5.2) while the maximum shear strain in the cruciform fillet remains similar for both models. Shear strain nodal values inside the gauge zone are smaller and less dispersed in Model 2 as confirmed by the lower corresponding SYRV value.

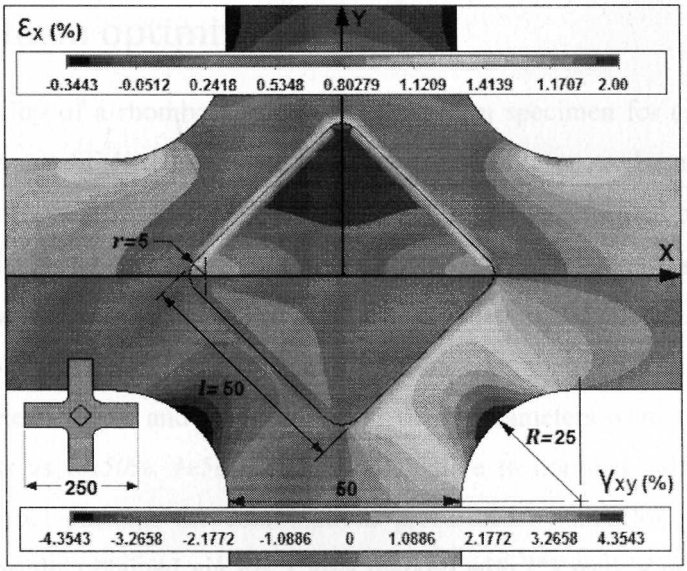

Figure 5.4. Model 2's FE strain field. Lay up for the reinforcement region is $[0]_5$, while for the gauge zone is [0] (that is, a single layer). All dimensions are given in mm.

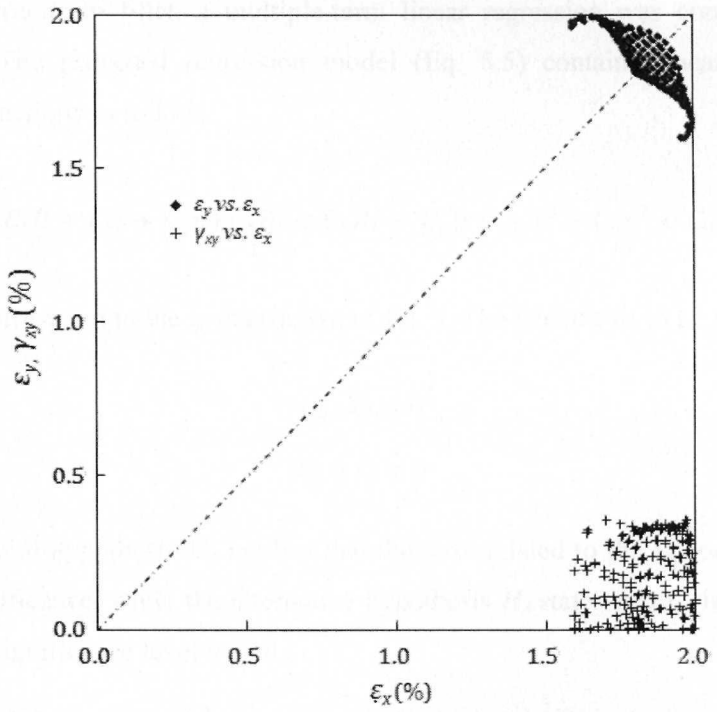

Figure 5.5. Gauge zone nodal strains ε_y vs. ε_x and γ_{xy} vs. ε_x corresponding to the proposed specimen (Model 2) for equi-biaxial imposed BC Ux=Uy=1.4838mm.

5.3. Cruciform optimization

Once the suitability of a rhomboid windowed cruciform specimen for creating a biaxial strain state was established, a geometrical optimization process based on design of experiments (DoE) was conducted. A set of simulations was performed based on a three-level full factorial surface response, where the BSRV and the maximum shear strain γ_{xy} at the arm fillets were taken, for all cases, as objective function and constraint, respectively, while l (rhomboid's side length), R (arm's fillet) and r (rhomboid's fillet) were designated variable parameters. Upper and lower limits for these parameters were selected based on preliminary tests as $R\pm50\%$, $l\pm50\%$ and $2r\pm r$, relative to nominal values employed in Model 2. Table 5.3 presents the combinations prescribed by the DoE, as well as their corresponding results obtained via FE. Cases marked with (*) were a priori neglected as they fall outside feasible design regions.

In order to determine how the different geometrical parameters affect the maximum γ_{xy} value at the cruciform fillet, a multiple-term linear regression was conducted for the response γ_{xy}. The proposed regression model (Eq. 5.5) contains linear, bilinear and quadratic interactions as follows:

$$\gamma_{xy} = C_0 + C_1R + C_2l + C_3r + C_4Rl + C_5Rr + C_6lr + C_7R^2 + C_8r^2 + C_9l^2 \qquad \textit{Eq. 5.5}$$

where C_i correspond to the i_{th} coefficient of Eq. 5. The hypothesis to be tested is:

$$H_0 : C_i = 0$$
$$H_A : C_i \neq 0 \qquad \textit{Eq. 5.6}$$

where the null hypothesis H_0 implies that the term related to the i_{th} coefficient has no statistical significance, while the alternative hypothesis H_A states that C_i is different from zero within a significance level α=0.05.

Several iterations were made in order to identify and eliminate the non-statistically significant factors; the results for the last iteration are shown in Table 5.4, which reveals that only the l and R factors were significant, given that the corresponding p value ($p \leq \alpha$) allows rejecting H_0.

Table 5.3. Factor levels defined for the DoE.

	R [m]	l [m]	r [% of l]	BSRV [-]	SXRV [-]	γxy [%]
1*	0.010	0.03	10	0.13732	0.06523	3.507
2	0.040	0.03	10	0.07765	0.04517	2.134
3	0.010	0.03	30	0.02331	0.02170	4.753
4	0.040	0.03	30	0.01023	0.01041	2.867
5*	0.010	0.07	10	1.70386	0.06645	8.024
6	0.040	0.07	10	0.05847	0.02353	3.970
7*	0.010	0.07	30	0.56771	0.15030	7.013
8	0.040	0.07	30	0.12431	0.08971	3.663
9	0.010	0.05	20	0.02133	0.03002	6.391
10	0.040	0.05	20	0.00103	0.00181	3.571
11	0.025	0.05	10	0.01359	0.01446	4.354
12	0.025	0.05	30	0.00246	0.00347	4.333
13	0.025	0.03	20	0.03981	0.03285	2.869
14*	0.025	0.07	20	0.13194	0.03322	4.936
15	0.025	0.05	20	0.00352	0.00586	4.467

Graphical results for the correlation are shown in Figure 5.6 as a contour map of γ_{xy} plotted into an l vs. R space. The feasible design region lies below the dark line, corresponding to combinations of R and l such that $\gamma_{xy} \leq 4\%$. This limit is equivalent to the shear strain failure reported for epoxy-glass TC [35], here defined as a restriction for the optimization process. A similar regression was conducted for the BSRV parameter; results for the last iteration are shown in Table 5.5. In this case, the coefficients of R, r, l, rl and l^2 were identified as significant ($p<0.05$). Values marked with (*) in Table 3 were neglected as all of them lie outside the feasible design region ($\gamma_{xy} \leq 4\%$). Plots were generated to analyze the BSRV behaviour against parameters R, r and l, as shown in Figure 5.7.

Table 5.4. Linear regression results for $\boldsymbol{\gamma_{xy} = C_0 + C_1 R + C_2 l}$.; $\alpha=0.05$; $R^2_{adj}=0.737$.

	Coef	SE Coef	T	P
$\boldsymbol{C_0}$	0.03875	0.00549	7.054	0
$\boldsymbol{C_1}$	-0.73721	0.14050	-5.247	0
$\boldsymbol{C_2}$	0.45256	0.10538	4.295	0.002

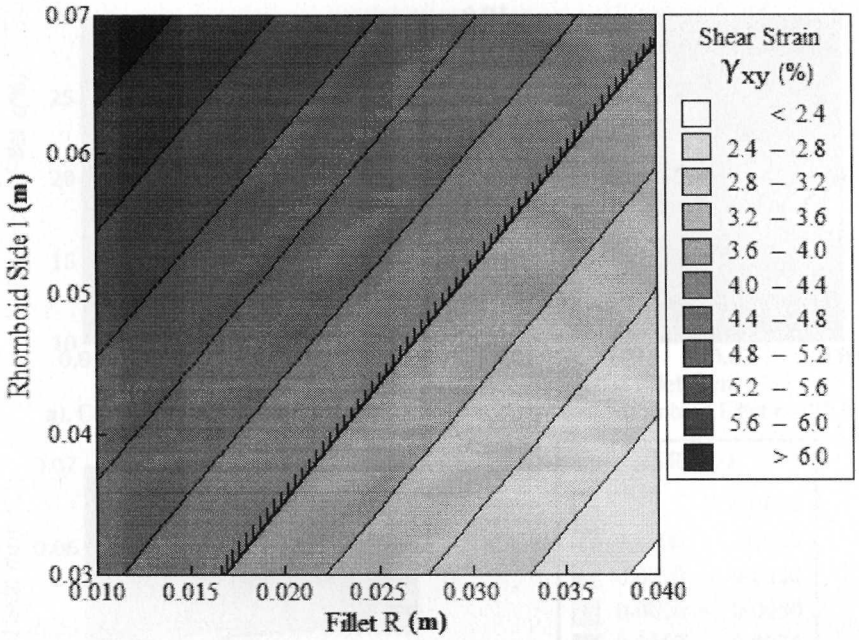

Figure 5.6. Response surface for the maximum shear strain γ_{xy} at the cruciform fillet vs. l and R parameters.

The feasible design region defined by the restriction $\gamma_{xy} \leq 4\%$ is graphically represented on the contour plots. Since the correlation predicts negative values for some regions, the condition BSRV>0 has been used as an additional restriction, graphically represented as another black line in the graphs. Contours plotted in the r vs. R space (Figure 5.7a) demonstrate that the parameter r has relatively little influence on the BSRV value. On the other hand, BSRV varies inversely with the cruciform fillet radius R, reaching a local minimum at R=0.04m for $0.42 \leq l \leq 0.5$ (Figure 5.7b).

Table 5.5. Regression results for $\gamma_{xy} = C_0 + C_1R + C_2l + C_3r + C_6lr + C_9l^2$; α=0.05; R^2_{adj}=0.975

	Value	Standard error	T	P
C_0	0.534	0.0339	15.762	0
C_1	-0.516	0.1976	-2.614	0.047
C_2	-18.355	1.1346	-16.177	0
C_3	-0.008	0.0007	-11.191	0
C_6	0.164	0.0146	11.262	0
C_9	163.395	10.8015	15.127	0

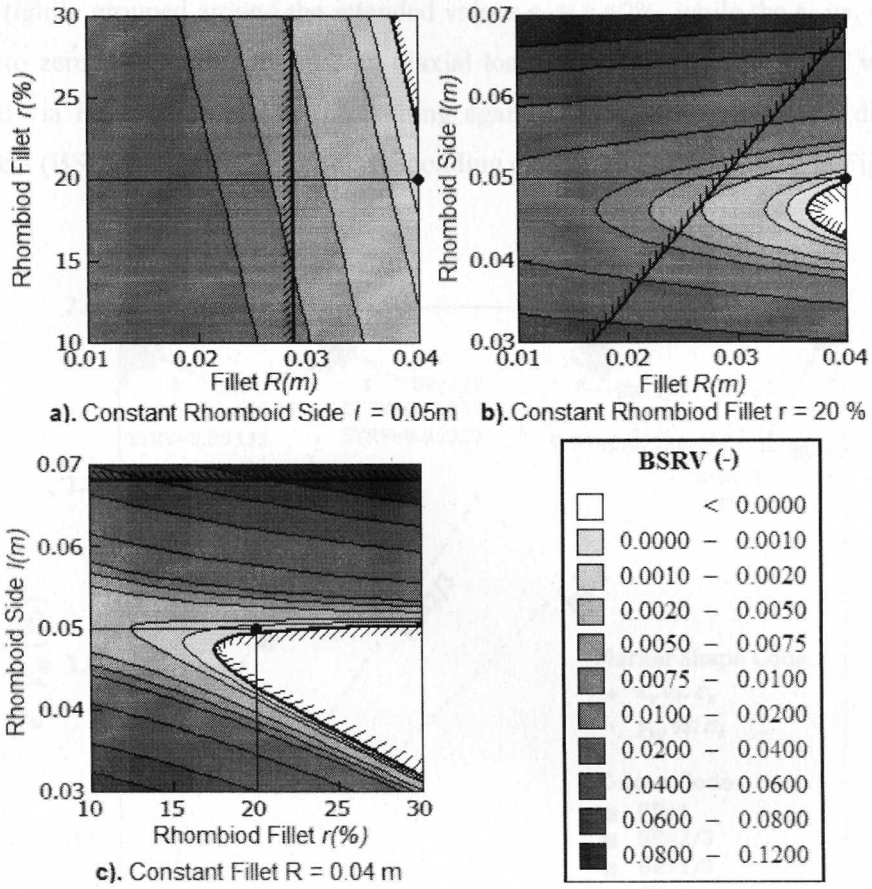

Figure 5.7. BSRV response surface vs: a) rhomboid fillet r and cruciform fillet R, b) rhomboid side l and cruciform fillet R, and c) rhomboid side l and rhomboid fillet r parameters.

BRSV values mapped into l vs. r space (Figure 5.7c) reveal an ample zone with low BSRV values, limited by l~0.05m. Since the condition BSRV≥0 excludes a certain portion of the l vs. r space, the requirement of a maximum gauge area (implying an R value as large as possible) was imposed as an additional constraint. Based on the above considerations, the following values were selected: R=0.04m, r=20% and l=0.05m, shown as black dots in Figure 5.7 a, b and c. The cruciform geometry resulting from the optimization process (Model 3, from here onwards) generates a significantly more homogeneous strain field than Models 1 and 2 (Table 2), as inferred from the FE calculated BSRV and SYRV values (BSRV=0.00103 and SYRV=0.00181). This is illustrated in Figure 5.8 where the nodal strain data cloud for BR=1 corresponding to ε_y

vs. ε_x is tightly grouped around the intended values $\varepsilon_x = \varepsilon_y$=2%, while the ε_y vs. γ_{xy} cloud is close to zero, as required by an equi-biaxial load state. Other biaxial ratios were also modelled via FE (BR=2/3, 1/3, 0), resulting again in lower values for both dispersion parameters (BSRV and SYRV); the corresponding clouds are also presented in Figure 5.8.

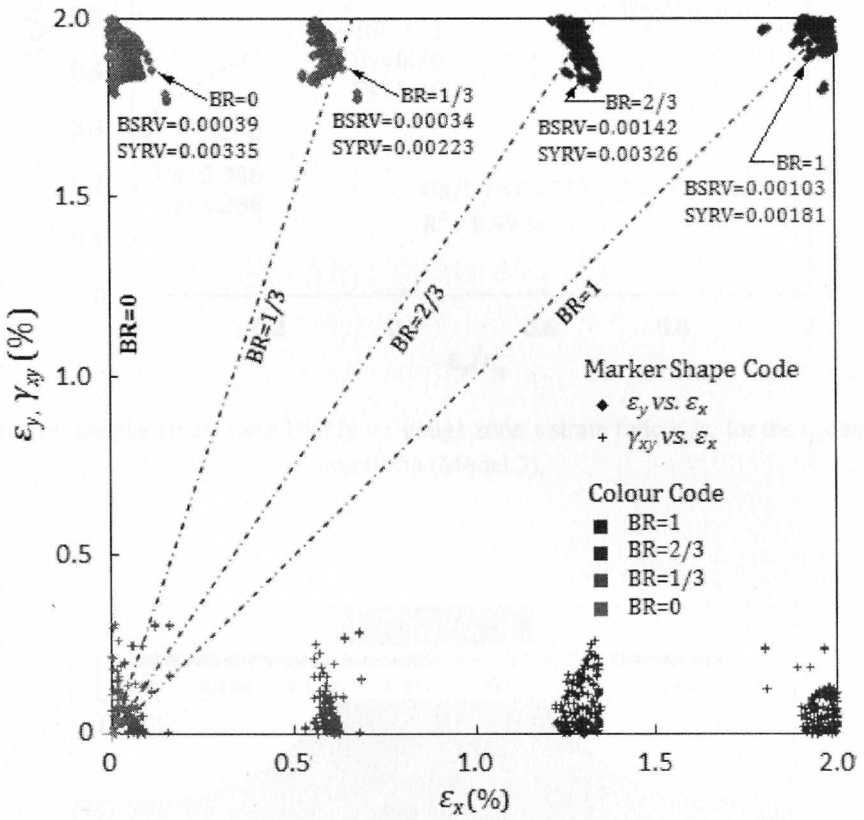

Figure 5.8. Optimized Model 3's FE nodal strain values inside the gauge zone corresponding to four different biaxial ratios BR.

The displacement ratio U_x/U_y varies nearly linearly with the intended BR values, as shown in Figure 5.9; remarkably, a strain ratio $\varepsilon_x/\varepsilon_y$=0 requires U_x/U_y=0.3 to overcome the transversal contraction due to material and specimen induced Poisson effect. Both characteristics, lower BSRV dispersion under any imposed BR and easy boundary conditions setting make Model 3 a very suitable choice to conduct full T-T failure envelope characterization.

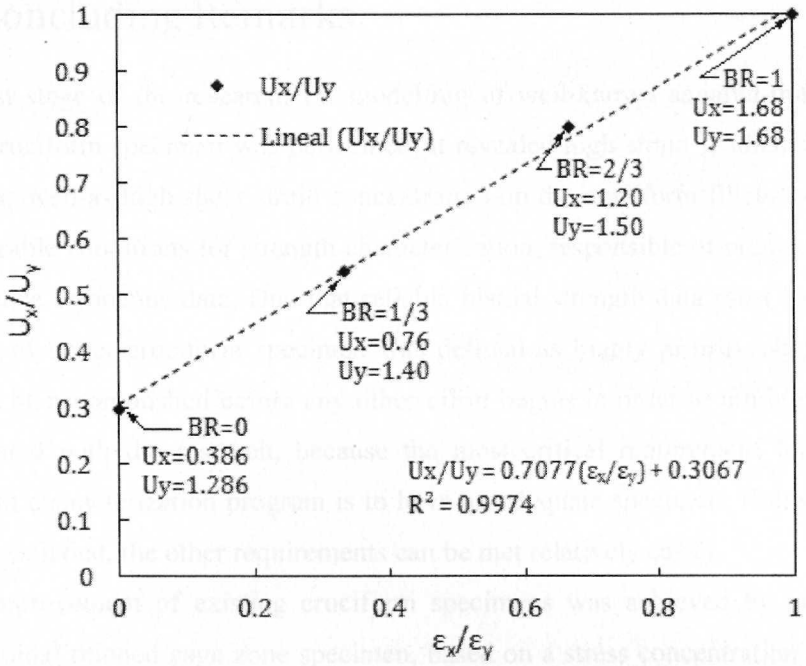

Figure 5.9. Displacement ratio Ux/Uy vs. gauge zone´s strain ratio $\varepsilon_x/\varepsilon_y$ for the optimized cruciform (Model 3).

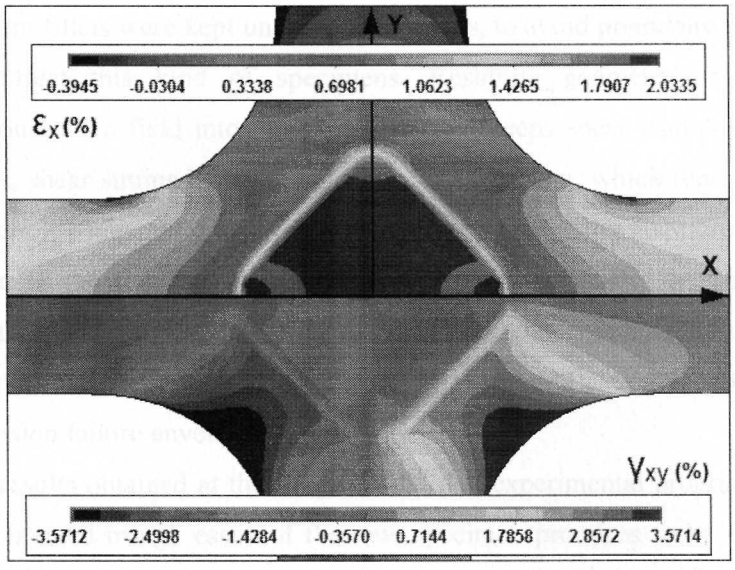

Figure 5.10. Displacement ratio Ux/Uy vs. gauge zone´s strain ratio $\varepsilon_x/\varepsilon_y$ for the optimized cruciform (Model 3).

5.4. Concluding Remarks

- As first stage of the research, FE modelling of well-known squared-thinned gage zone cruciform specimen was performed; it revealed high strain gradients into gage zone, as well as high shear strain concentration on the cruciform fillets, both highly undesirable conditions for strength characterization, responsible of premature failure and hence erroneous data. Due that reliable biaxial strength data must be obtained, design of better cruciform specimen was defined as highly priority objective, and should be accomplished before any other effort begins in order to minimize the risk associated with the research, because the most critical requirement for a biaxial strength characterization program is to have an adequate specimen; if this condition can be satisfied, the other requirements can be met relatively easily.
- The improvement of existing cruciform specimens was achieved by proposing a rhomboidal thinned gage zone specimen, based on a stress concentration qualitative analysis. FE analysis was conducted on the new geometry, which demonstrated the good characteristics if compared with the reference model. Then, an optimization based on design of experiments techniques were performed to achieve a highly homogeneous strain distribution into the rhomboidal gage zone while shear strains in the cruciform fillets were kept under failure values, to avoid premature failure which typically affect this kind of specimens. Resulting geometry generates very homogeneous strain field into the gage zone and keeps shear strains near to zero, while keeps shear strains in fillets below the failure value, which represents a great improvement if compared with other specimens reported in the literature.
- In addition to meeting the requirements for equibiaxial tests, the specimen was evaluated under various biaxial ratios, demonstrating that is practically insensitive to biaxial ratio, and hence can be used without any modification to obtain the full tension-tension failure envelope.
- Excellent results obtained at this stage ensure that experimental program is feasible and data obtained trough essay of the new specimen promises to be more reliable than these available in the literature. The next step consists on develop the biaxial testing apparatus capable to apply controlled loads to the cruciform.

Chapter 6.
Biaxial testing machine development

6.1. Biaxial testing machine specifications

As resulted from the literature review of biaxial testing devices, a set of requirements that must be met by an apparatus used impose biaxial tensile loads on the cruciform specimen were defined as follows: i). every axial load should be able to be controlled independently in order to test different biaxial load ratios, ii). the movement in the grips of each axis must be applied symmetrically, iii). it must ensure a free visual field in order to permit to make digital photographs of the specimen while the testing is running and iv). the mechanism must be able to absorb small misalignments in the charges to avoid the presence of spurious loads (torsion, shear and bending). Considering these requirements, an evaluation of biaxial testing commercial systems available in the market was conducted. Two commercial machines were identified, both operated by separate hydraulic actuators controlled electronically to ensure that the conditions i-iv were satisfied. Nevertheless, the inherent complexity of these systems and the lack of significant market demand are factors that influence the high costs of these devices, which rounds a million of dollars that is absolutely out of budget available for this research. Alternatives to these complex systems reported in the literature rely on the use of articulated mechanisms to be mounted on universal machines [Ref], but they fail to satisfy requirement i).

As result of these mishaps in the required equipment, design and construction of comparative low-cost biaxial testing machine based in mechanisms was identified as an excellent opportunity to contribute on the experimental effort to characterize composites materials.

6.2. Biaxial testing machine

The first machine's design by the ITESM's composites research team, in addition to the specifications initially defined, also should met the ability to perform fatigue tests. To permit this, the mechanisms should be capable to precisely revert it load direction, minimizing the backlash. With this extra requirement, a system based on power screw to apply loads were proposed; this system ensures the symmetry of loads application on every axis, while each independent axis shall be floating a rail system which permits a self-alignment operation; a cycloid reduction system was conceived to convert the relative low torque-high speed output from the electrical servo motors into very low speed-high torque output as required to drive the power screw. The resulting design is presented on Figure 6.1, which shown the general concept; more information about detailed design and operation principles can be found on [79].

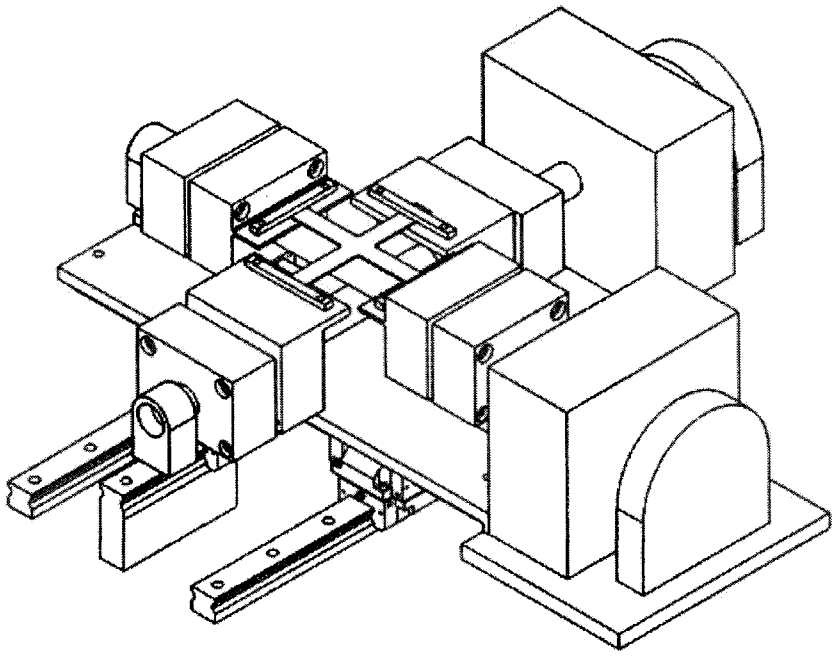

Figure 6.1 Biaxial, fatigue capable testing machine designed by the ITESM composites team.

Unfortunately, despite the design locks promised good performance, manufacturing cost far exceeded the budget allocated to the project because of the requirement of the ability to perform fatigue tests

This forced to return back to the drawing board to design a system capable of meeting the basic requirements while within budget. As suggested on literature, the most economical approach to perform biaxial tests is by using or mechanical rigs designed to be mounted on universal machines. Unfortunately this approach presents two major problems: not ensures an unobstructed vision over the specimen, and not permits to control both axis independently. However, the principle was adopted and adapted to design a specific machine.

The resulting apparatus is presented in the Figure 6.2a. and a photograph of the completed machine in Figure 6.2b. Here's how it works (numbers in parentheses refer to the components identified in the corresponding figures): the charges are applied through a slider-crank-slider symmetrical mechanism, which can meet the requirement ii: hydraulic piston (1), which is the first slider, is attached on it base to the machine frame and provides load drive, while it piston is linked by a revolute joints (2) to a pair of arms (3) arranged symmetrically, which are connected by cylindrical joints (5) to the blocks where the grips are installed holding the tab zone of the specimen (4); these cylindrical joints permits to absorbs small misalignment in the loads, as established in *iv*.

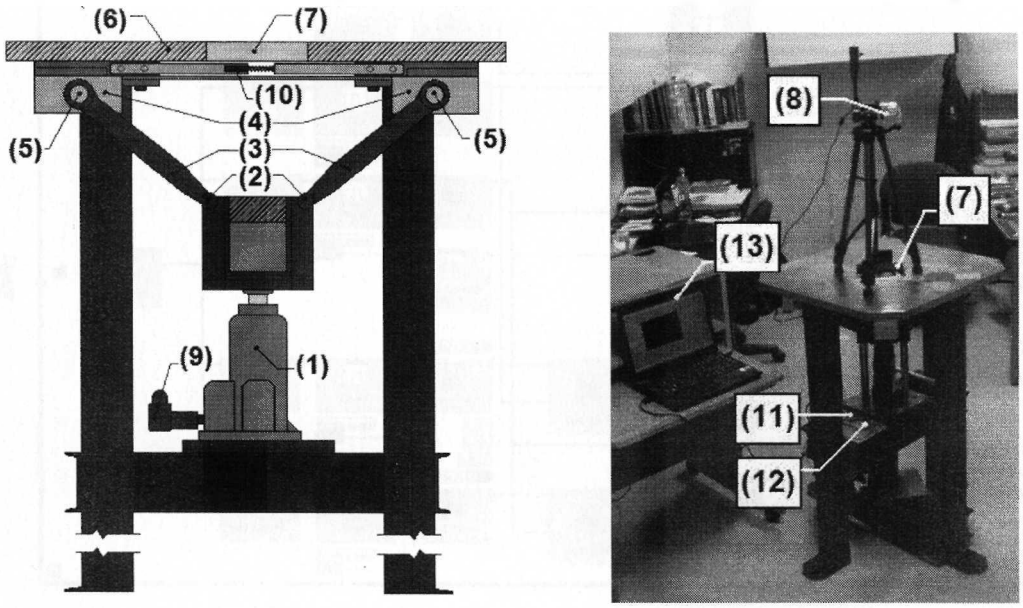

a. b.

Figure 6.2 a). Biaxial test machine´s single axis sketch. b). System general arrangement.

The grip blocks are lubricated and slides on the underside of a flat plate (6), which underwent a rectangular window (7) to allow a full field of view from the top of the machine, where installing a high definition digital camera (HDDC) (8), thereby satisfying the requirement iii.

A similar arrangement is perpendicularly installed respect the first, so as to ensure the independence of the load axis required by *i*. Data acquisition is done by measuring the pressure in the hydraulic cylinders (9) and correcting the information to take into account the geometry of the mechanism, while the displacements are measured directly in the grips through resistive displacement sensors (10); all the sensors are powered by a power board to provide a common voltage reference (11), and the signals are acquired through an National Instruments 8-channel analogical acquisition board (12). The information was stored and processed on a laptop (13) by using a Lab View routine, shown in the Figure 6.3. The cylinders actuation was manually controlled via a visual interface which displays a "strain director" on the control panel (Figure 6.4) which must be followed by the machine operators, one following each axis.

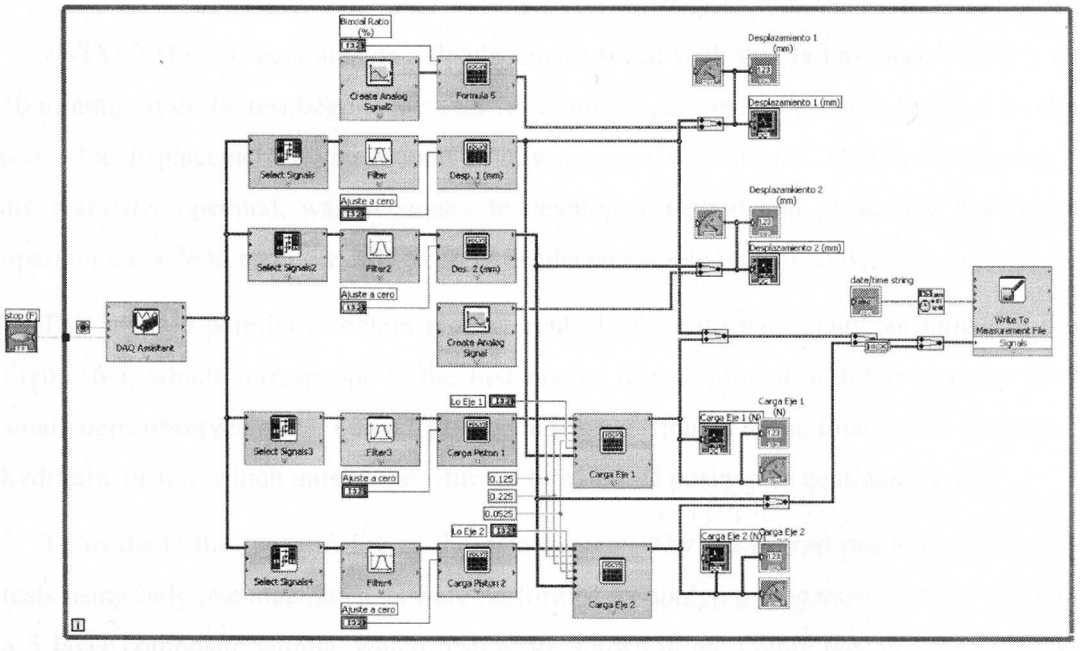

Figure 6.3. LabView data aquisition block diagram.

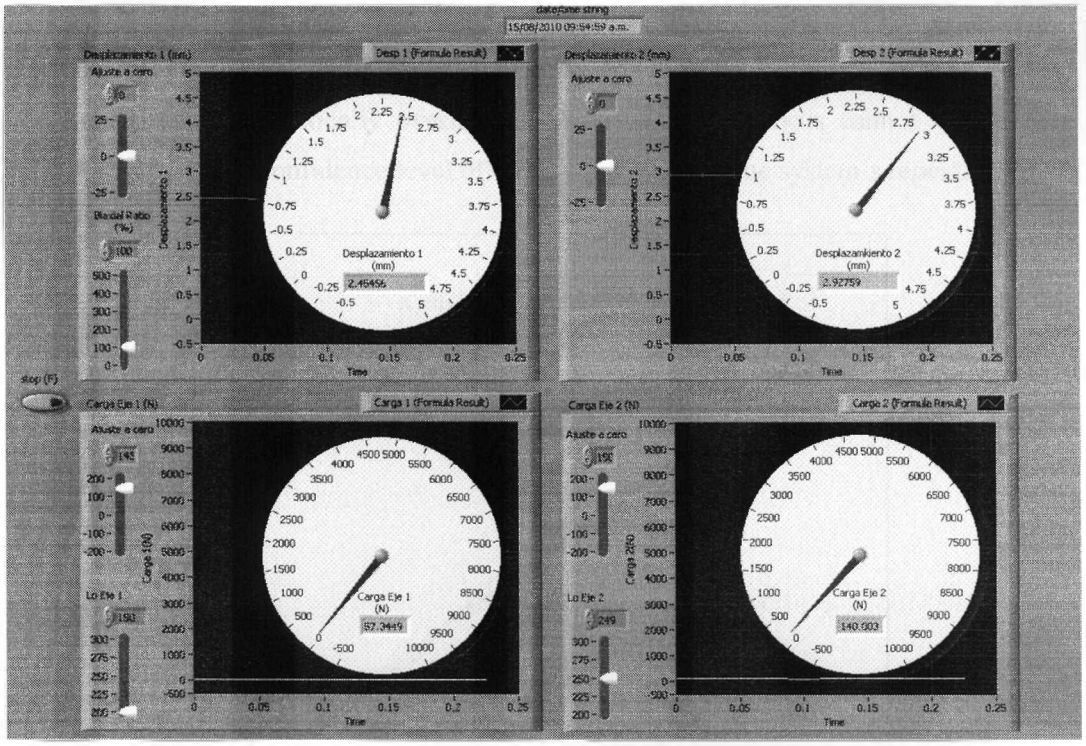

Figure 6.4. Biaxial machine´s control panel

ASTM 3039 [4] recommends a displacement speed such that failure occurs after 1 to 10 minutes after the test begins; then, an 1mm/min displacement rate were selected for the tests, due displacement values around 2mm were expected until fail. Due hydraulic piston are manually operated, was necessary to develop a method that makes the machine´s operator capable to meet the ASTM 3039 displacement rate recommendation.

This method permits to obtain precise control of the displacements, as shown in the Figure 6.5, which corresponds to the first biaxial test performed with the machine. The small steps observed at 25, 60 and 120 seconds are attributed to the final on the run of the hydraulic piston, which must to be returned to its initial position to continue the test.

To evaluate the repeatability of the data generated by the biaxial machine, a uniaxial tests using only one machine axis were performed by applying progressive higher loads to a 5 layer composite lamina, which results are shown in the Figure 6.6. In this plots, the discharge loads appears to be non-conservative, which results very estrange due the material stay within elastic region strain. This is due the load release rate cannot be

controlled, and is an almost instantaneous process; it results on relative high speeds between machine's lubricated plates, which dissipates considerable amount of energy. The load paths are practically overlapped, and statistical analysis cannot differentiate between them with a confidence level of 95%, which verifies the system's repeatability.

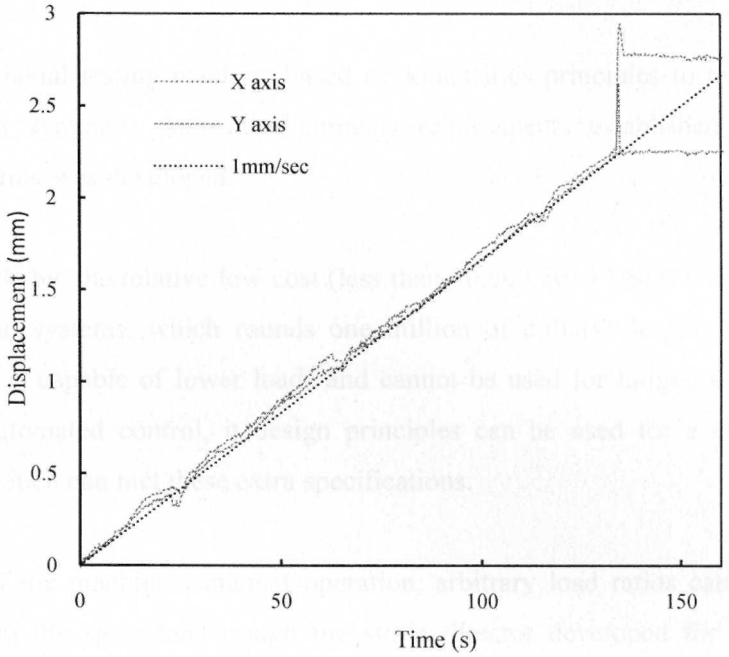

Figure 6.5 Displacements vs. time for test 5.

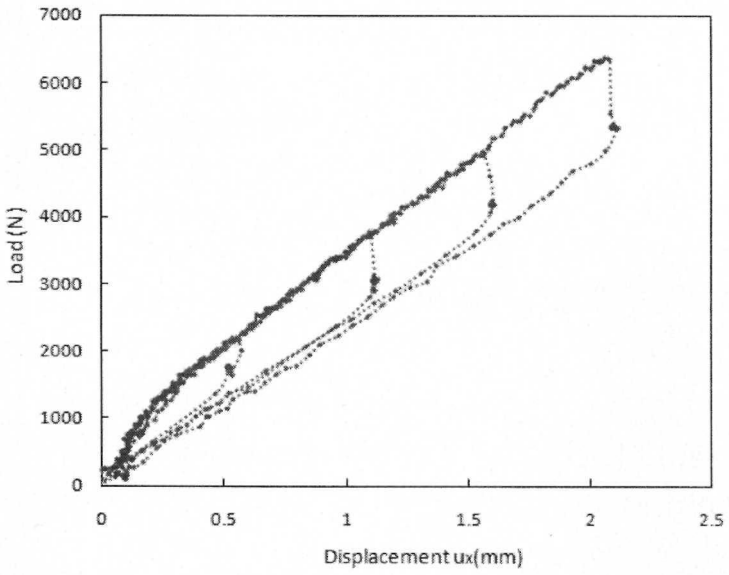

Figure 6.6 Displacements vs. time for test 5.

6.3. Concluding remarks

- A novel biaxial testing machine based on kinematics principles to meet the loads application symmetry and misalignments requirements established for perform biaxial testing was developed.

- It is remarkable the relative low cost (less than 10,000 2010 USD) if compared with commercial systems, which rounds one million of dollars; despite our apparatus obviously is capable of lower loads and cannot be used for fatigue testing due the lack of automated control, it design principles can be used for a more complex machine which can met these extra specifications.

- Despite of the machine's manual operation, arbitrary load ratios can be precisely imposed to the specimens trough the strain director developed for this purpose, meeting displacement ratios recommended by ASTM standards.

Chapter 7.
Experimental development

Experimental tests were conducted to validate the FE results obtained. The selected material was Epoxy West System 105/206 reinforced with fibreglass cloth style #7520, bidirectional plain weave 8.5 oz./sq. yd, with 18L x 18W threads per inch count. This is a representative TC of a wide range of industrial applications, which elastic properties correspond to those presented in Table 5.1.

7.1. Specimen manufacture

As stated by recent researches [20] the milling process typically employed to thin the gauge zone produces undesirable damage and stress concentrations in UD composites; for TC, milling would exacerbate this problem due to its more complex 3D structure, making this an unacceptable choice. The main concern is to preserve the integrity of the textile structure, especially when characterizing a single lamina. To generate a damage-free, single-layered gauge zone cruciform specimen, a novel manufacturing process was developed by the authors, explained below:

1). Non-impregnated fabric sheets required for 9 specimen reinforcement layers (24 sheets, separated each two by a polyethylene sheet) were fixed to a 6mm thick plywood base to ensure dimensional stability, with a printed grid to help proper fibre alignment of each cloth. The whole arrangement was cut into a square pre-form using a water jet, also removing the rhomboidal window corresponding to the gauge zone, as shown in the Figure 7.1. Afterwards, the material was oven-dried at 60°C during 12 hours to eliminate moisture.

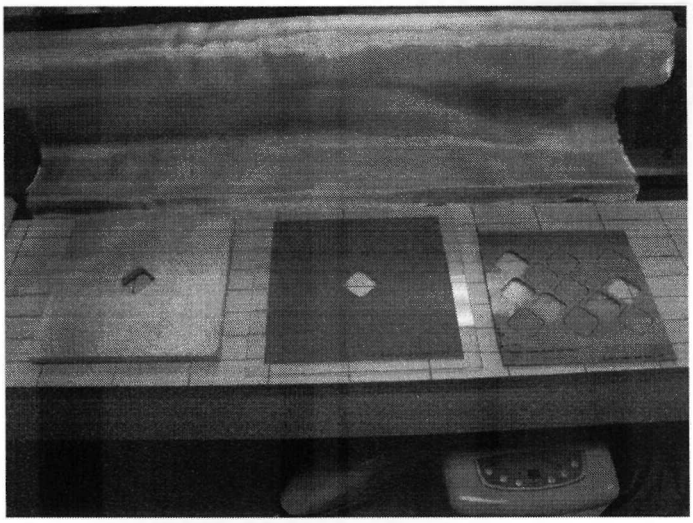

Figure 7.1. Rhomboid window cutted on the reinforcemetn layers and other auxiliary tools. .

2). The following numeric values inside brackets refer to indications given in Figure 7.2. Two reinforcement layers (1) corresponding to the bottom side of the cruciform specimen were placed in a lamination frame, consisting of a flat surface (2) surrounded by a square border (3) with a side length equal to that of the specimen. A pre-formed 2-layer rhomboid step (4) was located at the centre, corresponding to the location of the gauge zone, to ensure planarity of the central layer (5). The reinforcement layers were manually resin-impregnated and, immediately after this, the central layer (5) was placed and impregnated.

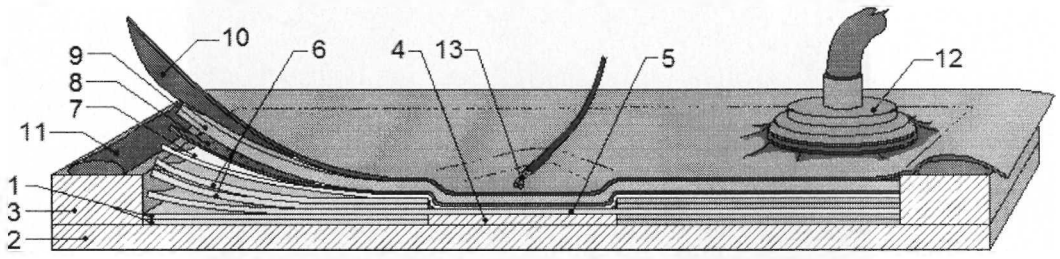

Figure 7.2. Arrangement for specimen manufacture.

Finally, the process was repeated for the last two reinforcement layers (6), as shown in Figure 7.3. Room environment was controlled during the lamination process at 80±2°C temperature and 50-60% relative humidity.

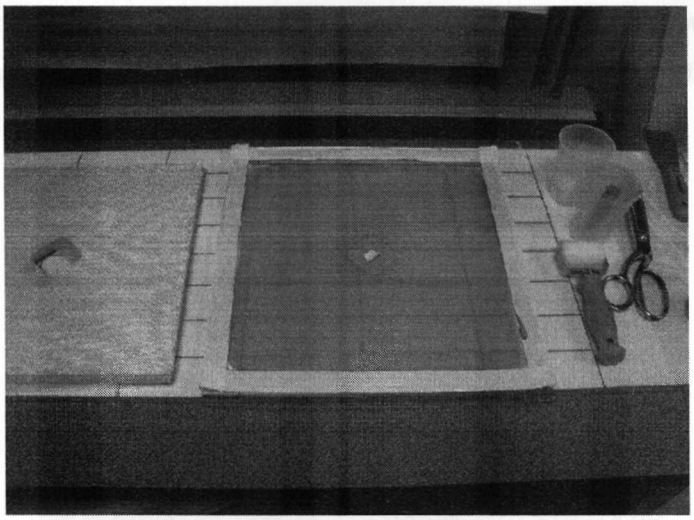

Figure 7.3. Resin impregnated textile ples.

Immediately after the impregnation process was completed, the laminate was placed in a vacuum bag consisting of a peel ply (7), perforated film (8), bleeder cloth (9) and the bag itself (10), using sealing tape to ensure vacuum seal (11). 0.8 bar vacuum pressure was applied through a valve located at a corner (12), sufficiently away from where the final shape would be cut.

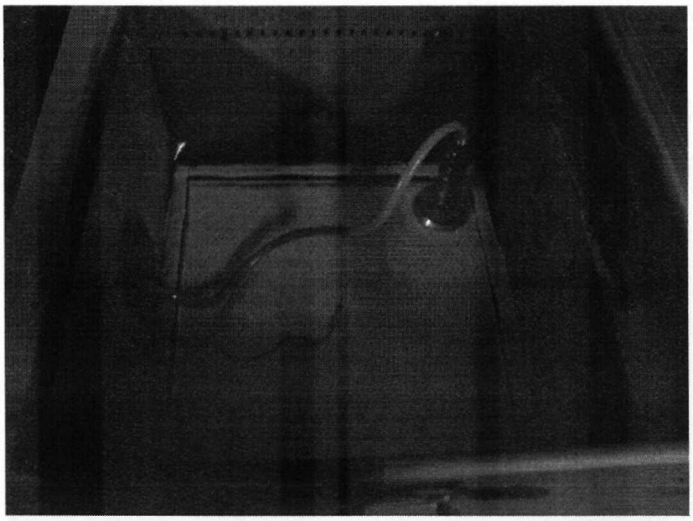

Figure 7.4.Laminate in the vaccum bag placed into oven to be cured.

The whole arrangement was cured during 4 hours inside a pre-heated oven at 80±2°C, as measured by a thermo-couple (13) located at the gauge zone, as shown in Figure 7.4

3). After curing, the final cruciform geometry was obtained through water jet cutting. Nine specimens were prepared meeting the dimensional specifications of Figure 7.5. All the 9 specimens are shown in Figure 7.6.

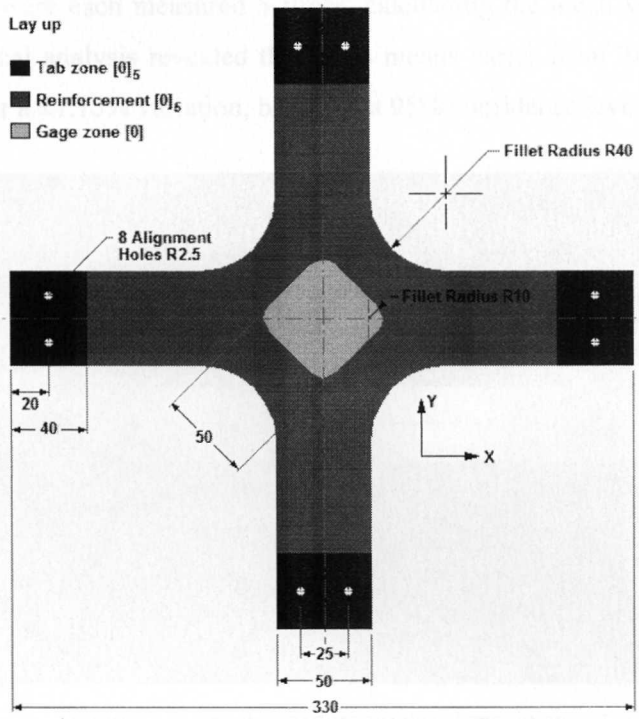

Figure 7.5. Optimized specimen specifications (Model 3). Dimensions are in mm.

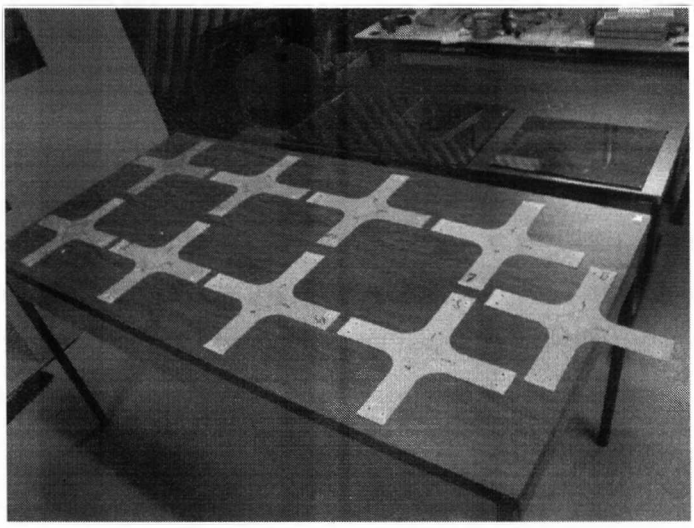

Figure 7.6. Nine cruciforms.

Given the labour-intense process required to prepare one specimen, a study was conducted to evaluate the repeatability of the process. The specimen's mass was selected as an indirect parameter to measure the effectiveness of the manufacture process. Masses of six specimens were each measured 5 times, calculating the mean values presented in Table 7.1; statistical analysis revealed that mass means varies from 285.27 to 291.76 g, that is, 281 ± 3g or a ±1.15% variation, based on a 95% confidence level.

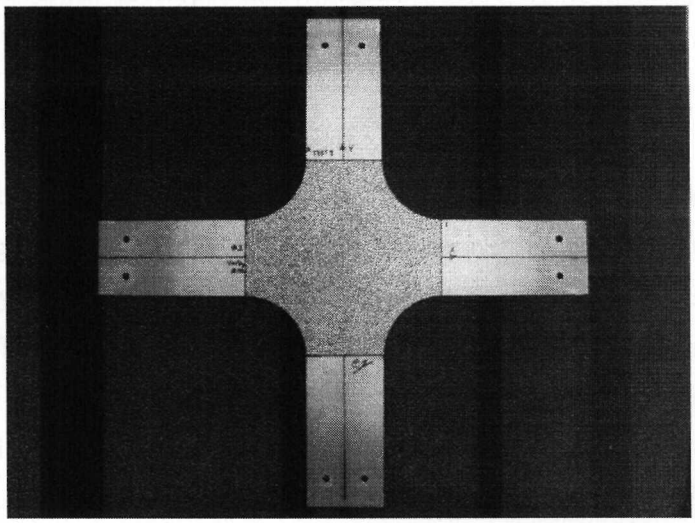

Figure 7.7. Speckle pattern prepared specimen.

As there is no official standard for biaxial specimens, the ASTM 3039 test standard for UD laminates [4] was used for comparison purposes, which allows a maximum variation of ±1% in width and ±4% in thickness for rectangular specimens in tensile tests. Assuming that mass is proportional to volume and no variation in length exists, the volume (and hence the mass) tolerance range can be calculated as (width±1%)*(thickness±4%)*(length). Normalizing dimensions, this equates to (1±.01)*(1±.04)*(1) = (0.9504, 1.0504) which represents a mass variation of around ±5%. Thus, the ±1.15% variation measured for the cruciform specimens complies with the ASTM criterion.

Table 7.1. Mean specimens mass (gr.)

Specimen	1	2	3	4	5	6
Mass (gr.)	290.69	290.62	292.08	286.45	284.06	287.18

To provide visual reference for the digital image correlation (DIC) strain field measurement [2],[43], specimens were painted with a black-dot random speckle pattern over a withe-mate primer, as shown in Figure 7.7. This technique was preferred over the sprayed technique reported in [43], as it might result in an inadequate control of the dot size distribution, leading to uncertainty in the DIC measurements. Additionally, five uniaxial, $[0]_5$ layup specimens were prepared in order to perform uniaxial tests to provide of precise input data for the further developed failure criteria.

7.2. Experimental set-up

To conduct an experimental validation of the optimized cruciform, the authors developed a biaxial testing machine capable of applying orthogonal independent tensile loads, thus capable of applying arbitrary biaxial load ratios while maintaining symmetric grip motion at each axis. The mechanism is able to cope with small load misalignments, avoiding spurious loads in the specimen (torsion, shear and bending). It also provides an unobstructed visual field of the specimen's gauge zone, which allows continuous DIC strain field measurements during the test. Specimens were mounted by gripping at the tab zones, via two alignment holes at corresponding locations in both the specimen and machine, thus ensuring a symmetric gripping as shown in Figure 7.8.

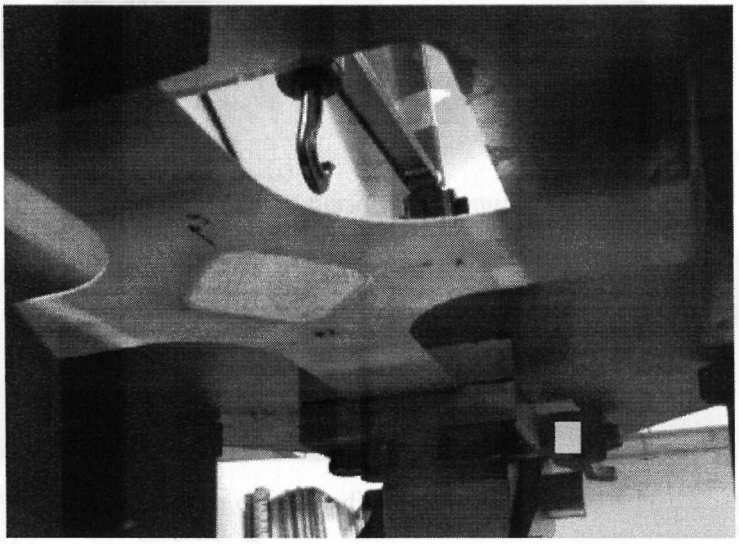

Figure 7.8 Cruciform specimen mounted in the biaxial test machine.

A pre-load of 500N was applied to each axis prior to tightening the mounting bolts. Then, preload and alignment bolts were removed, setting to zero the measured displacements and loads. A high-quality video of the specimen was recorded with a high definition cam coder (HDCC) with adjustable focus and exposure parameters functions for subsequent DIC analyses. A chronometer synchronized with the computer clock was placed near the specimen and inside the HDDC vision field, to ensure its inclusion in the captured images; this provided a time reference to relate each video frame with correspondent load data. After starting video recording and the data capture routine, biaxial displacements were applied at a rate of 1mm/min until final failure. This load rate was selected based on the ASTM 3039 standard [4], which recommends a displacement speed such that failure occurs after 1 to 10 minutes after the test starts.

Data acquisition and reduction was conducted as follows: two video frames were taken from the recorded video sequence, one corresponding to the test beginning and other just prior to the final failure, identified in the video sequence. Both images were fed into the open access software DIC2D (developed by Dr. Wang's team at the Catholic University of America) to obtain the full strain field (ε_x, ε_y and γ_{xy}).

7.3. Specimen validation

Experimental validation was carried out via testing of 6 specimens and following the methodology described in section 7.2. Three out of six tests (tests #1, #3 and #5) were considered completely successful, since they fulfilled all the requirements previously stated for a valid biaxial strength test. The partially successful Test #2 presented premature failure in the rhomboid boundary; this fact was traced back to a fibre misalignment in the gauge zone caused during the manufacture process.

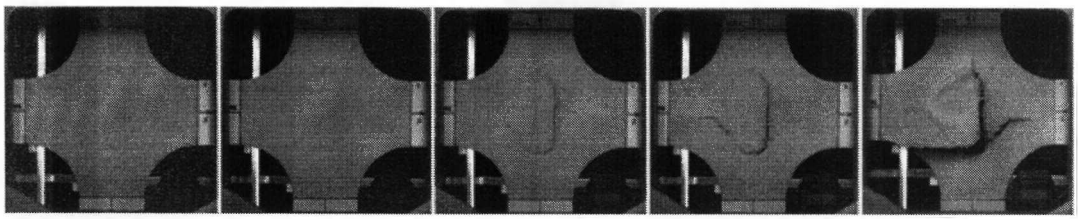

Figure 7.9. Final failure sequence corresponding to Test #5 recorded at 30 frames per second.

Tests #4 and #6 exhibited high shear strain at the gauge zone, evidence of load misalignment due to improper gripping procedure; both effects could be arguably attributed to the learning curve of the recently developed experimental procedure and not to the specimen itself.

The three successful tests covered a range of BR values in the vicinity of the critical condition BR=1: BR=1.5 (Test #1), BR=1.25 (Test #3), and BR=1 (Test #5). Figure 7.9 shows the final failure sequence corresponding to Test #5, representative of the three successful tests. It should be noted that the failure occurred well within the gauge zone as expected from the FE predicted strain fields. The final failure is clearly fibre-dominated, due it catastrophic nature; it is possible to identify the final failure onset region inside the rhomboidal gauge zone, as required for a successful test. To acquire the full strain field from all the DIC list data, an algorithm, described next was developed:

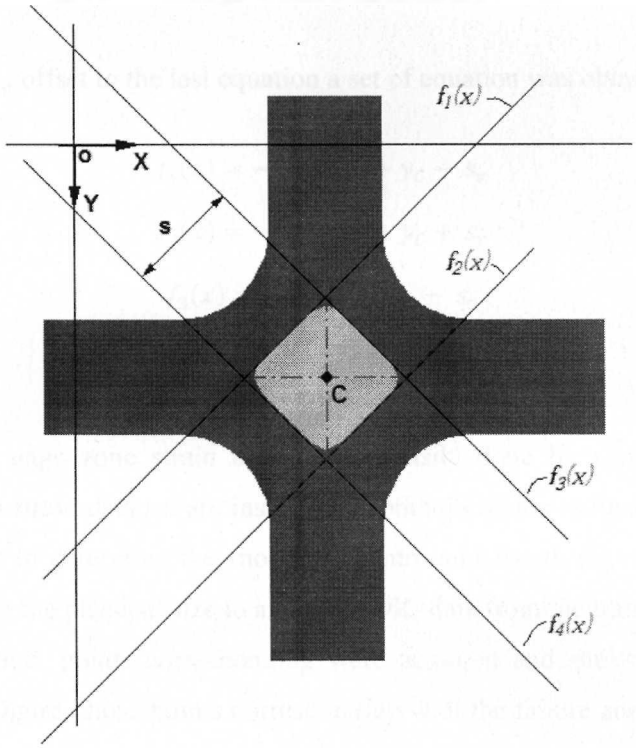

Figure 7.10. Auxiliary parameters for DIC data aquiring.

Just the strain values corresponding to rhomboidal gage zone must to be extracted from the full data list generated by the DIC analysis; to define a rhomboidal zone form which

data will be cropped, two auxiliary parameter were defined: the rhomboid's center C location coordinates (x_C, y_C) and the rhomboid side length s. Then, four lines defined by:

$$f_n(x) = m_n x + b_n \qquad n = 1,2,3,4 \qquad \textit{Eq. 7.1}$$

Were built, in order to form a rhomboidal zone by adjusting it slopes $m_1 = m_2 = -1$ and $m_3 = m_4 = 1$ and the parameter b_n, which must taken the absolute vertical distance from the point C to the lines defined by the functions $f_n(x)$ is defined as:

$$s_v = s\, Sin\, \frac{\pi}{4} \qquad \textit{Eq. 7.2}$$

A line with slope $m=1$ which passes through the point C is defined by the function:

$$f(x) = m(x - x_C) + y_C \qquad \textit{Eq. 7.3}$$

Summing an $\pm s_v$ offset to the last equation a set of equation was obtained:

$$\begin{aligned} f_1(x) &= -(x - x_C) + y_C - s_v \\ f_2(x) &= -(x - x_C) + y_C + s_v \\ f_3(x) &= (x - x_C) + y_C - s_v \\ f_4(x) &= (x - x_C) + y_C + s_v \end{aligned} \qquad \textit{Eq. 7.4}$$

Then, crop the gage zone strain data can be easily done by simply evaluating if coordinates of each strain data set are inside the rhomboid region defined by Eq. 7.4. The operator only must to determine the rhomboid centre and length (s), which must to be slightly smaller than the physical size to avoid the DIC data from the transition zone.

Using this method, points corresponding were acquired and shown in Figure 7.11. Also, in the same figure, those points corresponding with the failure zone identified from video recording were border-marked in white. From this figure is possible to determine that the maximum shear strain inside the gauge zone reached up to 25% of the maximum ε_y strain value, which is about twice the value predicted by FE analysis; however, failure occurs in regions inside the gauge zone with low shear strain values (around ±0.1%), so it can be considered that nearly pure biaxial load state was achieved at failure point. To

calculate the average biaxial ratio $\overline{BR}$ corresponding to each ε_y vs. ε_x cloud data, linear fits with forced zero offset were calculated, which slopes for each BR value are also shown in Figure 7.11. The ε_y vs. ε_x clouds shown in Figure 7.11 suggest that strength data obtained from the traditional data reduction method (based on applied forces and subsequent correction with by-pass factors can potentially produce erroneous data as the failure can occur, as shown for the case of Test #5, in a zone far apart from the data-cloud centre. BSRV and SYRV values were calculated from the experimental DIC data and are presented in Table 7.2. A descriptive statistical analysis shows that $\overline{BSRV} = 0.005971 + 0.00212$. This value is significantly higher than that of the FE model 3 with BR=1 ($\overline{BSRV} = 0.00103$).

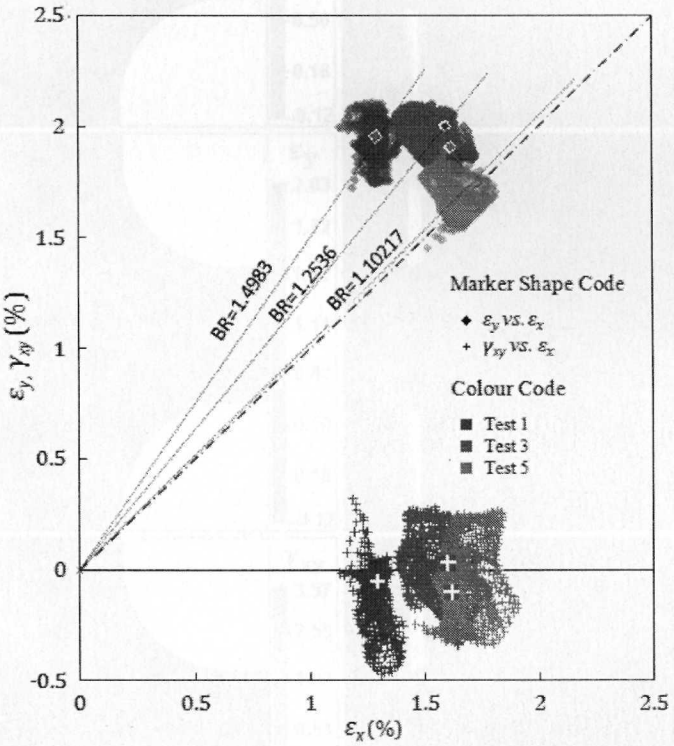

Figure 7.11. Experimental strain distributions inside the gauge zone (Model 3).

This is not surprising since the FE model only considers the influence of the geometrical parameters of the sample, neglecting the influence of the inherent experimental variability associated with material non-homogeneity, non-linearity, measurement inaccuracies and variation in specimens' dimensions.

Table 7.2. Experimental BSRV for gauge zone reduced from DIC data.

	Test #1	Test #3	Test #5
$\overline{\overline{BR}}$ (measured)	1.49831	1.25360	1.10217
BSRV	0.00505	0.00673	0.00612
SYRV	0.01071	0.00921	0.00842

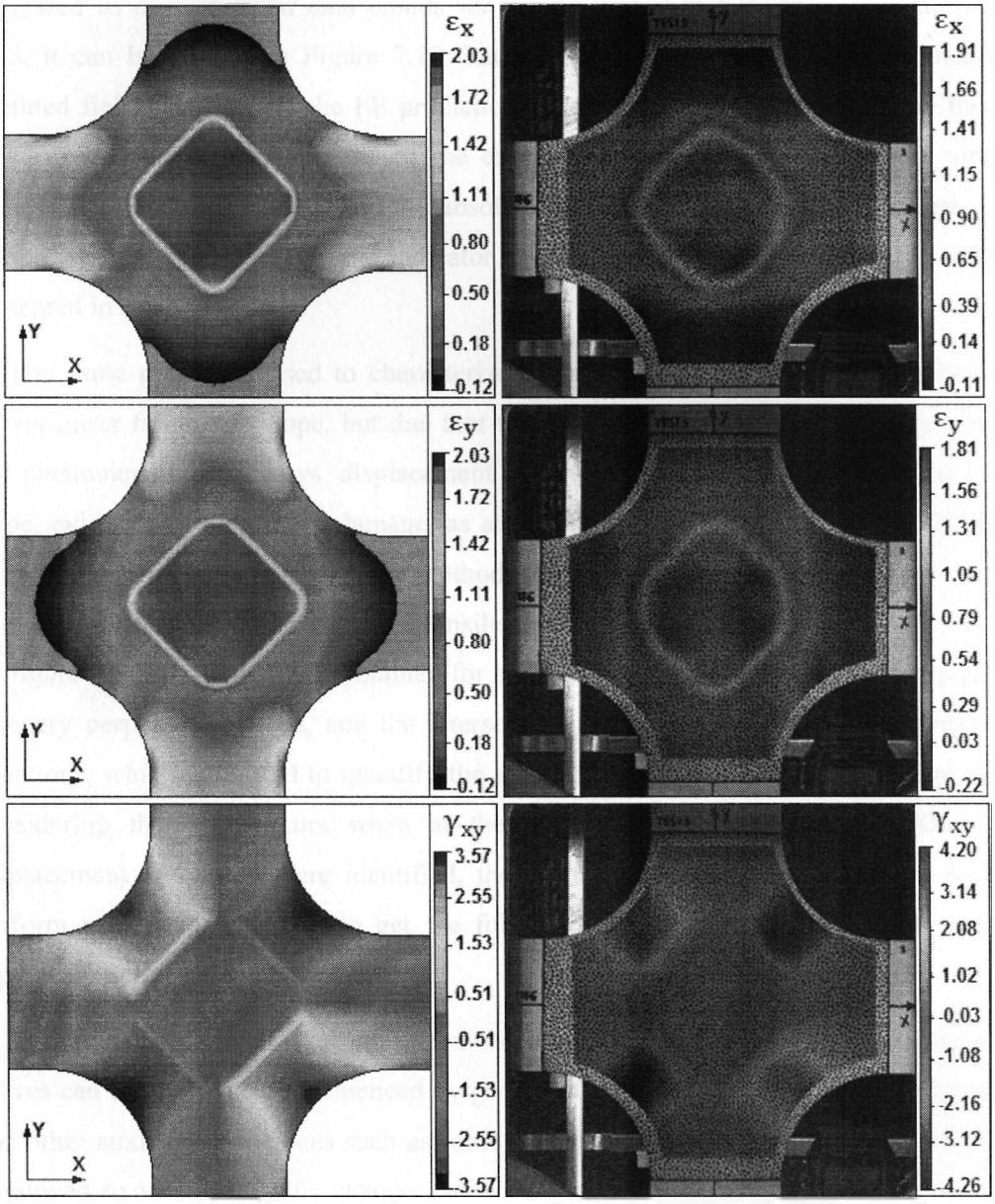

Figure 7.12. FE vs DIC strain field comparison for Test #5. First column corresponds to FE results, second column to experimental results. First, second and third rows present εx, εy and γxy (in %), respectively.

It should be noted, however, that the experimentally observed BSRV value is very low, even lower (by a factor of 3) than the FE-derived BSRV-values of the non-optimized specimens (Models 1 and 2), thus illustrating the very good homogeneity of the strain fields obtained with this novel geometry. This fact is also demonstrated by the remarkably low dispersion exhibited by the experimental εy vs. εx data clouds (Figure 7.11) as compared to the simulated data clouds for Model 3 (Figure 5.3). Regarding the strain field, it can be seen from Figure 7.12 that the agreement between the experimentally obtained field via DIC and the FE prediction is remarkably good. The DIC and the FE images show the same symmetry of the experimental shear strain pattern and similar homogeneity and smoothness, and the absolute strain values cover a similar range. This can be considered as an additional indicator of the success of the experimental procedure presented in this work.

The same procedure used to characterize the ultimate strain was used to obtain the matrix onset failure envelope, but due that there is a not significant visual indication of this phenomenon, the load vs. displacement plots were used to identify the change in the slope, evidence of the matrix damage, as shown in the Fig. 7.13; this method has been proposed as an extrapolation of the method employed for uniaxial tests defined by the ASTM 3039 standard for the uniaxial tensile characterization of composites [4], as shown in Figure 2.8. Linear fits were obtained for every linear segment of curves corresponding to every perpendicular axis, and the intersections were calculated solving the resulting equations, which permitted to quantify the strain corresponding at matrix damage onset, considering that this occurs when at the first observed slope change. Once the displacement and strain were identified, the digital image corresponding were used to perform a DIC analysis and to get the full field strain, in the same fashion that the previously described methodology.

Is important to remark that the use of the slope change in the load vs. displacements curves can be significantly influenced by geometrical effects and material's non-linearity, and other auxiliary techniques such as sonic emission or in-situ x-ray scanning should be employed to verify that this change can be effectively used as a matrix damage onset indication.

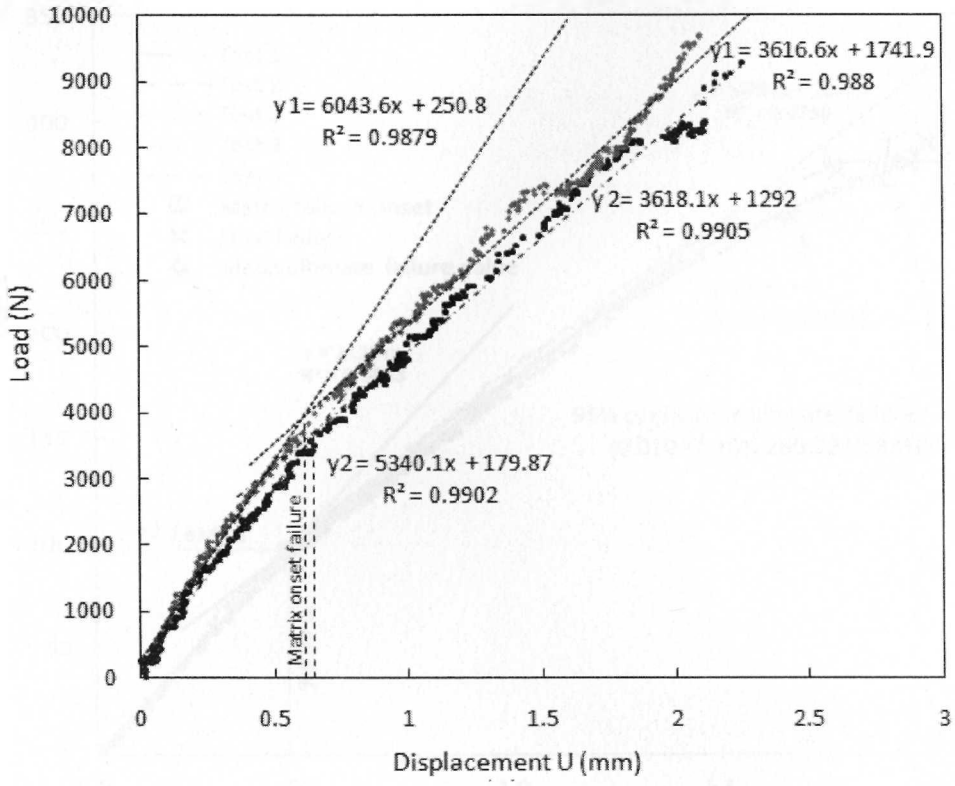

Fig. 7.13. Load vs diplacement for biaxial test #3.

In order to generate precise uniaxial data to be used as input data for the further developed failure criterion, uniaxial tests also were also performed, using a single axis of the testing machine. Due previous tests demonstrated that uniaxial single layer specimens are prone to premature failure due the edge damage produced during cut machining process, five layers specimens were tested, which can be cut without incur in significant edge damage. Details of specimens used are presented in Fig. 7.14.

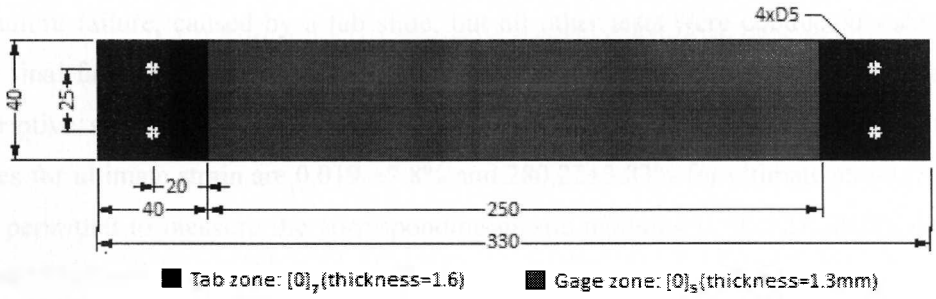

Fig. 7.14. Uniaxial test specimen dimensions. Dimensions are in mm.

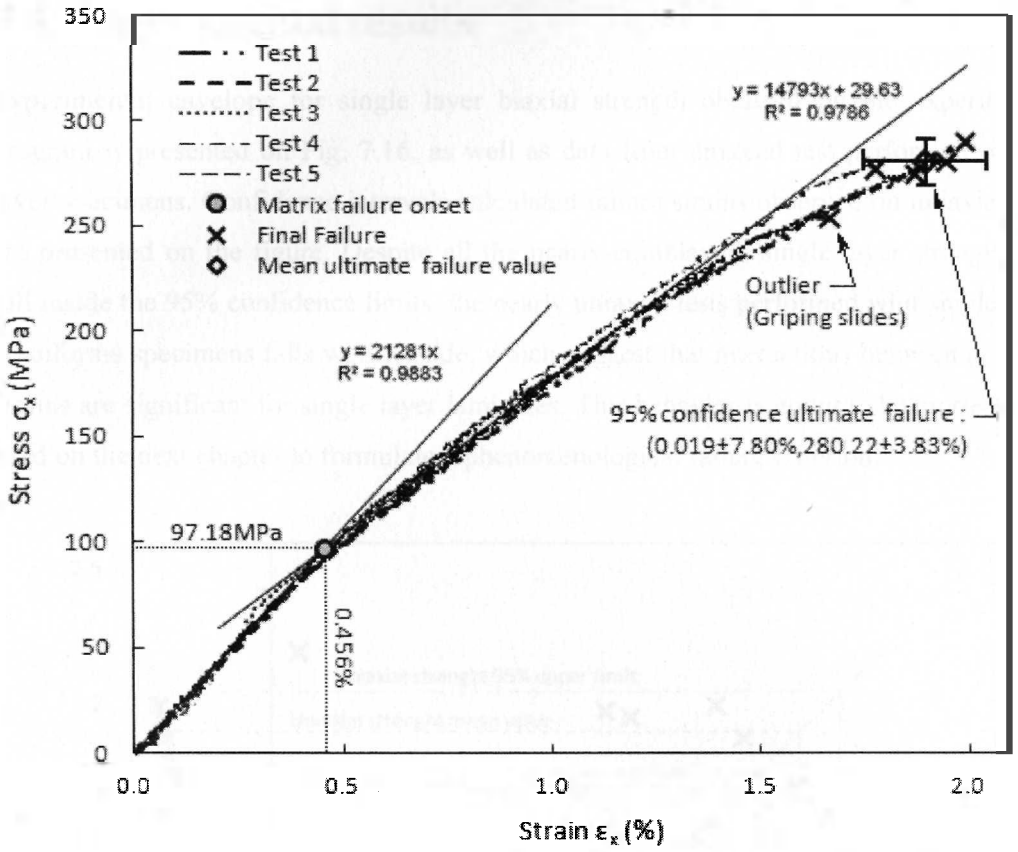

Fig. 7.15. Uniaxial testing strain/strain results.

Results of the five tests are presented in stress vs. strain plot in Fig. 7.15. Low dispersion is observed in the tests trend. The change in the curve has been calculated to establish the matrix onset failure strain, in the same fashion that is defined on Figure 2.8, resulting on a strain of 0.0456 and a stress of 97.18MPa, nearly one fourth and one third, respectively, of the ultimate values measured at final failure. Test number 1 exhibited a premature failure, caused by a tab slide, but all other tests were conducted successfully until final failure; measured strength data was relatively low dispersed, as revealed by a descriptive statistical analysis, which established whit a 95% of confidence that mean values for ultimate strain are 0.019 ±7.8% and 280.22±3.83% for ultimate stress. The tests also permitted to measure the corresponding elastic modulus E_x=E_y=21.28GPa, which is round 15% lower than expected from the tipycal values.

7.4. Experimental results

Experimental envelope for single layer biaxial strength obtained by the experimental program is presented on Fig. 7.16, as well as data from uniaxial test performed on five layer specimens. Confidence intervals calculated failure strains observed on uniaxial tests are presented on the figure. Despite all the nearly-equibiaxial, single layer strength data fall inside the 95% confidence limits, the nearly uniaxial tests performed whit single-layer cruciforms specimens falls well outside, which suggest that interactions between ε_1 and ε_2 strains are significant for single layer laminates. This behavior is going to be modeled and used on the next chapter to formulate a phenomenological failure criterion.

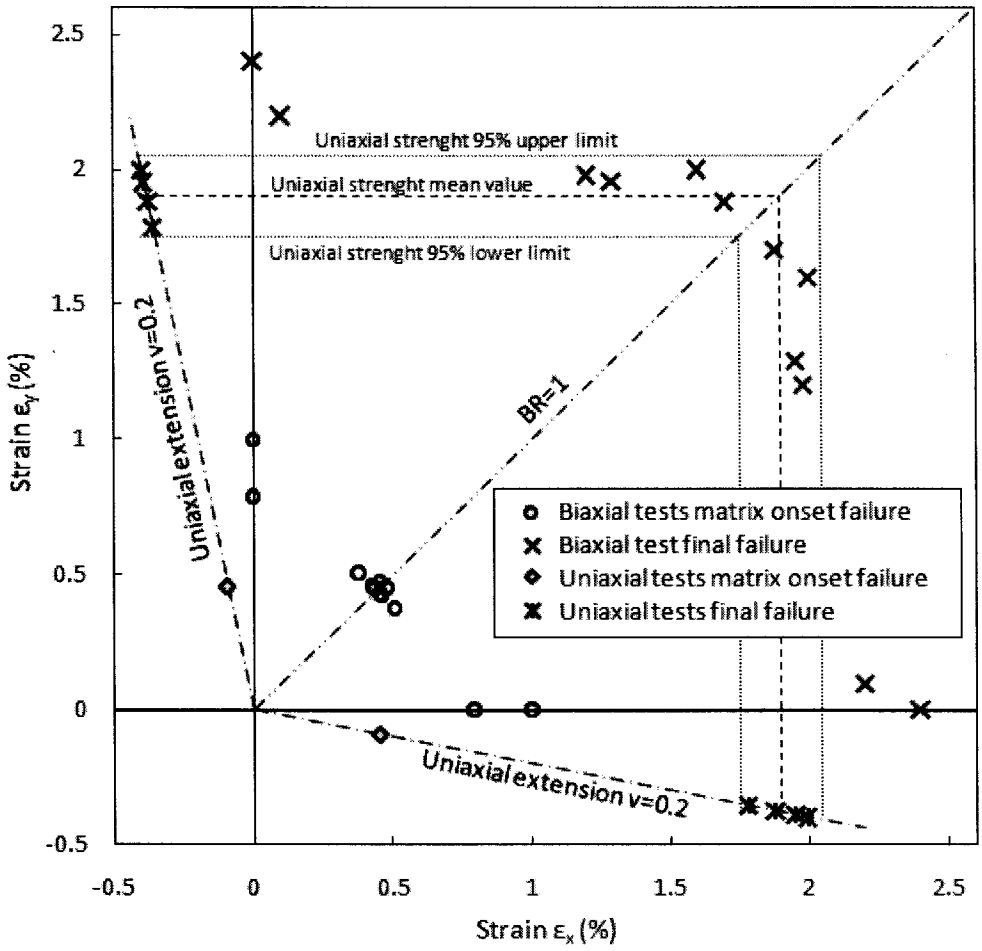

Fig. 7.16. Failure envelope data obtained from experimental program.

7.5. Concluding Remarks

- A novel manufacturing process, which avoids machining operations to generate the thinned gauge zone was developed, in an attempt to preserve the textile architecture from machining micro-damage. It consists on cutting the rhomboidal windows from the reinforcement layers prior it matrix impregnation by using water jet cutting machine. Despite high manual job is involved in the specimens manufacture process, it measured specifications were according to those extrapolated from ASTM 3039 for composite materials unidirectional samples.

- Validation of specimen's geometry and manufacturing technique was made through experimental testing, which were conducted on the own-developed biaxial machine. The cruciform's full strain field was measured via digital image correlation; results demonstrate, in close agreement with the results obtained from the FE simulations, that the specimen generates a significantly more homogeneous biaxial load state in the gauge zone than others reported in literature, and failure occurs, for all the tests, into the gage zone, as intended.

- Once the experimental methodology has been fully developed and validated, set of experimental data were obtained; the failure envelope obtained demonstrate that there exists interactions in the textile microstructure; this data will permit to formulate and validate an specific failure criterion.

Chapter 8.
Phenomenological Failure Criterion

8.1. Matrix damage onset failure criteria

Once experimental matrix failure envelope data was available, qualitative analysis permitted to establish similitude between this and Maximum Strain and Tsai-Wu criteria envelopes. To verify this, both criteria were mapped on $\varepsilon_1, \varepsilon_2$ strain space as shown in the .

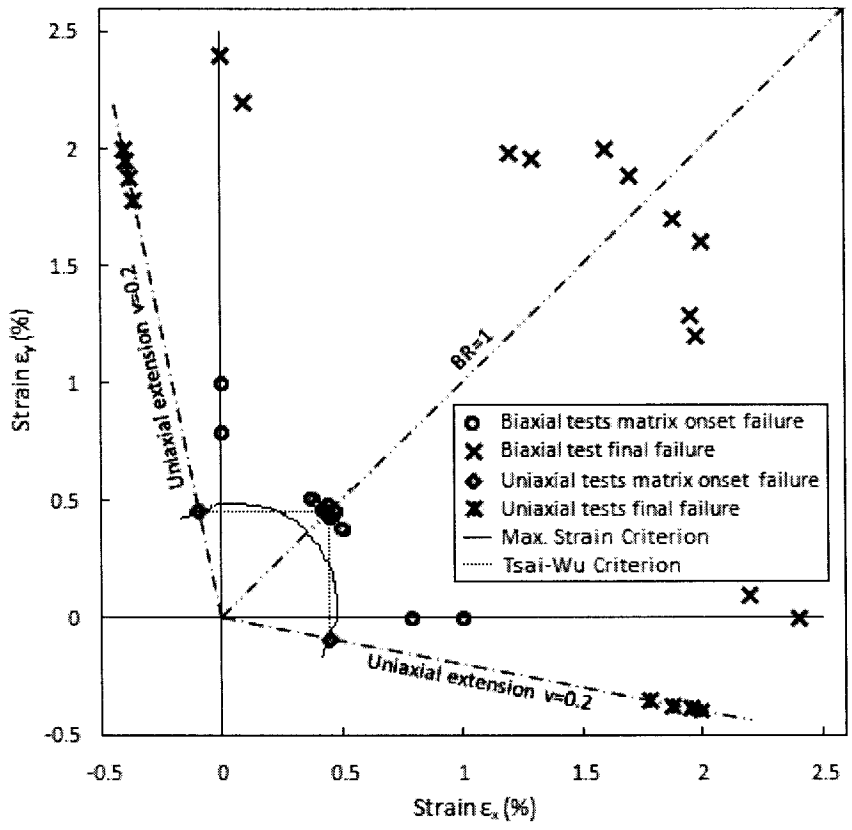

Fig. 8.1. Tsai-Wu and Maximum Strain criterion predictions for matrix failure onset as compared vs. experimental data.

For maximum stress criterion, the input damage was simply the stress for which the change in the stress-strain curve slope was detected, as defined on Fig. 7.15. For Tsai-Wu, additional parameters considered were F_{12}^{*}=-1/2 (the standard value used on literature), and compressive ultimate stresses were considered equal to the tensile stresses, defined in the same fashion than for the maximum stress case. Note that in that Tsai-Wu criterion is more conservative than maximum strain criterion, which predict very well the matrix onset failure for equibiaxial load conditions.

8.2. Ultimate strength failure criteria

8.2.1. Phenomenological derivation

Experimental data for T-T failure envelope of studied TC demonstrate that strain interactions are significant (which is not surprising due the entanglement of the yarns) and must to be included in the formulation of a successful failure criterion dedicated to TC. Since the experimentally obtained failure envelope not provides failure-mechanism insight enough by itself to formulate a phenomenological failure mode, other evidences taken during the research progress were used. Unlike dog-bone and rectangular specimens employed for uni-axial characterization, cruciform specimens avoid the free-edge effects on the gage zone and it associated out plane displacements; despite this, relative high displacements out the plane were identified when a preliminary uni-axial test were performed on a cruciform specimens mounted on a universal testing machine, as shown in Fig. 8.2a; it corresponds to the initial non-deformed state, while Fig. 8.2b. corresponds to the specimen loaded with an uni-axial force applied: is notorious the dark bands running along the gage zone in 45° direction, associated with the type of braid of the material (twill 2x2). This phenomena evidences some degree of interaction between the entangled yarns that plays an important role in the material´s behaviour, and presumable on it biaxial strength.

To formulate a failure criterion which takes on count this effect, the following conceptual mechanism is proposed: consider a biaxial TC unit cell (Fig. 8.3a.) to which a uni-axial load T is imposed: those yarns running parallel to the load tends to align in the load direction, forcing the transversal yarns to be pushed out of plane as sketched in Fig.

8.3b, and causing the undulations that caused the bands showed in Fig. 8.2b; for this condition, the strength will be maximum due the fibres alignment.

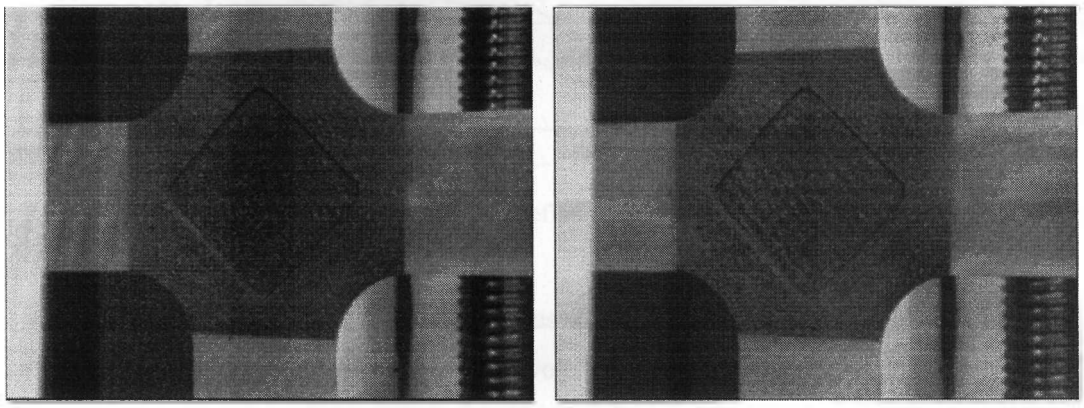

a. b.

Fig. 8.2. Out-plane tensile displacements.

On the other hand, when a equi-biaxial load state is imposed, the yarns are subjected to the same tension and no fibre alignment is permitted, resulting in a contact force between the yarns which ads a significant compression force on the fibres which must be quantified in order to determine the biaxial strength.

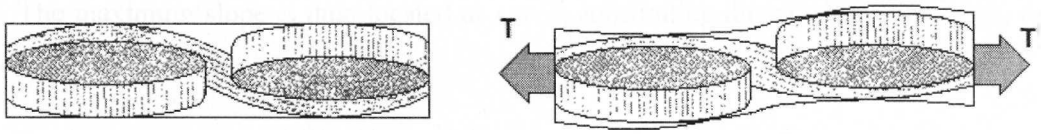

a. b.

Fig. 8.3. a). sketch of unit cell in non-deformed state and b.) subjected to uniaxial tensile load.

A phenomenological failure criterion was developed based on this interaction considering the following assumptions:

- Waviness of the central line of the yarns is nearly sinusoidal [7].
- Geometry of the unit cell is parameterized as a function of the non impregnated cloth: thickness t and length l, as defined in Figure 8.4.
- As isotropic-fragile material, individual fibres fail due shear stress.
- Changes in geometry are small enough to be neglected.

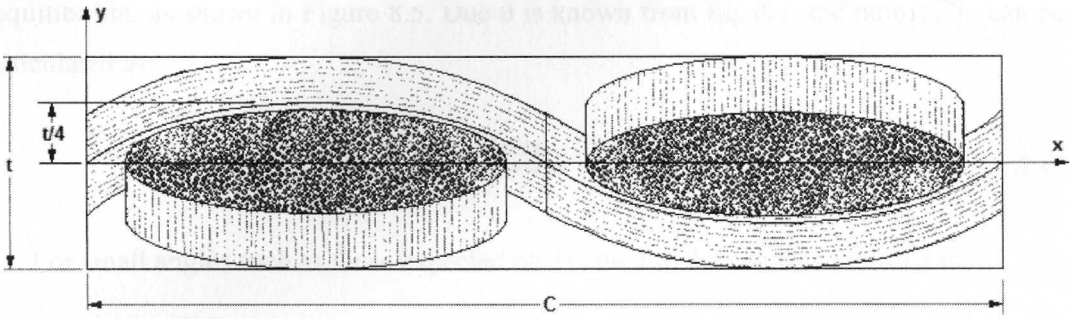

Figure 8.4 Geometrical parameters defined to model a plain weave unit cell.

Based on the Figure 8.4 and as stated by assumptions 1 and 2, the central yarn line will be defined as a sinusoidal function, with wavelength c and thickness t:

$$YP(x) = \frac{t}{4}\sin\left(\frac{2\,\pi\,x}{c}\right) \qquad \textit{Eq. 8.1}$$

And the slope of the yarn´s central line can be obtained by deriving Eq. 8.1 respect to

$$YP'(x) = \frac{dYP}{dx} = \frac{\pi\,t}{2\,c}\cos\left(\frac{2\,\pi\,x}{c}\right) \qquad \textit{Eq. 8.2}$$

The maximum slope is then located at x=c/2; substituting this condition in eq. Eq. 8.2 yields:

$$YP'_{max} = \left|YP'\left(\frac{c}{2}\right)\right| = \frac{\pi\,t}{2\,c} \qquad \textit{Eq. 8.3}$$

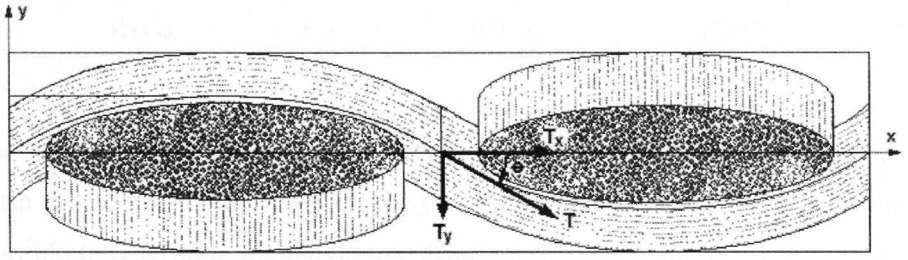

Figure 8.5 Tensile components in the yarns.

Given a tension T_x applied to the unit cell in x direction, a force component T_y normal to textile´s plane due the yarn misalignment θ must appear to maintain the system´s

equilibrium, as shown in Figure 8.5. Due θ is known from Eq. 8.3, the ratio T_y/T_x can be calculated as:

$$tan\,\theta = \frac{T_y}{T_x} \quad \xrightarrow{yields} \quad T_y = T_y\,tan\,\theta \qquad Eq.\ 8.4$$

For small angles such as those expected on TC the Eq. 8.4 can be simplified to:

$$\theta \approx \frac{T_y}{T_x} \quad \xrightarrow{yields} \quad T_x = \theta\,T_y \qquad Eq.\ 8.5$$

To study the validity of this simplification, common industrial plain weave textiles cloths parameters were collected (see Table 8.1) and YP'_{max} was calculated from it published thickness and count tread per inch. Results were plotted in Figure 8.6 with the normalized θ and $tan\ \theta$, as well as the function θ/tan θ. The last permits to evaluate the lost of accuracy respect to angle θ. Note that for all the studied textiles, independently of it material, the expected error is near or lower than 1%, which justify the simplification.

Table 8.1 Commercial plain-weave TC physical parameters

Style	Materal	Oz/yd2	Thickness (in)	Tread/In	YP'max
4533	S-Glass	5.8	0.009	18x18	0.1272
120-38	E-Glass	3.08	0.004	60x58	0.1822
3733	E-Glass	5.79	0.010	18x18	0.1413
7500	E-Glass	9.66	0.014	16x14	0.1539
1522	E-Glass	3.74	0.0055	24x22	0.0950
282	Carbon	5.8	0.0070	12.5x12.5	0.0687
120	Kevlar	1.8	0.0035	34x34	0.0934
281	Kevlar	5.0	0.010	17x17	0.1335

Once known the geometrical ratio between T_y and T_x, is reasonable to suppose that such ratio should be the same than for the yarn stresses due trigonometric similitude. Then it is possible to determine the maximum shear stresses for both, uniaxial and equibiaxial load cases (identified with sub-indexes $_{UD}$ and $_{BD}$, respectively) using the Morh circle as shown in Figure 8.7: for uniaxial tensile load, T_y component is null, and therefore so is the normal yarn stress σ_y. The maximum shear stress is then given by:

$$\tau_{xyUD} = \frac{\sigma_{xUD}}{2} \qquad \textit{Eq. 8.6}$$

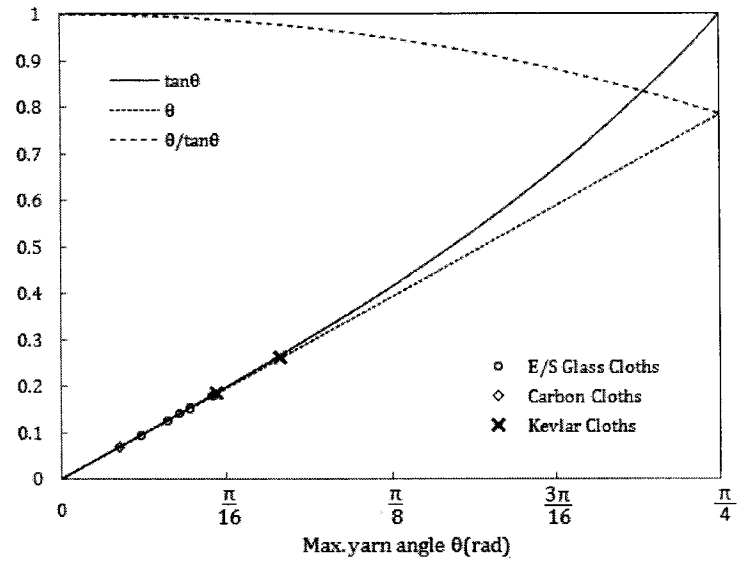

Figure 8.6 Error introduced by simplify *tan* θ to θ.

For equibiaxial load state, the maximum shear stress can be calculated as:

$$\tau_{xyBD} = \frac{\sigma_{xBD} - \sigma_{yBD}}{2} \qquad \textit{Eq. 8.7}$$

For this case $\sigma_{yBD} < 0$ due the compressive force acting on the yarn´s contact region. Is possible to express σ_{yBD} in terms of σ_{xBD} due it trigonometric similitude using Eq. 8.3 as:

$$\sigma_{yBD} = -(\frac{\pi\, t}{2\, c})\sigma_{xBD} \qquad \textit{Eq. 8.8}$$

Substituting Eq. 8.8 in Eq. 8.7 yields:

$$\tau_{xyBD} = \frac{\sigma_{xBD} + \sigma_{xBD}(\frac{\pi\, t}{2\, c})}{2} = \frac{\sigma_{xBD}}{2}\left(1 + \frac{\pi\, t}{2\, c}\right) \qquad \textit{Eq. 8.9}$$

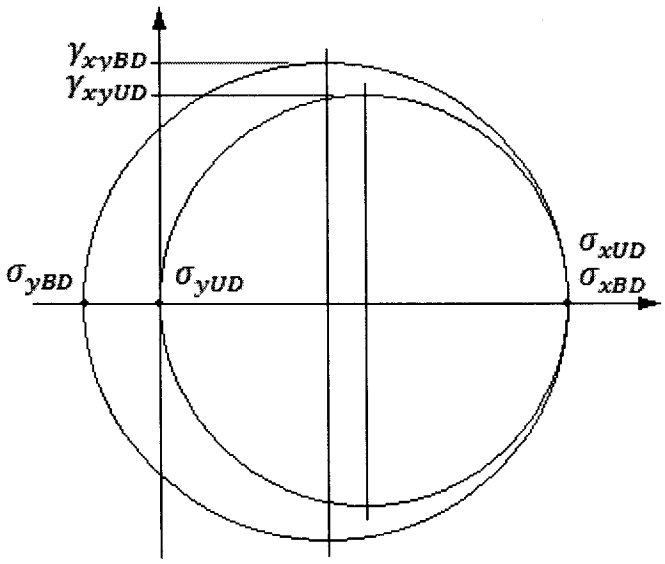

Figure 8.7 Morh circles for uniaxial and biaxial load cases on yarns.

Then, the shear stress ratio between uniaxial and biaxial load cases can be calculated as:

$$p = \frac{\tau_{xyUD}}{\tau_{xyBD}} = \frac{\sigma_{xUD}}{\sigma_{xBD}(1 + \frac{\pi\, t}{2\, c})} \qquad \textit{Eq. 8.10}$$

and given that:

$$\sigma_{xUD} = \sigma_{xBD} \qquad \textit{Eq. 8.11}$$

Eq. 8.10 reduces to:

$$p = \frac{\tau_{xyUD}}{\tau_{xyBD}} = \frac{1}{1 + \frac{\pi\, t}{2\, c}} \qquad \textit{Eq. 8.12}$$

This expression can be physically interpreted as the fraction of the uniaxial strength whose can be resisted by the textile under biaxial load. This can be expressed alternatively as a factor k that represents the reduction of the uniaxial strength due equibiaxial load as:

$$k = 1 - p = 1 - \frac{1}{1 + \frac{\pi\, t}{2\, c}} \qquad \textit{Eq. 8.13}$$

Simplifying Eq. 8.13 yields:

$$k = \frac{\pi t}{2c + \pi t} \qquad \textit{Eq. 8.14}$$

Assuming the yarn compression component changes proportionally to the biaxial ratio BR, the effective ultimate strain ε_f given certain BR can be expressed as:

$$\varepsilon_f = \varepsilon_{ux}(1 - k\,BR), \qquad BR = \frac{\varepsilon_1}{\varepsilon_2}, \quad \varepsilon_1 < \varepsilon_2 \qquad \textit{Eq. 8.15}$$

To express the Eq. 8.15 in failure criteria form, maximum strain must be reach the predicted effective value $\varepsilon_f = \varepsilon_2$; substituting this condition as well as k (Eq. 8.14) and $BR = \frac{\varepsilon_1}{\varepsilon_2}$ into Eq. 8.15, and dividing all the expression by ε_2, expression yields:

$$FC = \frac{\varepsilon_{ux}}{\varepsilon_2}\left(1 - \frac{\pi\, t\, \varepsilon_1}{(2c + \pi t)\varepsilon_2}\right) \qquad \textit{Eq. 8.16}$$

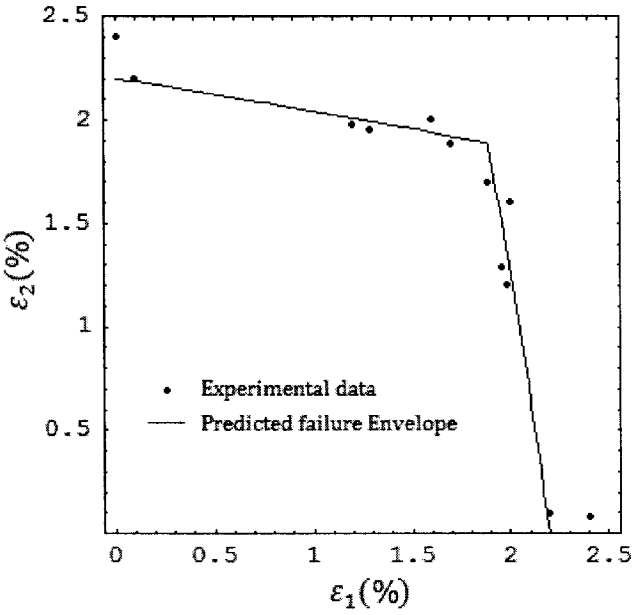

Figure 8.8 Failure envelope predicted by Eq. 8.16.

On this equation, FC≥1 predicts failure. Using the geometrical values derived from the material's manufacturer information (t=0.3mm, c=2.82mm) and using ε_{ux}=2.2, the

ultimate strain value measured form uniaxial tests performed with cruciform specimens, the failure envelope predicted by Eq. 8.16 is presented in ε_1-ε_2 space on Figure 8.8; is evident the good agreement between predicted failure envelope and the experimental data, and is remarkable the fact that only a two geometrical parameters and one experimental strength are required.

8.2.2. In-situ effect

If more than one layer are laminated together, the out-plane displacement is limited by the adjacent plies; then, if the number of layers are large enough, no yarn alignment will be possible even for uniaxial loads, and the maximum strain for all the envelope will tend to the failure strain measured on equi-biaxial tests. To account this effect in the model, a new parameter is introduced, a function of the number of layers f(NL), which in this case will be considered f(NL)=NL in order to evaluate the effect of the proposed modification; this parameter will multiply the length of the cell c in the equation (Eq.13). Also a parameter k_c is introduced to account the stress concentration effects between the yarns as follows:

$$k_n = 1 - \frac{1}{1 + k_c \frac{\pi\, t}{2\, c\, NL}} \qquad \textit{Eq. 8.17}$$

Rearranging Eq.16:

$$k_n = \frac{k_c\, \pi\, t}{2\, c\, NL + k_c\, \pi\, t} \qquad \textit{Eq. 8.18}$$

The effect of the f(NL) parameter is to reduce the slope of the failure envelope; also is necessary to force it to pass through the equi-biaxial failure strain, to modelling the phenomenology identified; to achieve this, the following function has been proposed, based on geometrical manipulation of the failure envelope:

$$\varepsilon_f = \varepsilon_{ux}\left(\frac{1-k}{1-k_n}\right)(1 - k_n\, BR) \qquad \textit{Eq. 8.19}$$

Rearranging Eq. 8.19 in failure criterion form:

$$FC = \frac{{\varepsilon_2}^2 NL\,(2\,c + k_c \pi\, t)}{\varepsilon_{ux}(2\,c\,NL - k_c\,\pi\,t(\varepsilon_1 - \varepsilon_2))} \qquad \textit{Eq. 8.20}$$

Criterion predicts failure when FC≥1. Failure envelopes predicted for NL=1,2,5,25, k_c=1(considering no stress concentration effects) and ε_{ux}=2.2% (the minimum observed for BR=∞ experimental tests) are shown in Figure 8.9. Note that for NL=1 it predicts the same failure envelope than the Eq. 8.16, (Figure 8.8), and conform the NL arises, the uniaxial strength becomes lower, until it tends to the same value observed for equibiaxial loads, as proposed. It can be interpreted as FC → Max Strain Criterion for n ≫ 1.

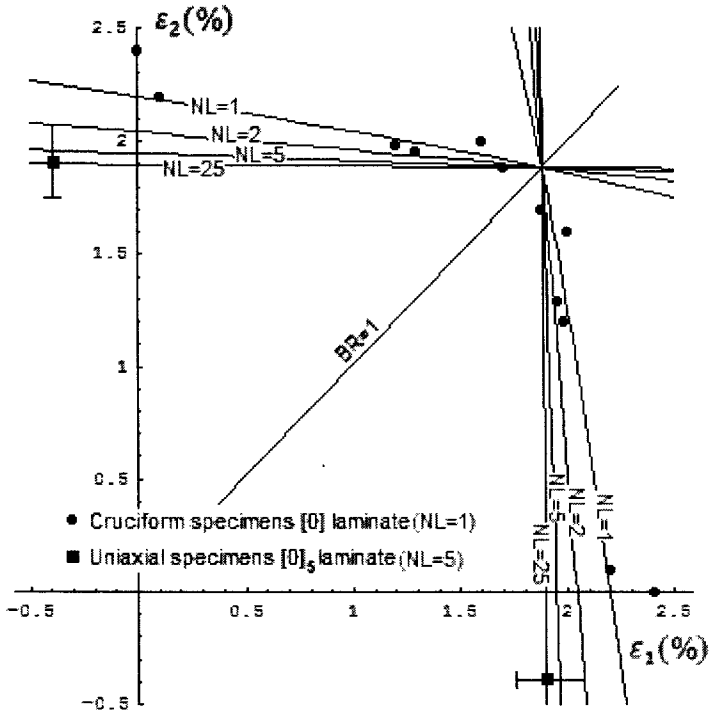

Figure 8.9 Failure envelope predicted by Eq. 8.20, using K_c=1.

8.2.3. Correction for account the Poisson ratio effect

On the aforementioned failure criterion formulation, an input parameter is ε_{ux}, which is the ultimate strain measured on uniaxial tests. For simplification purposes, is was assumed

that ε_{ux} value corresponds to a BR=∞, but due Poisson contraction effects the corresponding biaxial ratio is defined as:

$$BR = -\frac{v\,\varepsilon_{ux}}{\varepsilon_{ux}} \qquad \textit{Eq. 8.21}$$

To account this effect, Eq. 8.19 is modified by introducing the Poisson ratio v:

$$\varepsilon_f = \varepsilon_{ux}\left(\frac{1-k}{1-\frac{k_n}{1+v}}\right)\left(1-\frac{k_n}{1+v}\,BR\right) \qquad \textit{Eq. 8.22}$$

Expressing Eq. 8.22 in failure criteria form:

$$FC = \frac{\varepsilon_2\,(2\,c + k_c\,\pi\,t)\,\left(k_c\,\pi\,t\,v + 2\,c\,NL(1+v)\right)}{2\,c\,\varepsilon_{ux}\left(2\,c\,NL\,(1+v) + k_c\,\pi\,t\left(1-\frac{\varepsilon_1}{\varepsilon_2}+v\right)\right)} = 1 \qquad \textit{Eq. 8.23}$$

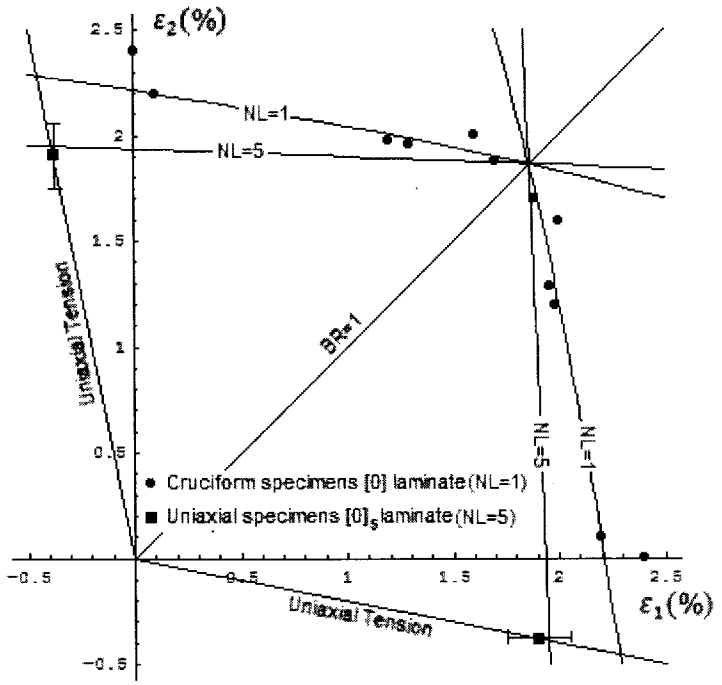

Figure 8.10 Failure envelope predicted by Eq. 8.20, using K_c=1.4 and ε_{ux}=2.3.

Failure envelope predicted by Eq. 8.23 is shown in Figure 8.10; for this case, k_c and ε_{ux} were adjusted to fit the experimental data, given ε_{ux}=2.3% and k_c=1.4. Is remarkable that

ε_{ux} extrapolated is very similar to these corresponding to BR=∞, and k_c has significant higher value (+40%) than for the models which neglected the Poisson effect. Considering that k_c represents a contact stress factor between the adjacent yarn's fibres, and that certainly some degree of contact stresses must be involved in the yarn interface, the fact that this value be greater than 1 is plenty justified.

8.3. Concluding Remarks

- Experimental data permitted to infer that maximum stress criterion is a good, conservative choice to predict the matrix initial failure, while Tsai-Wu criterion could fit better the initial failure envelope.

- A phenomenological failure criterion has been formulated based on the failure envelope and mechanical behavior observed during the experimental tests program. The proposed failure criterion requires of unit cell information: length and thickness, as well as number of layers to modeling the laminating in-situ effect, and the Poisson ratio to account the elastic properties of the material.

- This criterion permits to explain why some experimental failure envelopes reported in literature appears to be well explained by de maximum strain criteria, which not considers interactions between perpendicular failure modes, despite the entangled architecture of textile composites suggest that such interactions must be significant.

- The criterion has been formulated in closed form, and hence, is easy to implement and interpreting.

Chapter 9.
Conclusions and further work

9.1. Conclusions

1. About the "rhomboid cruciform specimen":

❖ FE analysis revealed that the cruciform specimens formerly used on composite materials biaxial strength characterization do not generate a deformation field as homogeneous as desirable.

❖ Rhomboid thinned gage-zone cruciform specimen proposed based on stress concentration considerations generates more homogeneous strain field than typical squared windowed cruciforms.

❖ Design of experiments based optimization process permitted to obtain a cruciform geometry capable to generate a very homogeneous strain field into the gage zone, while avoid premature failure outside this area. This makes the specimen suitable to be used on biaxial strength characterization experimental programs.

2. About the "biaxial testing machine":

❖ Low cost mechanisms based testing machine was developed, capable to perform biaxial tensile tests with arbitrary biaxial displacement ratio, while permits to absorb small misalignments and completely unobstructed visual field to the specimen.

- Despite non automatic displacement control was provided, a method which displays a displacement director permits to human operators to actuate the hydraulic cylinders with precision enough to met the requirements established by ASTM standards.

3. About the "experimental procedure":

- The specimen preparation methodology developed as part of this research permits to obtain a machining damage free specimen, essential condition to preserve the textile microstructure, while dimensional tolerances extrapolated from ASTM standards for uniaxial testing of composites materials can be met even with the large amount of manual work involved in the process.

- Use of DIC permitted to perform an experimental qualitative and quantitative validation of the FE calculated strain field of the optimized cruciform specimen, demonstrating excellent agreement between numerical and measured data.

- Experimental failure envelope for single layer plain weave textile composite demonstrates that interaction between textile constituents plays a significant role in the biaxial tensile strength.

4. About the "phenomenological failure criterion":

- A phenomenological based failure criterion has been formulated. It provides a very accurate prediction of the biaxial tensile strength of plain weave textile composites, using a set of a few physical parameters, which makes the criterion easy to implement.

- The understanding of the phenomenology at microscale level, permitted to extend the criterion to account for the in-situ effect due the stacking of layers and the Poisson effect.

9.2. Summary of contributions of this thesis

- The design of rhomboid thinned window gage zone cruciform specimen capable to generate nearly ideal strain distributions for strain characterization of biaxial tensile strength of textile composites, and arguably useful for other kind of composites.
- The methodology to prepare single layer, machining damage free cruciform specimens.
- The design, building, calibration and operation of a low cost biaxial testing machine by less than 10K USD. This equipment will permit to continue the research on the biaxial strength characterization.
- The use of DIC as primary measurement system avoids inaccuracies introduced when strength data is reduced from forces and displacements applied to the cruciform.
- The matrix onset failure of plain weave textile composite under biaxial tensile loads can be conservatively predicted by the maximum stress criterion, and probably more accurately by Tsai-Wu criterion.
- The experimental evidence that interactions between constituents of textile composite play a significant roll on it tensile biaxial strength.
- The understanding of how the in-situ effect can hide these interactions when more than one single layer is laminated.
- The formulation of a simple to implement, phenomenological based failure criteria for plain weave TC, which considers lamination in situ effects and the elastic properties of material and requires only a few, physically significant parameters.
- A very important contributions for practical engineering design activities derived of the last is the possibility that if not detailed failure envelope is available for a bidirectional, plain weave textile composite under biaxial tensile loads, the final failure envelope can be reasonable well predicted by the maximum strain criterion, using as input data the ultimate strength measured on uniaxial tests of thick laminates (thick means laminates with high number of layers, 5 or more can be used)

9.3. Suggestions for future work

- To achieve a full validation of the proposed failure criterion, biaxial tests for different laminates must be performed; also, uniaxial tests for different number of plies laminates must be conducted.

- On this work, the stress concentration parameter k_c has been used as a fit parameter; instead this, as part of future work, analytical derivation of k_c must be pursued.

- Despite experimental data evidences that number of layers plays a significant role in the biaxial tensile strength, detailed research to quantify it value should be conducted.

- To extend the usability of the criterion to a general laminates, interactions of normal strains with shear strains must be modeled; then, experimental program designed to characterize this effects must be conducted. This shall include a specific specimen and test equipment design.

References

[1] AlKhalil MFS, Soden PD, Kitching R, Hinton MJ. The effects of radial stresses on the strength of thin-walled filament wound GRP composite pressure cylinders. International Journal of Mechanical Sciences 1996; 38(1):97-120.

[2] Antoniou AE, Van Hemelrijck D, Philippidis P. Failure prediction for a glass/epoxy cruciform specimen under static biaxial loading. Composite Science and Technology 2010; 70(8):1232-1241.

[3] Arellano D, Sepúlveda G, Elizalde H, Ramírez R. "Enhanced cruciform specimen for biaxial testing of fibre-reinforced composites." International Materials Research Congress. Cancun, 2007.

[4] ASTM Standard D 3039/D 3039M, Standard Test Method for Tensile Properties of Polymer Matrix Composite Materials, 2000.

[5] ASTM Standard D 6507 – 00. Standard Practice for Fiber Reinforcement Orientation Codes for Composite Materials. 2000.

[6] ASTM Standard D6856–03, Standard Guide for Testing Fabric-Reinforced TextileComposite Materials, 2003.

[7] Barbero EJ, Trovillion J, Mayugo JA, Sikkil KK. Finite element modeling of plain weave fabrics from photomicrograph measurements. Composite Structures 2006;73(1)41-52.

[8] Bing P, Kemao Q, Huimin X, Anand A. Two-dimensional digital image correlation for in-plane displacement and strain measurement: a review. Measurement Science and Technology 2009; 20(6): 1-17.

[9] Bird JE, Duncan J. Strain hardening at high strain in aluminum alloys and its effect on strain localization. Metallurgical and Materials Transactions A 1981; 12(2): 235-241.

[10] Boehler JP, Demmerle S, Koss S. A New Direct Biaxial Testing Machine for Anisotropic Materials. Experimental Mechanics 1944; 34(1): 1-9.

[11] Camanho PP, Dávila CG, de Moura MF. Numerical simulation of mixed-mode progressive delamination in composite materials. Journal of Composite Materials 2003; 37(16): 1415–1438.

[12] Chaudonneret M, Gilles P, Labourdette R, Policella H. Machine d'essais de traction biaxiale pour essais statiques et dynamiques. La Recherche Aérospatiale 1977:299-305.

[13] Clay SB. Biaxial Testing Apparatus. United States of America Patent 5905205. 18 May 1999.

[14] Crookston JJ, Long AC, Jones IA. A summary review of mechanical properties prediction methods for textile reinforced polymer composites. Proceedings of the Institution of

Mechanical Engineers, Part L: Journal of Materials: Design and Applications 2005; 219(2):91-109.

[15] Daniel IM, Gdoutos EE, Wang KA, Abot JL. Failure Modes of Composite Sandwich Beams, International Journal of Damage Mechanics 2002; 11(4): 309-334.

[16] Deo RB, Starnes JH, Holzwarth RC. Low-Cost Composite Materials and Structures for Aircraft Applications. Presented at the RTO AVT Specialists' Meeting on "Low Cost Composite Structures", Loen, Norway, 7-11 May 2001; published in RTO-MP-069(II).

[17] Dudderar TF, Koch, Doerries DE. Measurement of the shapes of foil bulge-test samples. Experimental Mechanics 1977; 17(4): 133-140.

[18] Doyle JF, Phillips JWP. Manual on experimental stress analysis. Society for Experimental Mechanics (U.S.). Society for Experimental Mechanics, 1989.

[19] Ebrahim L, Van Paepegem W, Degrieck J, Ramault C, Makris A, Van Hemelrijck D. Strain distribution in cruciform specimens subjected to biaxial loading conditions. Part 1: Two-dimensional versus three-dimensional finite element model. Polymer Testing 2010; 29(1):7-13.

[20] Ebrahim L, Van Paepegem W, Degrieck J, Ramault C, Makris A, Van Hemelrijck D. Strain distribution in cruciform specimens subjected to biaxial loading conditions. Part 2: Influence of geometrical discontinuities. Polymer Testing 2010; 29(1):132-138.

[21] Echaabi J, Trochu F, Gauvin R. Review of Failure Criteria of Fibrous Composite Materials. Polymer Composites 1996; 17(6):786-798.

[22] Fawaz, Z. Étude analytique, numérique et expérimentale portant sur la rupture et la fatigue biaxiales des lamelles renforcées de fibres. PhD Thesis, Sherbrooke: Université de Sherbrooke, 1992.

[23] Ferron G, Makinde A. Design and Development of a Biaxial Strength Testing Device. Journal of Testing and Evaluation (ASTM) 16, no. 3 (May 1988).

[24] Ferron, G. Dispositif perfectionné d'essais de traction biaxiale. France. 26 Septembre 1986.

[25] Fessler H, Musson JK. A 30 Ton Biaxial Tensile Testing Machine. Professional Engineering Publishing 1969; 4(1): 22-26.

[26] Forest Products Laboratory. 1999. Wood handbook--Wood as an engineering material. Gen. Tech. Rep. FPL-GTR-113. Madison, WI: U.S. Department of Agriculture, Forest Service, Forest Products Laboratory.

[27] Gdoutos EE, Gower M, Shaw R, Mera R. Development of a Cruciform Specimen Geometry for the Characterisation of Biaxial Material Performance for Fibre Reinforced Plastics. Experimental Analysis of Nano and Engineering Materials and Structures. Springer Netherlands, 2007. p. 937-938.

[28] Gre´diac M. The use of full-field measurement methods in composite material characterization: interest and limitations. Composites: Part A 2004; 35(7-8):751-761.

[29] Gupte AA. Optimization of Cruciform Biaxial Composite Specimen. In: Master on Science Thesis. South Dakota State University, 2003.

[30] Hashin Z. Failure criteria for unidirectional fibre composites. Journal of Applied Mechanics. 1980; 47; 329-334.

[31] Hayhurst DR. A Biaxial-Tension Creep-Rupture Testing Machine. Professional Engineering Publishing 1973; 8(2): 119-123.

[32] Hull D, Clyne TW. An introduction to composite materials. 2nd edition. Cambridge University Press, 1996.

[33] Hill, R. Elastic Properties of Reinforced Solids: Some Theoretical Principles. Journal of Mechanics and Physics of Solids1963; 11: 357–372.

[34] Hinton, M. J. and Soden, P. D., Predicting failure in composite laminates: the background to the exercise. Composites Science and Technology, 1998; 58, 1001.

[35] Huang Z-M. Fatigue life prediction of a woven fabric composite subjected to biaxial cyclic loads. Composites: Part A 2002; 33(2):253-266.

[36] Jackson KE, Kellas S, Morton J. Composite Laminates Loaded in Tension and in Flexure Scale Effects in the Response and Failure of Fibre Reinforced. Journal of Composite Materials 1992; 26(18): 2674-2705.

[37] Kaddour AS, Hinton MJ. Instructions To Contributors Of The Second World-Wide Failure Exercise (Wwfe-II): Part(A).

[38] Karkkainen RL, Sankar BV, Tzeng JT. Strength prediction of multi-layer plain weave textile composites using the direct micromechanics method. Composites: Part B 2007; 38(7-8): 924-932.

[39] Kawai M, Morishita M, Tomura S, Takumida K. Inelastic behavior and strength of fiber-metal hybrid composite: Glare. International Journal of Mechanical Sciences1998; 40(2-3): 183-198.

[40] Key CT, Schumacher SC, Hansen AC. Progressive failure modelling of woven fabric composite materials using multicontinuum theory. Composites: Part B 2007; 38(2):247–257.

[41] Kim JH, Ryou H, Lee MG, Chung K, Youn JR, Kang TJ. Micromechanical modelling of fiber reinforced composites based on elastoplasticity and its application for 3D braided glass/Kevlar composites. Polymer Composites 2007; 28(6):722-732.

[42] Kwon HJ, Jar PYB, Xia Z. Characterization of bi-axial fatigue resistance of polymer plates. Journal of Materials Science 2005; 40(4):965– 972.

[43] Lecompte D, Smits A, Bossuyt S, Sol H, Vantomme J, Van Hemelrijck D, Habraken AM. Quality assessment of speckle patterns for digital image correlation. Optics and Lasers in Engineering 2006; 44(11):1132-1145.

[44] Lomov SV, Huysmans G, Luo Y, Parmas RS, Prodromou A, Verpoest I, Phelan FR. Textile composites: modelling strategies. Composites: Part A 2001; 32(10):1379-1394.

[45] Marsh G. Boeing's 787: trials, tribulations, and restoring the dream. Reinforced Plastics 2009; 53(8): 16-21.

[46] Marsh G. Composites lift off in primary aerostructures. Reinforced Plastics 2004; 8(4): 22-27.

[47] Marsh G. Flying high with the self-build movement. Reinforced Plastics 2002;46(1): 26-30.

[48] Makinde A, Thibodeau L, Neale K. Development of an apparatus for biaxial testing using cruciform specimens. Experimental Mechanics 1992; 32(2): 138-144.

[49] Matthews FL, Rawlings RD. Composite Materials: Engineering and Science. Chapman & Hall 1994.

[50] Mayes JS, Hansen AC. Multicontinuum Failure Analysis of Composite Structural Laminates. Mechanics of Composite Materials and Structures 2001; 8(4): 249–262.

[51] MIL-HDBK-17-5. Composite materials handbook volume 5. Ceramic matrix composites volume 5 of 5. Department of defense handbook 2002.

[52] Mönch, E., and D. Galster. "A Method for Producing a Defined Uniform Biaxial Tensile Stress Field." British Journal Of Applied Physics 14, no. 11 (1963).

[53] MSC.Dytran Theory Manual, MSC Software, 2005.

[54] Ng RK, Yousefpour A, Uyema M, Ghasemi MN. Design, Analysis, Manufacture, and Test of Shallow Water Pressure Vessels Using E-Glass/Epoxy Woven Composite Material for a Semi-Autonomous Underwater Vehicle. Journal of Composite Materials 2002; 36(21): 2443-2478.

[55] Paris F. A Study of Failure Criteria of Fibrous Composite Materials, NASA/CR- 2001-210661, March 2001.

[56] Pascoe KJ, de Villiers JWR. Low Cycle Fatigue of Steels Under Biaxial Straining. Journal of Strain Analysis 1967; 2(2).

[57] Pinho ST, Dávila CG, Camanho PP, Iannucci L, Robinson P. Failure Models and Criteria for FRP Under In-Plane or Three-Dimensional Stress States Including Shear Non-Linearity, NASA/TM-2005-213530. February 2005.

[58] Peters ST. Handbook of composites, 2nd edition. Chapman and Hall, 1998.

[59] Post D, Han B. *Chap 22*, "*Moire Interferometry*," Handbook on Experimental Mechanics, W. N. Sharpe, Jr., ed., Springer-Verlag, NY, 2008.

[60] Puck A, Schürmann H. Failure Analysis of FRF Laminates by Means of Physically Based Phenomenological Models. Composites Science and Technology 1998; 58; 1045-1067.

[61] Raymer DP. Aircraft design: a conceptual approach, 2nd edition. American institute of aeronautics and astronautics; Washington D.C., 1992.

[62] Rho JY, Kuhn-Spearing L, Zioupos P. Mechanical properties and the hierarchical structure of bone. Medical Engineering & Physics 1998; 20(2):92-102.

[63] Rengifo L. La construcción con tierra. Trabajo de investigación: el adobe, la quincha y el tapial. Universidad Nacional de Ingeniería 1995, Lima, Perú.

[64] Sadegh AM, Cavallaro P, Quigley C. Biaxial and shear testing apparatus with force controls. United States of America. 17 April 2007.

[65] Sepúlveda CG. Biaxial Testing of Composite Materials: Technical Specifications and Experimental Set-up *Maestría en Ciencias con Especialidad en Sistemas de Manufactura* México Mayo 2009

[66] Shivakumar KN and Smith SA. In Situ Fracture Toughness Testing of Core Materials in Sandwich Panels. Journal of Composite Materials 2004; 38(8): 655-668.

[67] Schultheisz CR, Wass A. Compressive Failure of Composites, Part I: Testing and Micromechanical Theories. Prog. Aerospace Sci. 1996; 32(1): 1-42.

[68] Soden PD, Hinton MJ, Kaddour AS. Biaxial test results for strength and deformation of a range of E-glass and carbon fibre reinforced composite laminates: failure exercise benchmark data. In: Failure Criteria in Fibre Reinforced Polymer Composites: the World-Wide Failure Exercise. Oxford: Elsevier Science LTD, 2004, p. 52-96.

[69] Soden, P. D., Hinton, M. J. and Kaddour, A. S., Lamina properties, lay-up configurations and loading conditions for a range of fibre reinforced composite laminates. Compos. Sci. Technol. 1998; 58; 1011.

[70] Soden PD, Kaddour AS, Hinton M.J. Recommendations for designers and researchers resulting from the world-wide failure exercise. Composites Science and Technology 2004; 64(3-4): 589–604.

[71] Standard Practice for Fibre Reinforcement Orientation Codes for Composite Materials. ASTM D6507, American Society for Testing and Materials, West Conshohocken, PA.

[72] Steven Huybrechts, Arup Maji, Jennifer Lao, Peter Wegner and Troy Meink. Validation of the Quadratic Composite Failure Criteria with Out-of-Plane Shear Terms, Journal of Composite Materials 2002; 36; 1879. DOI: 10.1177/0021998302036015250

[73] Suarez JA, Buttitta C et al. Novel Composites for Wing and Fuselage Applications. In: Report Number: NAS 1.26:201612. Langley Research Center, Bethpage, NY, Sep, 1996.

[74] Swanson SR, Smith LV. Comparison of the biaxial strength properties of braided and laminated carbon fibre composites. Composites: Part B 1996; 27(1):71-77.

[75] Tsai SW, Wu EM. A general theory of strength for anisotropic materials. Journal of Composite Materials 1971; 5: 58-80.

[76] Tsai SW. Strength characterisation of composite materials, Tech. Rep. NASA CR-224, National Aeronautics and Space Agency (1965).

[77] Turon A., Camanho PP, Costa J, Dávila CG. An interface damage model for the simulation of delamination under variable-mode ratio in composite materials. Tech. Rep. NASA/TM-2004-213277, National Aeronautics and Space Administration, U. S. A. (2004).

[78] Ward MB, Epstein JS, Lloyd R. Self-aligning Biaxial Load Frame. United States of America Patent 5279166. 18 January 1994.

[79] Vargas-Cortés PV, Arellano-Escárpita DA, Elizalde-Siller HR, Ramírez-Mendoza RA, Sepúlveda-Castro G. Máquina para pruebas biaxiales con mecanismo autocentrador. Patente Publicada. México. Solicitud: 2008-12-18. No. MX/a/2008/016309.

[80] Welsh JS, Adams DF. An experimental investigation of the biaxial strength of IM6/3501-6 carbon/epoxy cross-ply laminates using cruciform specimens. Composites: Part A 2002; 33(6):829-839.

[81] Welsh JS, Adams DF. Development of an Electromechanical Triaxial Test Facility for Composite Materials. Experimental Mechanics 2000; 40(3): 312-320.

[82] Welsh JS, Mayes JS, Biskner A. 2-D biaxial testing and failure predictions of IM7/977-2 carbon/epoxy quasi-isotropic laminates. Composite Structures 2006; 75(1-4):60-66.

[83] Welsh JS, Mayes JS, Key CT, McLaughlin RN. Comparison of MCT failure prediction techniques and experimental verification for biaxially loaded glass fabric-reinforced composite laminates. Journal of Composite Materials 2004; 38(24):2165-2181.

[84] Yamada SE, Sun CT. Analysis of Laminate Strength and Its Distribution. Journal of Composite Materials 1978; 12; 275-284.

[85] Youssef, Y. Résistance des composites stratifiés sous chargement biaxial: validation expérimentale des prédictions théoriques. PhD Thesis, Sherbrooke: Université de Sherbrooke, 1995.

[86] Yu Y, Wan M, Wu X, Zhou X. Design of a cruciform biaxial tensile specimen for limit strain analysis by FEM. Journal of Materials Processing Technology 2001: 67-70.

[87] <http://www.uni-stuttgart.de/ifu/forschung/einrichtungen/werkstoffpruefung/index.en.html#kreuz> (2008)

[88] <http://www.sheffield.ac.uk/aerospace/staff/soutis/res-interests.html> (2011)